Effects of disease-causing mutations of podocin on podocyte biology

Valeryia Kuzmuk

A dissertation submitted to the University of Bristol in accordance with the requirements for award of the degree of PhD in the Faculty of Health Sciences

Bristol Medical School

PhD Thesis 2019

Word Count: 44,029

Abstract

The slit diaphragm component podocin is the protein product of the *NPHS2* gene, which is mutated in a subset of patients with autosomal recessive steroid-resistant Nephrotic Syndrome (SRNS) that manifests as early childhood onset of proteinuria, focal segmental glomerulosclerosis (FSGS) and fast progression to end-stage renal disease (ESRN). Most disease-causing mutations of podocin result in its incorrect intracellular trafficking leading to aberrant formation/function of the slit diaphragm complex. Among these, the most frequent mutation is R138Q (57.5%), which alters the intracellular trafficking of podocin to the plasma membrane (PM), leading to its retention in the endoplasmic reticulum (ER). Interestingly, the most frequent worldwide mutation (F508del) of the cystic fibrosis transmembrane conductance regulator (CFTR) is also retained in the ER. Our collaborators have shown that this is due to aberrant interaction of this mutant with cytokeratin 8 (K8). Disruption of this interaction leads to the correction of the F508del-CFTR processing defect leading to its expression at the plasma membrane.

Standard *in vitro* techniques were used to understand the effects of R138Q mutation on podocin trafficking and biology and to characterize the nature of R138Q-Keratin 8 interaction in podocin's bona fide cell type, the kidney podocyte. Furthermore, a conditional podocin knock-in mouse carrying a R140Q mutation, the mouse analogue of human R138Q, was created using doxycycline-inducible Cre-recombinase technology that allows for the study of the effects of the mutation in postnatal life and represents an ideal model for pharmacological studies.

In this study, a previously unknown mechanism for the intracellular retention of the R138Q podocin mutant was identified. First, I demonstrated that Keratin 8 may physically interact with the R138Q podocin, and that ablation of K8 expression using shRNA in human R138Q-expressing cells led to the correct association of podocin with lipid raft microdomains at the plasma membrane and the recovery of the adhesive function of the mutant cells. Excitingly, interruption of this interaction in the R138Q podocin mutant podocytes with a small molecule compound also results in the correct targeting of the mutant protein to the plasma membrane and restores its function. The involvement of keratin 8 network in the misfolded protein response was further demonstrated *in vivo*, where a continuous 28-days treatment with a small molecule compound prevented the development of proteinuria in the *NPHS2*$^{flox/R140Q}$ mice. Together, these results show that the disruption of the K8-R138Q interaction potentially using chaperone drugs already developed in the Cystic Fibrosis (CF) field may provide a novel therapeutic target for SRNS patients bearing the R138Q mutation. I have also identified a novel binding partner of podocin, and a new gene mutated in NS.

This thesis is dedicated to:

My dad for his unconditional love and support

Acknowledgments

This work contains the results of three years' worth of intense but rewarding work, which I have thoroughly enjoyed. I would like to thank all members of Bristol Renal, past and present, for being so helpful and encouraging.

Firstly, thank you must go to Kidney Research UK and Nephrotic Syndrome Trust, who awarded me a PhD scholarship, which funded this work to help those in need. I would particularly like to thank you my supervisors Dr Gavin Welsh and Prof Moin Saleem. Gavin has always been very supportive and helpful. Gavin has believed in my ability and was always there to share the ups and downs of the research. Equally, Moin has helped me to understand the purpose of my research and shown me the clinical relevance of it. His support and encouragement have been invaluable. I have been very lucky to have been supervised by both of you and I am looking forward to continue working with you in the future. Thank you should also go to Dr Rebecca Foster for letting me to work under her animal license. Extra special thanks must be addressed to Dr Ruth Rollason for being such an amazing lab supervisor and friend. For all your help with teaching me new techniques and the many coffee and lunch breaks.

Outside of the laboratory, I would like to thank you Professor Aleksander Edelman for allowing me to spend time in his lab in Paris and for significant advice on data analysis. Also, huge thanks must go to Professor Corinne Antignac (INSERM, France) for the collaboration during this project.

Finally, but by no means least, I must thank my amazing friends and family, who as always have been a source of immense support throughout. Thank my parents, Alexander and Maya, for both the emotional and financial support. Thank you for your interest and enthusiasm in what I am doing. To my Dasha, words cannot express how grateful I am for all the support she has given me. To my sister Stefania, thanks for making my mood always better and being a little ball of happiness.

Author's Declaration

I declare that the work in this dissertation was carried out in accordance with the requirements of the University's Regulations and Code of Practice for Research Degree Programmes and that it has not been submitted for any other academic award. Except where indicated by specific reference in the text, the work is the candidate's own work. Work done in collaboration with, or with the assistance of, others, is indicated as such. Any views expressed in the dissertation are those of the author.

Signed: Date:

Declaration

Some of the work described in Chapter 6 has been taken from "*TBC1D8B* Loss-of-Function Mutations Lead to X-Linked Nephrotic Syndrome via Defective Trafficking Pathways" paper (https://doi.org/10.1016/j.ajhg.2018.12.016). I was a joint first author and contributed significantly to the writing of the manuscript; where work was not done by me, I have acknowledged it in the text.

Signed: Date:

Contents

List of Figures

List of Tables

List of Abbreviations

A1AT	Alpha-1 antitrypsin
ATP	Adenosine Triphosphate
CD2AP	CD2-Associated Protein
CF	Cystic Fibrosis
CFTR	Cystic Fibrosis Transmembrane Conductance Regulator
CK	Cytokeratin
CNF	Congenital NS of the Finnish Type
CP	Capping Protein
DAD	Diaphanous Autoregulatory Domain
DID	Diaphanous Inhibitory Domain
DNA	Deoxyribonucleic Acid
DT	Diphtheria Toxin
EM	Electron Microscopy
ER	Endoplasmic Reticulum
ES	Embryonic Stem
ESL	Endothelial Surface Layer
ESRD	End-Stage Renal Disease
FAK	Focal Adhesion Kinase
FH1	Formin Homology 1
FH2	Formin Homology 2
FPE	Foot Process Effacement
FSGS	Focal Segmental Glomerulosclerosis
GAG	Glycosaminoglycan
GAP	GTPase-activating protein
GBM	Glomerular Basement Membrane
GDP	Guanosine Diphosphate
GEF	Guanine nucleotide exchange factor
GEnCs	Glomerular Endothelial Cells
GFB	Glomerular Filtration Barrier
GTP	Guanidine Triphosphate
HEK	Human Embryonic Kidney
IF	Immunofluorescence
IF	Intermediate Filament
INF2	Inverted Formin 2
K	Keratin
K18	Cytokeratin 18
K8	Cytokeratin 8
KI	Knockin
KO	Knockout
MM	Metanephric Mesenchyme
mRNA	messenger RNA
MSD	Transmembrane Domain

MST	Microscale Thermophoresis
NaCl	Sodium Chloride
NBD	Nucleotide-Binding Domain
NS	Nephrotic Syndrome
PAN	Puromycin Aminonucleoside
PAS	Periodic acid-Schiff
PCR	Polymerase Chain Reaction
PFA	Paraformaldehyde
PHB	Prohibitin Homology
PM	Plasma Membrane
PM	Podocin Mutant
PTM	Post-Translational Modification
qPCR	Quantitative PCR
R-domain	Regulatory Domain
RNA	Ribonucleic Acid
rtTA	reverse tetracycline-controlled Transcriptional Activator
SD	Slit Diaphragm
SH3	Src Homology 3
shRNA	short hairpin RNA
SRNS	Steroid-Resistant Nephrotic Syndrome
Tet-O	Tetracycline-responsive promoter element
TIRF	Total Internal Reflection Fluorescence
TRP	Transient Receptor Potential
TRPC6	Transient Receptor Potential Canonical Channel-6
UB	Uretic Bud
WH2	Wiskott-Aldrich Syndrome Homology Region 2
WT	Wild-Type

Chapter 1: General Introduction

1.1 The Kidney

The (human) kidneys are a pair of bean-shaped filtering organs approximately 5 inches in length, located towards the posterior muscular wall of the abdominal cavity. The kidneys (Figure 1.1) process the plasma portion of blood and, in so doing, they perform several fundamental functions, including secreting hormones, such as calcitriol and erythropoietin [1], regulating blood pressure via renin production [2] and gluconeogenesis. The principal function of the kidneys, however, is the excretion of metabolic waste products, such as creatinine and urea, into the urine as soon as they are produced as a result of protein catabolism. This waste removal is achieved by filtering the blood, thus maintaining its water/ion balance, and is carried out by the nephrons. The typical adult human kidneys process approximately 180 litres of primary urine devoid of macromolecules per day at the filtration rate of 125 ml/min.

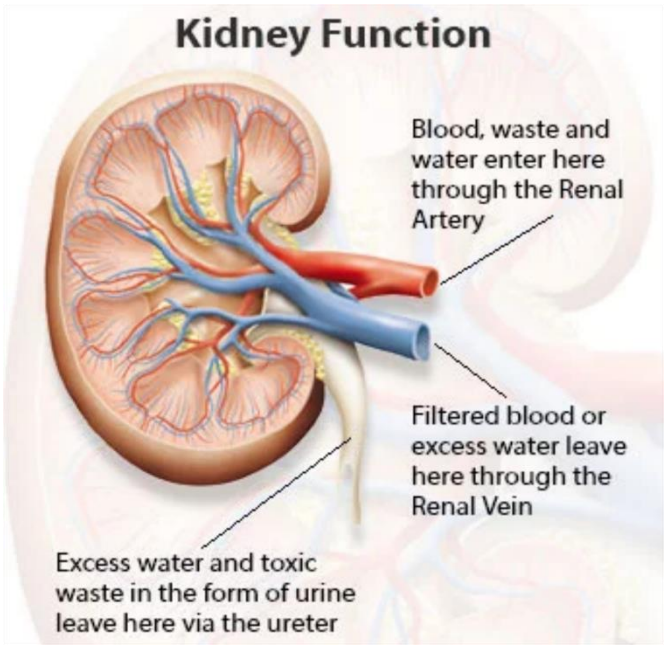

Figure 1.1 A cross section of the human kidney. Unfiltered blood enters the human kidney via the renal artery and leaves via the renal vein once filtered. Urine containing the excess waste products and fluid is excreted from the kidney via the ureter. Image reproduced from [3].

There are approximately 2 million nephrons present in each human kidney. Each nephron is composed of the renal corpuscle and a tubule (Figure 1.2) [4]. The renal corpuscle is the part of the nephron that forms cell and protein free filtrate from blood; more precisely a specialised bundle of capillaries called the glomerulus is responsible for this filtration process [5]. As filtrate made by the glomerulus leaves the renal corpuscle, it enters the proximal convoluted tubule, where substances, such as amino acids, glucose, albumin and LMWPs, are reabsorbed back into the bloodstream [4]. The filtrate then enters a long, U-shaped duct called the loop of Henle, which aids the recovery of water and NaCl from the urine. Once the filtrate passes through the ascending limb of Henle, it reaches the distal convoluted tubule, which reabsorbs calcium and sodium and regulates the pH of urine [6]. Finally, the filtrate enters the collecting duct, which concentrates urine from the nephron.

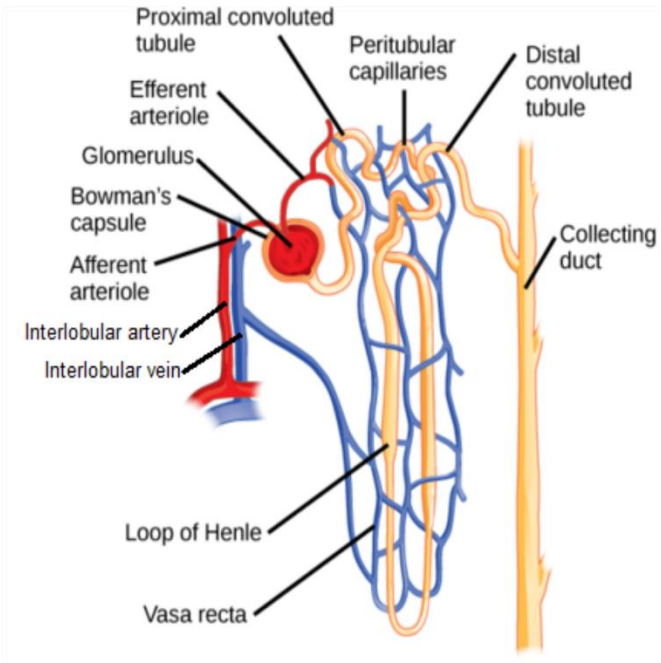

Figure 1.2 The Nephron. Filtrate made by the glomerulus leaves via the proximal convoluted tubule, onto the loop of Henle, the distal convoluted tubule and finally reaches the collecting duct. Image modified from [7].

1.2 The Glomerulus and its development

As mentioned above, one of the central roles of the human kidney is to filter blood through primary urine production in the glomerulus [8]. The mammalian glomerulus is a highly complex vascular bed that serves as a filter, restricting the passage of cells and high molecular weight proteins into the blood circulation, while allowing water, small

molecules, sugars and electrolytes to pass though [9]. The glomerulus is composed of a capillary tuft surrounded by the Bowman's capsule, which directs the filtered primary urine to the tubular system for further processing [10]. Abnormalities to the glomerulus at any stage of life ultimately lead to a severe disease, so proper development and maintenance of this structure is required.

Renal development has been previously studied in various animal models, such as zebrafish and mice, which allowed the characterization of three distinct stages of the kidney's differentiation ontogenetically. These are the pronephros, which mature into the mesonephros, which further develop into the metanephric kidney [11]. In comparison to the pronephros and mesonephros, the metanephric kidney represents a stable structure, and its development is defined by reciprocal crosstalk between the metanephric mesenchyme (MM) and the uretic bud (UB), leading to the formation of the renal vesicle around the 5^{th} week of gestation in humans [12],[13] .The MM will further give rise to all proximal parts of the nephron, while the UB will branch into collecting ducts, renal calyces and the rest of the urinary tract system [14].

The inductive signals of the UB drive the condensation of the MM towards the renal vesicle, while also result in a mesenchymal-to-epithelial transition, thus marking the beginning of the future nephron development [15]. The comma-shaped bodies are formed after this initial condensation, which further undergo morphological changes to give rise to the S-shaped body, also known as the precursor structure of the glomerulus [15]. At this stage of the glomerular development three main components can be found: a layer of visceral epithelial cells, known as podocytes, a thin layer of Bowman's capsule, and a capillary loop made of immature endothelial cells [9]. It remains unclear how the podocytes cover the outside of the capillary loop. However, what's known is that at the beginning of this process, both the podocytes and the capillary endothelial cells develop their own basal lamina, which fuse with each other forming a thick basement membrane, called the glomerular basement membrane (GBM) [9]. The outcome of this fusion results in the podocytes and endothelial cells being brought into close proximity to each other, allowing podocytes to undergo a significant transformation [9]. During this transformation the podocytes gain some mesenchymal-like features, although remaining an epithelial cell, and start to lose their lateral cell attachments, except the ones at the basal membrane (Figure 1.3) [9]. At this point, podocytes almost completely enwrap the capillary loops. Finally, the mature podocytes cell bodies that have become independent

of each other, develop several large branch-like projections, from which many smaller foot processes extend and interdigitate with those of neighbouring podocytes to form slit diaphragms (discussed in detail below) [9].

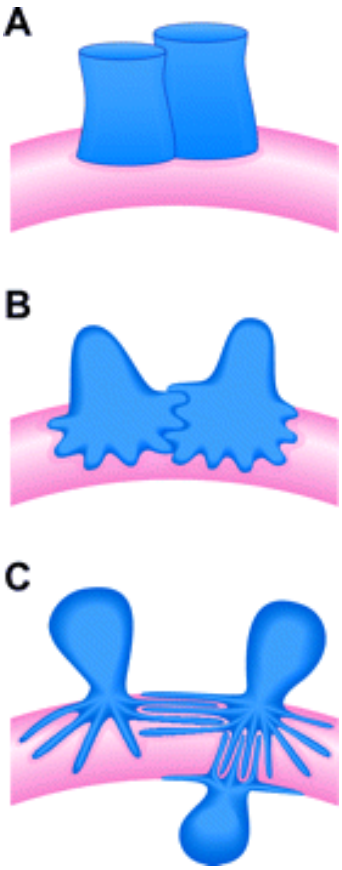

Figure 1.3 A model of the podocyte and foot process assembly. (A) Two immature columnar podocytes are attached along their lateral membranes. (B) Podocytes lose their lateral membrane attachments and begin to interdigitate at the basally attached regions. (C) Independent of each other, podocytes are still attached through their interdigitated foot processes. Adapted from Quaggin and Kreidberg [9].

Maturation of the glomerular capillaries begins with a single capillary loop composed of endothelial progenitors invading itself into the vascular cleft and requires primitive podocytes to produce angiogenic factors, such as VEGF-A [16]. As the development progresses, the capillary loop starts to divide into six to eight loops [17]. The endothelial cells of the capillaries gain a perforated-like appearance, such that now there are slit-like openings on either side of the GBM: the actual filtration slits between interdigitating foot processes of podocytes and holes through the endothelial cells themselves [9]. Following the endothelial cells, specialized smooth muscle cells, known as mesangial cells, also migrate through the vascular cleft, where they are suggested to help extend the capillary

loops into branches and respond to different physical stimuli [9]. The finding discussed in this section has led to the conclusion that the proper development and interaction of both podocytes and glomerular endothelial cells results in the formation of the glomerular filtration barrier (GFB).

1.3 The Glomerular Filtration Barrier

The glomerulus, being situated in the most proximal part of the nephron, acts as a key functional regulator for renal ultrafiltration [15]. The filter itself represents a three-layered structure consisting of the intervening glomerular basement membrane (GBM), glomerular endothelial cells (GEnCs) and glomerular epithelial cells, known as podocytes, and lies between the glomerular vasculature and Bowman's capsule (Figure 1.4) [18]. The filtration barrier serves as a selective sieve restricting the passage of macromolecules according to their size, charge and shape, while being freely permeable to water and small solutes in plasma. It's believed that the flow of the glomerular filtrate takes an extracellular route, beginning from the innermost fenestrated endothelium, then across the GBM, and finally through the slit diaphragm of podocytes [10]. Diseases affecting either one or any of the layers result in the presence of high amounts of albumin in the urine, the condition known as proteinuria. Therefore, each of the three core layers has its own role in filtration specificity, which will be outlined in more detail below, and their physicochemical and signalling interplay is essential for maintenance of the GFB integrity in both health and disease [19].

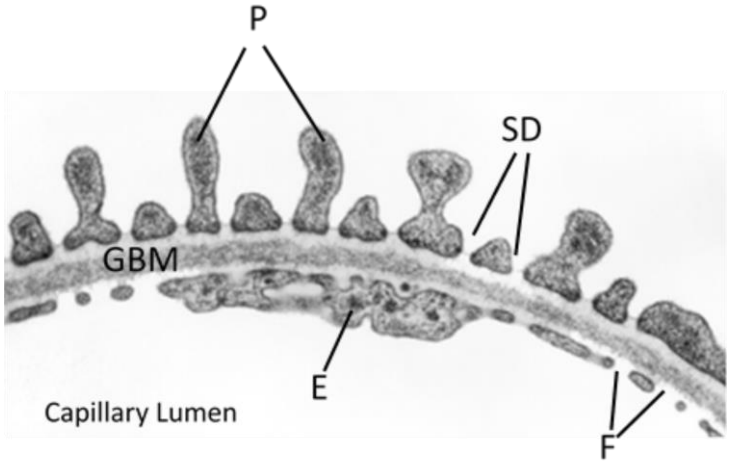

Figure 1.4 The Glomerular Filtration Barrier. Transmission electron micrograph of a cross section of the GFB, which is composed of three main components: glomerular endothelial cells (E) with fenestrae (F) (Layer 1), glomerular basement membrane (GBM) (Layer 2) and

podocyte foot processes (P) that interdigitate creating the slit diaphragm (SD) (Layer 3). Adapted from Pavenstädt *et al* [20]**.**

1.3.1 Layer 1: The Glomerular Endothelial Cells

The glomerular vasculature is made of afferent and efferent arterioles, and the capillary tuft. Blood enters the glomerulus via the afferent arteriole and exits via the efferent one. Within the glomerulus, the afferent arteriole instantly divides into the glomerular tuft, which acts as a functional unit for blood filtration [21]. Unlike the afferent and efferent arterioles, the GEnCs monolayer lines the capillary side of the GFB and is the first point of contact of the plasma with the GFB. The glomerular capillaries show increased permeability to water and small solutes, when compared to most other capillary beds. This high hydraulic conductivity is partly due to the GEnC monolayer having a fenestrated appearance, caused by transcellular pores, known as fenestrae, that cover it [21]. The fenestrae themselves are 60-100 nm wide and cover around 20-50% of the glomerular capillary surface area, thus establishing glomerular capillaries as an essential part of the renal ultrafiltration (Figure 1.5A) [22].

The development of the GEnC monolayer has been widely studied in rodent models. The earliest GEnC emerge from mesenchyme, also known as angioblasts, drifting into the cleft of the glomerulus at the S-shaped body phase of development; these cells have cuboidal appearance and lack fenestrations [23]. During the capillary loop phase podocytes are observed on the adverse side of the maturing GBM, and the endothelial cells start to proliferate, where their cytoplasm narrows down before fenestration's formation [24]. At this stage the fenestrations have diaphragms, which disappear as the glomerular endothelium progressively matures and as podocyte foot processes start to develop [24]. Therefore, it has been stated that the GEnC fenestration's formation runs in parallel with podocyte foot processes maturation [23].

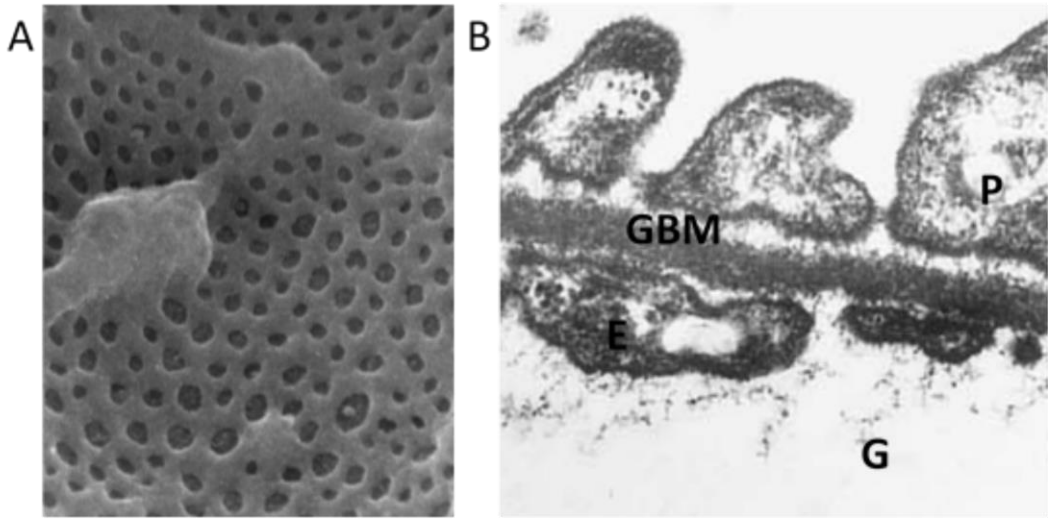

Figure 1.5 The Glomerular Endothelial Cells. (A) Scanning electron micrograph of a highly fenestrated glomerular endothelium. Adapted from Kamba *et al* [25].(B) Transmission electron micrograph of the GFB, showing that the luminal side of the glomerular endothelium is covered by a fine layer of glycocalyx (G). Adapted from Rostgaard and Qvortrup [26].

Due to the large size of the fenestrae in comparison to albumin for example, the idea that the GEnCs could play an essential role in protein filtration was contentious. However, recent studies have demonstrated that the glomerular endothelium does indeed take part in the barrier function because of its negatively charged surface [21]. The luminal side of the glomerular capillaries and the fenestral surface are covered by the glycocalyx, a thick (200-500 nm) layer as determined by electron microscopy (Figure 1.5B) [27]. The glycocalyx mainly consists of negatively charged glycoproteins and proteoglycans [22]. Furthermore, absorbed plasma components within the glycocalyx form a broader layer called the endothelial surface layer (ESL) [28]. The strong negative charge of the surface layer causes fenestrae to become narrower and more restrictive [21]. Enzymatic digestion of various ESL elements caused increased albumin permeability across the endothelium together with decreased ESL depth and loss of charge on the glomerular endothelial surface layer [29]. Analogously, the importance of the ESL was demonstrated in mice models, where adriamycin perfusion also resulted in the glomerular ESL shrinkage, thus supporting the theory that GEnCs contribute to the charge-selectivity of the GFB [30].

The proteoglycans are critical for the glycocalyx formation, and consist of a core protein and covalently attached glycosaminoglycan (GAG) side chains [31]. Five types of GAG side chains have been defined, namely, heparan sulphate, dermatan sulphate, chondroitin

sulphate, keratan sulphate and hyaluronic acid [32]. Interestingly, hyaluronic acid is the only nonsulphated, uncharged side chain linked to cell surface proteins instead of any core proteins [32]. GEnCs are considered to produce the most abundant proteoglycan, known as heparan sulfate [33]. Heparanase III and human heparanase are enzymes that specifically cleave heparan sulphate, and have been reported to increase the albumin permeability across the monolayer, whilst resulting in no change in trans-endothelial electrical resistance [31]. Interestingly, neuraminidase treatment led to the removal of almost all of the glycocalyx, which consequently decreased trans-endothelial electrical resistance and elevated albumin influx *in vitro* [31]. Taken together, these findings suggest that the human endothelial cell glycocalyx is involved in the size and charge restriction of protein passage, which might explain why patients with preeclampsia, a disease associated with a glomerular lesion known as endotheliosis, present with protein in the urine due to their loss of the endothelial cell glycocalyx [34],[35].

1.3.2 Layer 2: The Glomerular Basement Membrane

After passing through the first layer of the GFB, the filtrate next contacts the GBM - an essential element of the GFB derived from the fusion of the individual basal membranes of both podocytes and GEnCs during glomerulogenesis. Similar to other basement membranes, the preeminent components of the GBM are type IV collagen, nidogen, laminin and heparan sulfate proteoglycans [36]. However, past studies have demonstrated that the GBM has its own specific protein isoforms, which are essential for correct glomerular development and function. In particular, what distinguishes the GBM is the expression of the following isoforms - laminin α5β2γ1, collagen IV α3α4α5 and agrin [37]. These specific protein isoforms are able to create an interwoven meshwork of 300 to 350 nm in thickness believed to play a role in both size- and charge- selective properties of the GFB [38]. Despite the fact that the composition of the GBM has been studied for a while, there is still a debate about its role as the primary filter compared to that of podocytes and endothelial cells.

Laminin characterizes a family of evolutionary conserved glycoproteins that are able to interact with each other in a non-random manner to create at least 15 various αβγ heterotrimers, which are produced by different cell types and secreted into the extracellular space [39]. Interestingly, the extracellular space is where the laminin polymerization occurs that is essential for the initiation of basement membrane development, as seen by a number of *in vitro* and *in vivo* studies [39]. Laminin 521

(α5β2γ1) is the main laminin present in the mature GBM secreted by both endothelial cells and podocytes. As glomeruli progress through their development, laminins (αβγ heterotrimers) undergo developmental transitions within the GBM [40]. Specifically, laminin 111 (α1β1γ1) is mainly present in the earliest epithelial cells of the nephron, and its expression then shifts to laminin 511 (α5β1γ1) and finally to laminin 521 (α5β2γ1) upon further development [41]. It has been shown that mutations in laminin prevent these developmental transitions from occurring revealing their significance. Laminin β2 chain deficient mice, for example, show massive proteinuria due to GBM dysfunction and die in the perinatal stage [42], while in humans mutations in β2 gene lead to Pierson's syndrome [22].

Similar to all collagens, collagens type IV are also secreted as heterotrimers consisting of three α chains whose sequence contains multiple Gly-X-Y repeats, which are believed to add the flexibility to the collagen network [43]. Analogous to laminin transitions, GBM type IV collagen also undergoes developmental transitions during glomerulogenesis. At the early stages of the development, collagen IV α1 and α2 chains, secreted by both podocytes and endothelial cells, are mainly expressed [44]. Upon maturation of the glomerulus, podocytes start to synthesize the α3α4α5 trimers, which then polymerize to form the triple-helical type IV collagen network of the mature GBM [45]. This highly organized type IV collagen network gives flexile strength and support to the capillary wall. This explains why mutations in the genes encoding any one of the type IV collagen α3, α4, or α5 chains can lead to severe abnormalities in the GBM. Heterozygous null mutations in collagen IV α3 or α4, for example, cause benign familial hematuria, also well known as thin basement membrane disease, while in the homozygous state these mutations result in autosomal recessive Alport syndrome characterized by progressive renal failure [37].

Concerning the other two components of the GBM, nidogens and heparan sulfate proteoglycans, such as agrin, little is known about their developmental transitions during glomerulogenesis. Both nidogen 1 and nidogen-2 are found in the mature GBM although interestingly lack of their expression in mice has no significant influence on the glomerular filtration [39]. Similarly, ablation of agrin in the GBM results in no dramatic defects on glomerular permeability, even though it causes a drastic anionic charge reduction [46]. Overall, it has been suggested that the GBM plays a small part in charge-selectivity, but it acts primarily as domain for the endothelial glycocalyx, as the proteoglycans are able to stabilize the membrane by binding to laminin and collagen IV [47].

1.3.3 Layer 3: The Podocytes

The final layer of the GFB is composed of podocytes, also known as glomerular visceral epithelial cells, which are terminally differentiated, highly specialized epithelial cells with a complex and unique 3D cellular cytoarchitecture found on the urinary side of the GFB [19]. Glomerular podocytes are endowed with an epithelial polyanion cell surface coat, which is mainly comprised of podocalyxin, a heavy glycosylated protein [48]. The podocyte is able to synthesize podocalyxin itself inserting it into the apical side of the plasma membrane, where it is believed to maintain the filtration slit opening [49]. It has been demonstrated that puromycin aminonucleoside-treated (PAN) rats present with heavy proteinuria due to the reduced sialylation of podocalyxin, thereby highlighting the importance of the negatively charged surface of podocytes [50]. Healthy fully differentiated podocytes have voluminous cell bodies, which resemble the body shape of an octopus, with numerous projections subdivided into the larger major processes and the finer foot processes (Figure 1.6) [21]. Typically, the podocyte's cell body protrudes 5 to 10 primary processes, which are further projected into multiple foot processes [51]. Recently, using a block-face scanning electron microscopy, Ichimura *et al*. demonstrated that the foot processes were projected from the podocyte's cell body via ridge-like prominences, suggesting that the podocytes are anchored to the GBM [52]. More precisely, these prominences provide an adhesion platform for the direct anchorage of the cell body and primary process to the GBM, while also serving as linkers to connect the foot processes to the cell body and primary process [52].

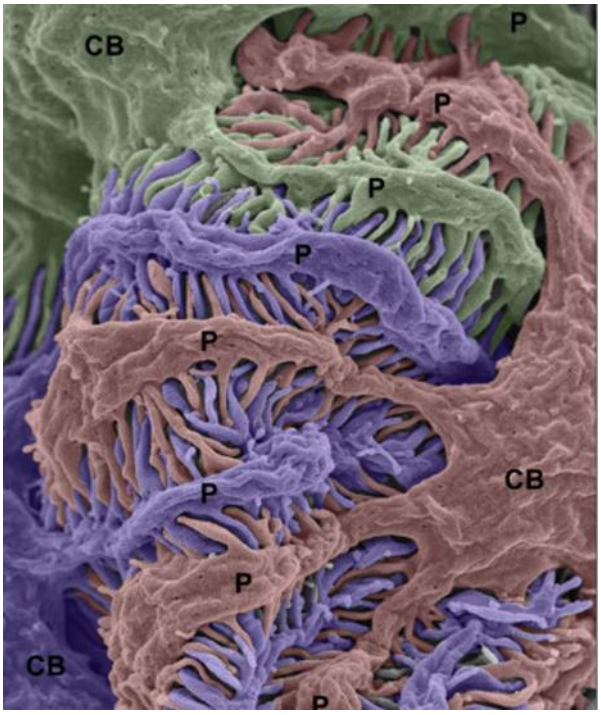

Figure 1.6 Conventional scanning electron micrograph of podocytes enwrapping a glomerular capillary. Each podocyte is individually coloured. Interdigitating foot processes can be observed extending from each primary process. (CB=cell body, P=primary process). Adapted from Ichimura *et al* [52].

There is a close link between podocyte morphology and the actin cytoskeleton. The two types of processes in podocytes are defined by their well-developed internal cytoskeletal systems, which play an essential role in sustaining cell structure and the maintenance of the processes [53]. The core cytoskeletal components of the major processes are microtubules and intermediate filaments, such as vimentin, whereas actin-rich filaments dominate in the foot processes [53]. Therefore, this might help to explain why only the foot processes are affected in glomerular disease. There are two different actin-based structures found in foot processes during development and after injury, which are lamellipodia and filopodia that are responsible for their movement and extension [54]. In addition, focal adhesion complexes are involved in movement, while also allow for the tethering of the foot processes to the GBM, thus preventing their detachment within the glomerular structure [54]. Podocyte movement occurs, when the foot processes exhibit opposing forces that pull on the cell body by extending the protrusions; thereby, each movement results in the re-establishing of the new adhesion point once the lamellipodia move forward [55]. Furthermore, actin is also involved in the intracellular trafficking

within the podocyte foot process; an example is the actin-based motor protein, Myoc1, which transports the podocyte protein NEPH1 to the podocyte cell membrane [56].

The podocyte cell bodies enwrap the outer surface of the glomerular capillaries by extending foot processes that interdigitate with those of neighbouring podocytes forming specialized cell-to-cell junctions called slit diaphragms [20]. The slit diaphragm contains proteins, such as zona occludens-1 [57] and P-cadherin, which are commonly found in tight and adherens junctions respectively, however it lacks E-cadherin and has a porous structure [58]. The slit diaphragm represents a dynamic multiprotein apparatus that consists of integral membrane proteins, ion channels, scaffolding and signalling proteins (Figure 1.7). This multiprotein complex must accomplish essential tasks, such as acting as a filter as well as anchoring the podocyte to the GBM. It has become the main focus of research since the discovery of single-gene mutation in slit diaphragm proteins that were found to be responsible for the development of Nephrotic Syndrome (NS) (discussed in more detail below). The first such protein discovered was the transmembrane protein nephrin, a member of the immunoglobulin superfamily, which has been identified at the podocyte slit diaphragm (discussed in further detail below) [59]. Its homophilic interaction with nephrin from an adjacent podocyte is considered to be the "pore" of the slit diaphragm [60]. Nephrin's intracellular domain is able to interact with proteins, such as podocin, to facilitate actin polymerization into specific arrangements, which is essential for foot process architecture [60]. This is supported by the fact that single-gene mutations in actin-binding proteins, such as α-actinin-4 and inverted formin 2, result in hereditary nephrotic syndrome, in which foot processes show abnormalities [61],[62]. Being such a specialized complex, the slit diaphragm has recently been appreciated to function as a signalling platform controlling podocyte cell survival, endocytosis, and polarity, along with actin cytoskeleton organization [63]. Thus, gene defects in a number of components of the slit diaphragm have been associated with nephrotic syndrome in humans.

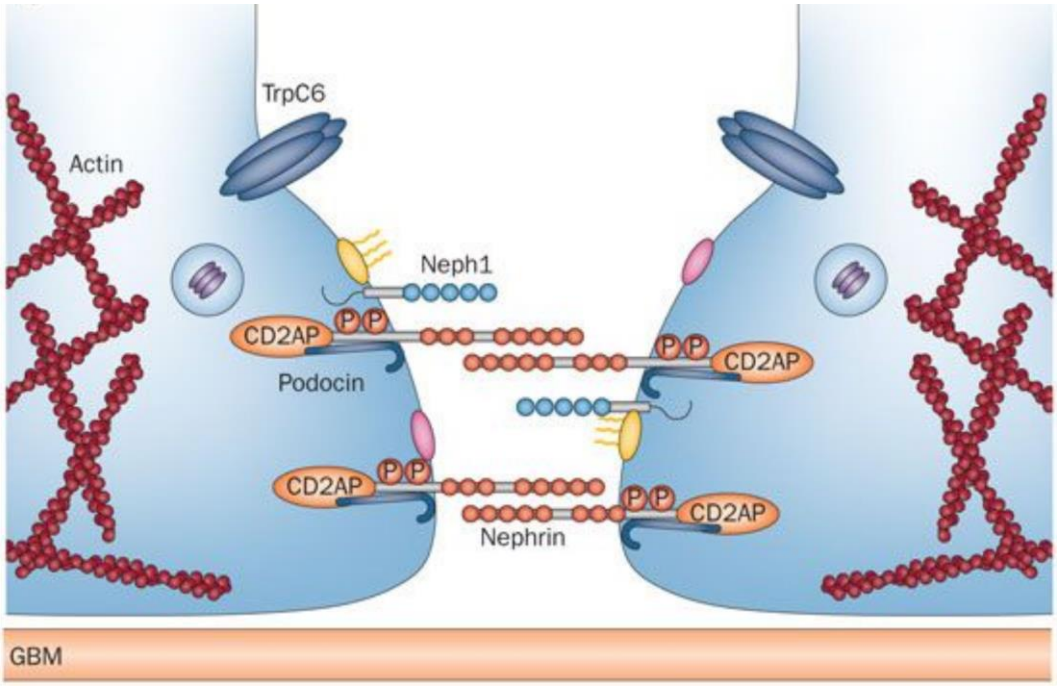

Figure 1.7 A cartoon illustration of the main molecular elements of the podocyte slit diaphragm. Reproduced from Grahammer *et al* [64].

The podocyte slit diaphragm itself acts as a final barrier in the GFB ultrafiltration, which means that the occurrences of foot process effacement (FPE) are problematic for GFB permeability. Disruption of foot process architecture results in FPE, a proteinuria-correlated process activated by podocytes in response to the injurious stimuli [65]. Podocyte effacement is, indeed, a very complex and dynamic process involving various phosphorylation-driven and signalling based events [54]. The actual term FPE describes the physical loss of the interdigitating pattern of foot processes of neighbouring podocytes, where the two distinct phases are distinguished. During the first stage, foot processes retract and change their shape into irregular broadened projections, causing slit diaphragms being either lost or displaced [66]. The second phase, also known as the complete stage of FPE, describes the formation of flattened disk-like projections spread along the GBM, which eventually merge with the cell bodies [67] Interestingly, FPE seems to be reversible and is a consequence of active actin filament reorganization subsequent to intracellular signals [68]. The best example of reversibility of FPE arises from patients with minimal change disease upon treatment, while in contrast focal segmental glomerulosclerosis (FSGS) patients present with more severe and irreversible FPE [19]. Based on the available data, podocytes have a unique structure-function relationship

placing them in the centre of thinking with regard to the direct link to genetic forms of NS.

1.4 Nephrotic Syndrome and genes identified

Dysfunction of the glomerular filtration barrier, leading to extensive leakage of plasma proteins into the urine and podocyte foot processes effacement observed by electron microscopy, is detected in many inherited and acquired nephropathies [69]. The clinical indication is nephrotic syndrome (NS), described as a triad of heavy proteinuria (>40 mg/m^2/hr), oedema and hypoalbuminaemia (<3.0 g/dL), and which often results in end-stage renal disease (ESRD), accounting for 15% of the cases in the European population [70]. Even though NS is linked to various types of renal disease, the most common form (90%) identified in children is idiopathic NS, which progresses in the absence of any clinical features of primary extrarenal disorder [70]. In rare cases, childhood NS can be caused by the systemic inflammation or autoimmune disorders or can be due to infections, toxins , drugs or other inherited renal diseases [71].

Clinically, NS can be classified into two groups by the response to steroid therapy: steroid-sensitive NS (SSNS) and steroid-resistant NS (SRNS). Most patients with idiopathic NS initially respond well to steroids and enter the remission stage with a good renal prognosis; however, around 90% of these patients will relapse, with another half of those becoming steroid-dependent [70]. The remaining 10% are recognized to have SRNS. However, this fails to explain why some patients who originally respond to steroid treatment later become resistant. As mentioned before, NS is considered to be the most prevalent glomerular disease of childhood, with an incidence of around 2 in 100,000 children [72]. Approximately 20% of children will be steroid resistant, with a further 60% of these cases presenting with focal segmental glomerulosclerosis (FSGS), indicated by biopsy [73]. FSGS is described as scarring of the glomerulus that includes several distinct changes, where only a segment of the glomerulus and some, but not all, glomeruli are affected [74]. Progression to ESRD is closely correlated with the development of FSGS. Therefore, because most cases of genetic NS are clinically steroid-resistant with pathologically prevalent FSGS, genetic NS is hard to treat, has poor renal prognosis and often results in ESRD.

The majority of the SRNS genetic forms show structural alterations in the glomerulus or, more precisely, the podocyte. Molecular research work on the genetics of hereditary NS

has revealed the podocyte as a key player in regulating glomerular filtration, whose structure and function are essential in the maintenance of the slit diaphragm membrane [73]. The ongoing identification of genetic defects in podocyte-specific genes has undoubtably expanded our understanding of pathophysiology in genetic NS in regard to clinical onset, diagnosis, therapeutic and prognostic approaches [75]. To date, around 75 genes including those encoding nephrin, transient receptor potential canonical channel-6 (TRPC6), CD2AP, α-actinin-4 and podocin, have been reported to cause NS, and yet more remain to be identified (Table 1.1). Proteins affected by genetic mutations have been found to be expressed at various intracellular locations within the podocyte, such as cell membrane, mitochondria, nucleus and cytoskeleton. The significance of several of them, including nephrin, CD2AP and podocin, which participate in the slit diaphragm assembly, has been shown by the presence of heavy proteinuria, when they are mutated [76]. The major ones will be discussed in further detail below.

NPHS1	AR	CNS/NS
NPHS2	AR	CNS, NS – childhood and adult onset
CD2AP	?	Early-onset NS, HIV nephropathy
TRPC6	AD	Adult onset NS
NUCLEAR PROTEINS		
WT1	Sporadic; AD	Adult onset NS, Denys–Drash and Frasier Syndromes
LMX1B	AR	Nail–Patella Syndrome/NS only
PAX2	AD	Adult onset NS
ACTIN CYTOSKELETON AND SIGNALING		
ACTN4	AD	Adult onset NS
INF2	AD	Familial/sporadic NS; Charcot-Marie-Tooth
SYNPO	?	Adult onset NS
APOL1	Complex; AR	Adult onset NS
MYO1E	AR	Early or adult onset NS
MITOCHONDRIAL		
COQ2	AR	Mitochondrial disease/isolated nephropathy
COQ6	AR	NS with sensorineural deafness
ZMPSTE24	AR	Mandibuloacral dysplasia with NS
GBM		
LMNA	AD	Familial partial lipodystrophy + NS
COL4A3	AR	Alport's disease

COL4A4	AR	Alport's disease
COL4A5	X-linked	Alport's disease

Table 1.1 Some of the genes directly associated with NS. Modified from Bierzynska *et al* [77].

1.4.1 Nephrin

Recent advances in the study of genetic diseases with malfunction of the glomerular filtration barrier provide useful models to explain the physiological mechanisms whereby such disorders occur. One of the most serious such conditions is congenital NS of the Finnish type (CNF), caused by mutations in *NPHS1* gene encoding nephrin, the first podocyte protein discovered [76]. These mutations result in the complete deletion or partial truncation of the protein, therefore, revealing its significance in the maintenance of the GFB [78]. CNF is an autosomal-recessive disorder that progresses itself in utero and results in massive proteinuria at birth or shortly after it [78]. Although the disease is detected in the population worldwide, it is highly frequent in Finland with an incidence of 1:10,000 birth [79]. In most cases, CNF causes death at the neonatal stage, however, in early childhood it can be treated by dialysis and correct nutritional support followed by kidney transplantation [80]. Originally CNF was considered as a GBM disease, however no mutated genes coding for fundamental elements of the basement membranes were identified. Using the positional cloning approach, Kestilä *et al.* found a novel gene located in the 150 kb region of chromosome 19, which was defective in the majority of CNF patients studied, and called it *NPHS1* [78].

Nephrin, the gene product, is a 1241-residue putative transmembrane protein consisting of a short intracellular domain, an extracellular domain containing eight IgG-like motifs, and one proximal fibronectin type III-like motif (Figure 1.8A) [81]. Two cysteine residues linked by a disulphide bridge are present in each IgG-like motif, and these motifs in consequence are able to adopt a globular shape [81]. These IgG-like motifs are known as type C2 and identified in proteins involved in cell-matrix or cell-cell interactions [81]. Therefore, nephrin belongs to the Ig superfamily of cell adhesion molecules, and is exclusively localized to the podocyte slit diaphragm [59]. Based on the domain structure and specific location, it has been stated that nephrin molecules assemble in the slit diaphragm to form the porous substructure, with pores the size of albumin or smaller (Figure 1.8B) [60]. Thus nephrin is a crucial determinant of glomerular ultrafiltration, as

seen in a mouse model that presented massive protein leakage, foot processes effacement and absence of slit diaphragms, when the *NPHS1* gene was inactivated [82].

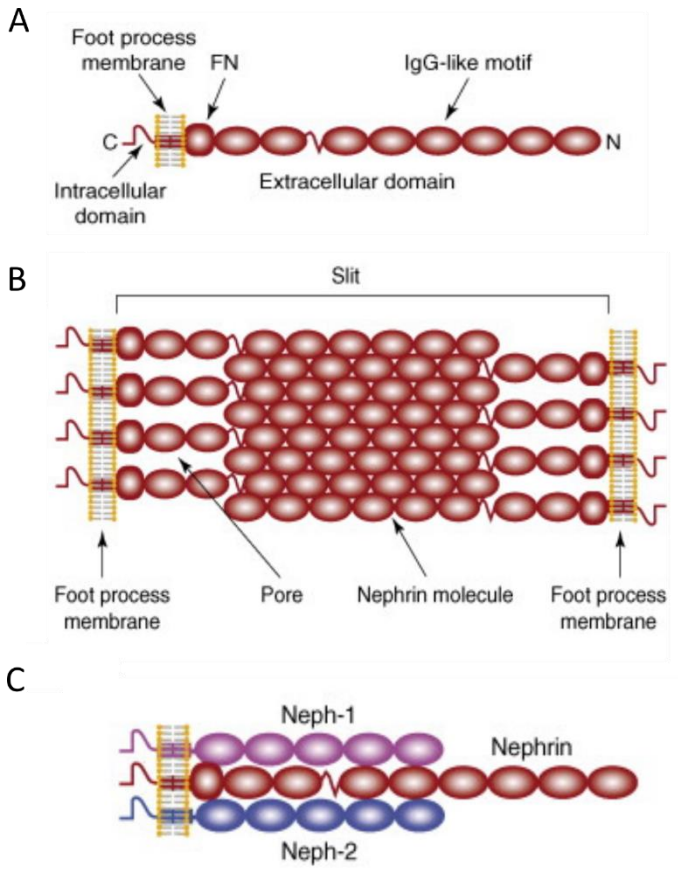

Figure 1.8 Structure and interactions of nephrin. (A) Nephrin's structure consisting of a C-terminal intracellular domain, followed by a single transmembrane domain, and a N-terminal extracellular domain made of one fibronectin type III-like motif and eight IgG-like motifs. (B) Nephrin molecules from adjacent podocytes interact in the middle of the slit diaphragm through homophilic interactions to form the porous substructure. (C) The extracellular domain of nephrin is also believed to interact with shorter Neph molecules, thus maintaining the slit diaphragm structure. Adapted from Patrakka and Tryggvason [81].

The extracellular domain of nephrin has ten potential N-glycosylation sites, nine of which indeed undergo N-linked glycosylation, which is essential for the correct folding and trafficking of nephrin to the plasma membrane [83]. Furthermore, the extracellular domain of human nephrin interacts with the recently discovered Neph family of proteins, and hence, extracellularly nephrin is believed to be involved in maintaining the slit diaphragm ultrastructure. In fact, this interaction has been previously seen *in vivo* between Neph and nephrin homologs in *Drosophila melanogaster*, and was shown to be crucial for the cell-junction formation [84]. The Neph family members (Neph1, Neph2, and

Neph3) are transmembrane proteins with a shorter extracellular domains consisting of five IgG-like motifs that are structurally related to nephrin [81]. These proteins are found in a variety of tissues, and in the glomerulus Neph 1 and Neph 2 are specifically localized to the slit diaphragm [85]. The interactions of nephrin and Neph 1 are highlighted to be essential for maintenance of glomerular filter integrity, as injection of appropriate doses of both anti-nephrin and anti-Neph1 antibodies into rats results in proteinuria [86]. The function of Neph 2 at the glomerular slit diaphragm remains to be identified.

Nephrin's intracellular domain consists of 154 amino acids, including several tyrosine residues that can become phosphorylated, suggesting that nephrin is involved in intracellular signalling [81]. Both *in vitro* and *in vivo* experiments have demonstrated that nephrin is directly tyrosine-phosphorylated by Fyn, the Src family kinase member [87]. This phosphorylation activates the PI3K/AKT pathway, which protects podocytes from apoptosis. Nephrin tyrosine phosphorylation also leads to the recruitment of the SH2-SH3 domain-containing Nck family of adaptor proteins and regulates actin cytoskeleton dynamics [88].

1.4.2 CD2-associated protein (CD2AP)

CD2AP is an 80 kDa multidomain protein consisting of three Src homology 3 (SH3) domains at the N-terminus, followed by a proline-rich region, a potential actin binding domain and a coiled-coil domain at the extreme C-terminus, suggesting that it functions as an adaptor protein (Figure 1.9) [89]. It was originally described as a protein involved in T-cell activation and found to be expressed in all tissue apart from the brain. In the kidney, where the ultrafiltration takes place, CD2AP was shown to play a crucial role. In fact, in glomerular podocytes CD2AP interacts with nephrin via its C-terminal domain and localizes to the slit diaphragm as seen by immunoelectron microscopy [90]. Loss of CD2AP expression in the glomerulus initially results in epithelial cell injury, which further leads to mesangial matrix expansion, glomerulosclerosis and global foot process effacement [91]. Accordingly, mice lacking CD2AP present with severe NS and die of renal failure soon after birth, while heterozygous mice develop a glomerular disease at 9 months with lesions mimicking those of human FSGS [92]. The renal phenotype of these mice was completely rescued by the expression of CD2AP in podocytes, therefore, highlighting the important function of CD2AP in the kidney or more precisely the podocyte [93].

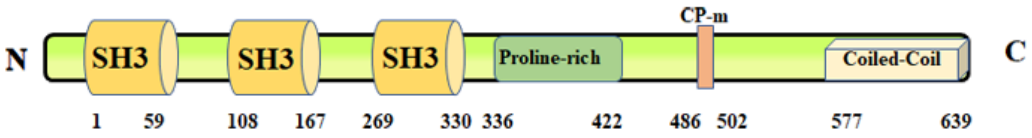

Figure 1.9 Schematic representation of the CD2AP protein. Three SH3 domains are located at the N- terminus, followed by a proline-rich region. A coiled-coil domain and an actin capping protein (CP) binding motif are found at the C-terminus. Reproduced from [94]

CD2AP is an intracellular protein that acts as a linker protein, which is involved in podocyte slit diaphragm assembly, different signalling pathways, actin cytoskeleton regulation and endocytosis [89]. Like nephrin, CD2AP is able to bind an intermediary protein, p85, via its N-terminal domain, therefore recruiting PI3K to the plasma membrane and initiating the nephrin-induced PI3K/AKT signalling pathway to have antiapoptotic effects in podocytes [95]. Moreover, *in vitro* experiments have demonstrated that the interaction between podocin, nephrin and CD2AP stimulates AKT and, in turn, regulates gene expression, actin cytoskeleton remodelling and apoptosis. Podocytes lacking CD2AP show increased apoptosis and defects in the *CD2AP* gene lead to proteinuria in mice, suggesting that CD2AP is a crucial component of the glomerular filtration barrier [91].

1.4.3 TRPC6

Another important component of the glomerular slit diaphragm is the ion-channel TRPC6, a member of the large transient receptor potential (TRP) superfamily, which has been shown to play a pathogenic role, when mutated [96]. This superfamily is best known for their ability to mediate Ca^{2+} release and function as cellular detectors aiding osmolar and fluid flow sensing [97]. Therefore, the discovery of TRPC6 in podocyte foot processes suggests that Ca^{2+} signalling is required for healthy podocyte structure and function and as a result for the maintenance of a proper GFB.

The mammalian TRP superfamily is made up of proteins with the highest homology to *Drosophila* TRP [98]. All TRP channels consist of six transmembrane domains that assemble as tetramers to form cation-permeable pores, and have been grouped into seven subfamilies in mice and six in humans, including the classical or canonical TRPC proteins, according to the amino acid sequence homology [98]. In general, they are ubiquitously expressed, and have diverse functions. TRP channels are composed of an N-terminal cytoplasmic domain containing several ankyrin repeats (four in the case of TRPC6), followed by a membrane domain with 6 transmembrane segments, where a pore-

forming region is located between segments 5 and 6 and a C-terminal cytoplasmic domain that has a TRP sequence (Figure 1.10) [99]. The 25-residue TRP sequence is highly conserved among all the TRP channels and comprises a motif called TRP box 1, followed by a proline-rich region known as TRP box 2 [99]. Coiled-coil sequences have been identified in both the amino- and carboxy- domains with an additional calmodulin and IP_3 receptor-binding domain known as CIRB region found in the COOH-terminal [96],[99]. Coiled-coil sequences, ankyrin repeats and proline-rich regions are believed to be essential for protein-protein interactions, while the domain structure opens a window for unique associations with other proteins [99]

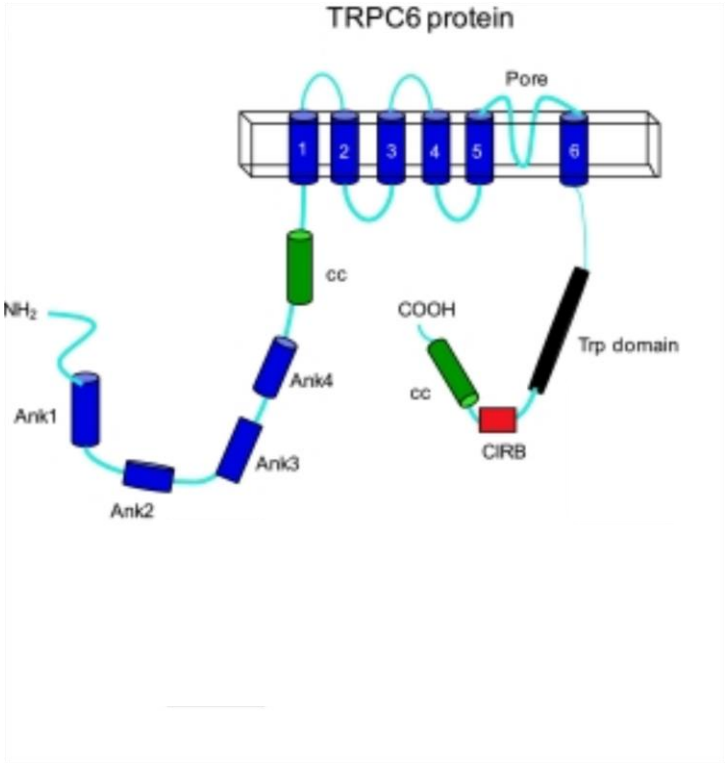

Figure 1.10 Schematic representation of the TRPC6 domain structure. Human disease-causing mutations known to cause FSGS are found in both the amino- and carboxy-domains and indicated in boxes. Reproduced from Dryer and Reiser [99]

There is around 65% of identity between TRPC4 and TRPC5, while TRPC1 and TRPC2 are almost unique [100]. TRPC6, a member of the canonical TRPC subfamily, is a receptor-operated channel leading to the influx of calcium [96]. Although all TRPC subfamily members respond to phospholipase C (PLC) signals, TRPC3, 6 and 7 share around 70-80% identity at the amino acid level and have been grouped together due to the ability to heteromerize with each other and their diacylglycerol (DAG)-sensitivity [100].

Winn *et al*. were the first to identify a point mutation in the *TRPC6* gene in a large family with autosomal dominant FSGS [101]. To date, there are 10 disease-causing mutation identified in human *TRPC6* gene shown in Figure 1.10, some of which are gain-of-function mutations resulting in an elevated influx of Ca^{2+} into the cells, while the others lead to longer opening channel function, once activated [101]. Interestingly, patients with mutations in the *TRPC6* gene present with FSGS with no other pathological phenotype observed, even though TRPC6 is widely expressed in variety of tissues. One possible explanation for this is that TRPC6 plays an essential role in the assembly of the filtration slit or the structure is highly susceptible to even slight changes in Ca^{2+} dynamics [99].

This prompted further research to study the renal expression of TRPC6. TRPC6 is broadly expressed throughout the kidney in tubules and glomeruli. However, most of the TRPC6 expression is confined to podocytes, where it localizes within both major processes and foot processes, and to the slit diaphragm [102]. Interestingly, TRPC6 expression was also detected in glomerular endothelial cells [102]. The precise role of TRPC6 in the podocyte is still unknown, but it is thought to be involved in mechanosensory events at the slit diaphragm or in signalling to the actin cytoskeleton via calcium-dependent pathways [103]. TRPC6 channels can interact with podocin and nephrin at least in cultured podocytes, and these interactions are likely to be key for the maintenance of these channels at the filtration slits [104]. Podocin was demonstrated to control the activity of TRPC6 in a cholesterol-dependent fashion, where podocin interacts with and alters the lipid microenvironment around the channel, thus leading to its activation in response to deformation of the plasma membrane [105], [99]. Moreover, TRPC6 was shown to interact with nephrin at or near the slit diaphragm, where this interaction is believed to regulate the gating and trafficking function of the channel [88]. This interaction is able to sense mechanical stimuli, which further activates Ca^{2+} signalling cascades leading to alterations in cytoskeletal dynamics of podocytes [99]. For example, nephrin ectodomain engagement leads to local activation of Src kinases, such as Fyn, which in turn results in tyrosine phosphorylation of the TRPC6 channel and an increase in its activity, thus altering the cytoskeletal dynamics [88], [106]. Furthermore, it has been shown that overexpression of TRPC6 in cultured podocytes results in the loss of actin stress fibres, leading to rearrangement of the podocyte actin cytoskeleton [107]. A similar outcome was observed in neonatal nephrin knockout mice [102]. Altogether, there is some evidence to propose that TRPC6 channel activity at the slit diaphragm of the podocyte is needed for controlled regulation of podocyte structure and function.

1.4.4 Inverted formin 2 (INF2)

While mutations in the *TRPC6* gene are best characterized as causes of familial FSGS, in recent years more candidate genes, such as *INF2*, have been reported. The *INF2* gene encodes protein INF2, a member of the formin family of actin-regulatory proteins. INF2 is highly expressed in the kidney as well as in glomerular podocytes, which are believed to initiate the majority of forms of FSGS.

Similar to other formin family members, INF2 is composed of an N-terminal diaphanous inhibitory domain (DID), and a C-terminal diaphanous autoregulatory domain (DAD) and formin homology domains (FH1 and FH2) [108]. Additionally, the N-terminal part generally has a regulatory function and includes an overlapping Rho binding domain, while the C-terminal DAD domain can also act as a monomeric G-actin binding Wiskott-Aldrich syndrome homology region 2, known as WH2 domain [109]. The mammalian formin INF2 has a unique biochemical feature, it is able to accelerate polymerisation and depolymerisation of actin *in vitro*, and it displays ER and cytoplasmic localizations in podocytes [108]. This dual catalytic activity is dependent on both the FH2 and WH2 acting in pair [108]. Mutations in the *INF2* gene were first identified by Brown *et al.* in 11 unrelated families with FSGS [62]. The described disease-causing *INF2* mutations were all found to be located within the DID, an autoinhibitory domain, and they all caused non-conservative substitutions in highly conserved amino acid residues. The DID domain binds the DAD domain of INF2, which results in autoinhibition of INF2-mediated actin depolymerisation [108]. Interestingly, FSGS-associated mutations, such as E184K and R218Q, in the DID domain were shown to alter INF2 and F-actin localization in transfected podocytes, while they didn't prevent INF2-mediated accumulation of actin filaments [62]. The finding that mutations in the podocyte-specific formin INF2 cause FSGS demonstrates that the precise regulation of actin polymerisation is essential for proper podocyte function.

1.4.5 Podocin

Podocin is the protein product of the *NPHS2* gene that is mutated in a subset of patients with autosomal recessive SRNS, which manifests as early childhood onset of proteinuria, fast progression to ESRN and FSGS [69]. Podocin is a 42 kDa podocyte specific integral membrane protein, and is a member of the stomatin family of proteins [69]. Using the positional cloning approach in 2000, the human *NHSP2* gene was found to be located on

chromosome 1q25-q31 and specifically expressed in the podocytes of developing and mature glomeruli [69]. Using *in situ* hybridization and immunohistochemistry methods, the expression profile of podocin has been studied both during human embryogenesis and kidney maturation, and in the podocytes [110]. Podocin was initially detected in human embryos at 5 weeks of gestation, which represent the earliest developmental phase studied [110]. The *NPHS2* transcript was not found in any embryonic structures apart from the mesonephros, or more specifically it was expressed in the mesonephric future podocytes from the S-shaped body and in the presumptive podocytes of metanephric kidneys at a later stage [110]. Interestingly, podocin protein was only detected much later than the transcript. Podocin expression is elevated throughout glomerular development and remains high in podocytes of mature kidneys [110].

In podocytes, podocin is exclusively localized to the slit diaphragm, where it is involved in mechanotransduction events [104]. This crucial localization of podocin to the slit diaphragm is underscored by the fact that mice lacking podocin present with massive proteinuria, foot process effacement and absence of slit diaphragms [111]. Similar to all stomatin-like proteins, podocin is an integral protein of 383 amino acids consisting of an N-terminal domain, a short membrane domain and a C-terminal domain. Podocin has a unique topology with a single membrane domain forming a hairpin-like structure due to both the N- and C-terminal tails facing the cytoplasmic side of the slit diaphragm (Figure 1.11) [112]. It also has a single hydrophobic domain, which embeds podocin into the inner leaflet of the lipid bilayer, and the prohibitin homology (PHB) domain that facilitates podocin binding to cholesterol in the PM and acts as a lipid recognition motif [105]. This binding results in cholesterol being recruited to the TRPC6 ion channel complex at the slit diaphragm, which, in turn, suggests that podocin binds and mediates TRPC6 mechanosensory activity [103]. It has been demonstrated that podocin reduces mechanosensitivity of TRPC6 channels, so a failure of podocin to function correctly leads to hyperactivation of the TRPC6 channels at the slit diaphragm [113]. Therefore, mutations in genes encoding either podocin or TRPC6 could lead to severe glomerular diseases due to possible Ca^{2+} overflow. Interestingly, podocin oligomerises into clusters, and nephrin molecules assemble at the slit diaphragm, where CD2AP acts as an adapter to connect the entire structure. The presence of the intact podocin at the slit diaphragm is essential for the recruitment of nephrin to the plasma membrane and for podocyte intracellular signalling as a whole [114].

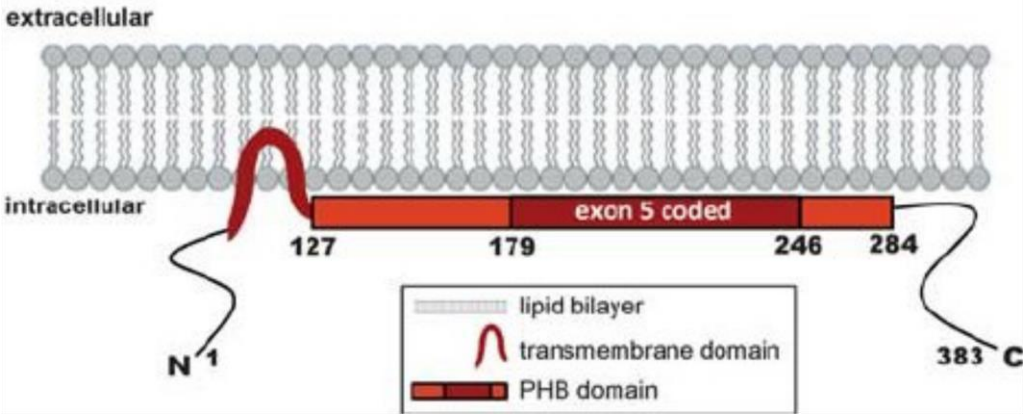

Figure 1.11 Schematic representation of membrane orientation of podocin. A single membrane domain forms a hairpin-like structure with both the N- and C-terminal tails facing the cytoplasmic side of the slit diaphragm. Podocin also contains a single hydrophobic domain and PHB domain. Adapted from Relle *et al* [115].

Multiple experimental studies show that podocin in its oligomeric form localizes to lipid raft microdomains in the slit diaphragm, where it recruits and colocalizes with nephrin. As mentioned previously, the slit diaphragm of podocytes is essential for the correct function of the GFB and is assembled in lipid rafts. These are highly dynamic specialized plasma membrane microdomains 10-200 nm in diameter enriched in glycosphingolipids, cholesterol and a number of signal transduction molecules, which are found in all eukaryotic cells (Figure 1.12) [116]. In comparison with the rest of the plasma membrane, there is 5-8-fold increase in cholesterol in lipid rafts, which is able to interact with glycosphingolipids via its hydrophobic side chains [117]. Therefore, having such a unique lipid composition, rafts have been suggested to function in many cellular processes, such as polarized sorting of membrane proteins, endocytosis and signal transduction [116].

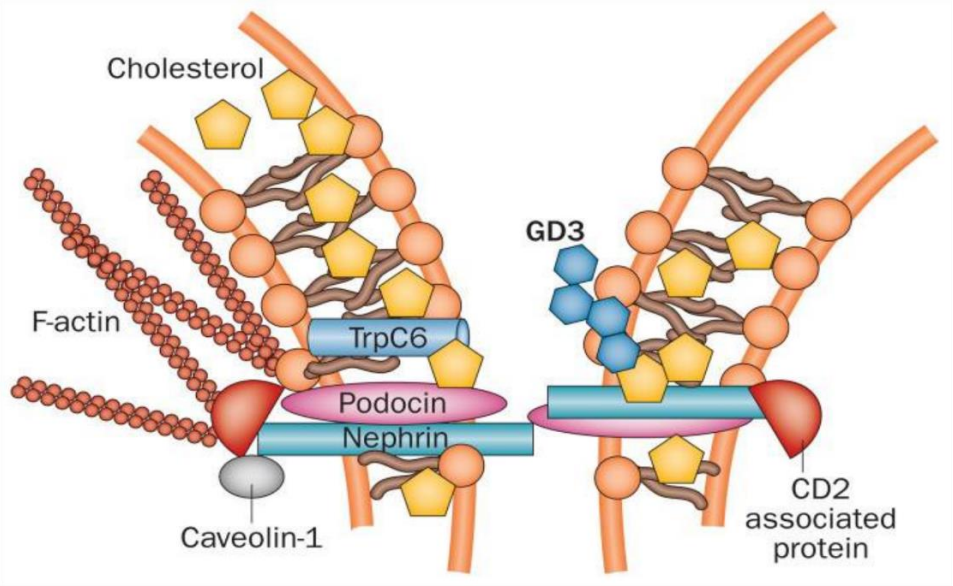

Figure 1.12 Lipid rafts structure in the slit diaphragm. Podocin contains PHB domain that allows binding to cholesterol leading to the assembly of multiprotein complexes, such as between podocin, nephrin and TRPC6. Different lipids are highlighted in various shades of orange. Reproduced from Fornoni *et al* [118].

Lipid raft targeting of nephrin enhances its signalling activity from the slit diaphragm, which results in regulation of the podocyte actin cytoskeleton and glomerular permselectivity. Thus, it has been suggested that disease-causing podocin mutants might still colocalize with nephrin, but fail to target it to lipid rafts either because they cannot be intracellularly trafficked to the PM or they get to the PM, but are not recruited into rafts [119]. Apart from strong functional interaction between podocin and nephrin, podocin also binds CD2AP and TRPC6 via its C-terminus, demonstrating an important link between the slit diaphragm and the actin cytoskeleton [120]. Indeed, the complex formed allows for the attachment of the slit diaphragm to the actin filaments, therefore embedding the complex into the lateral part of the podocytic plasma membrane [121]. Taken together, podocin serves as a scaffolding protein involved in the organization of the SD complex and the mediation of its filtration function [122].

1.4.5.1 Disease-causing podocin mutation R138Q

Nowadays, genetic causes of SRNS are being progressively acknowledged. Mutations in the *NPHS2* gene were first reported in children with autosomal-recessive SRNS and FSGS, followed by sporadic childhood and adult-onset SRNS cases. As stated before, mutations in podocin result in the dysfunction of the GFB with the variable age of onset and FSGS being prevalent on the renal histology. Patients with homozygous or compound

heterozygous mutations usually develop SRNS before 6 years of age that in the majority of paediatric cases rapidly progresses to ESRD with an extremely low frequency of recurrence after renal transplantation [120]. Late-onset patients are considered to be over 18 years of age and found to inherit a mutation and a non-neutral polymorphism, meaning that a variant is relatively common and doesn't cause a disease until in a combination with a certain mutation [123]. Interestingly, both N- and C-terminal cytoplasmic tails of the podocin may be affected by the mutations, which include loss-of-function mutations, along with missense changes [124].

Indeed, missense mutations appear to represent the largest group of *NPHS2* mutations accounting for 42 % of a total of the 126 mutations of *NPHS2* reported to date [120]. The most frequent mutation identified in 42 of 73 families with two pathogenic mutations is the p.R138Q (c.413G>A) mutation in exon 3 [125]. Paediatric patients carrying truncating mutations (nonsense or frameshift), or homozygous p.R138Q, present with a severe, early-onset from of SRNS, which is found in 98.2% of cases studied [125]. The replacement of arginine residue at position 138, which is highly conserved amongst the stomatin-like family of proteins and is crucial for podocin function, with glutamine results in podocin with the R138Q mutation [69]. Functional data have shown that this protein is retained in the endoplasmic reticulum (ER) and loses its ability to target nephrin to lipid raft microdomains, therefore augmenting its signalling [119]. By screening the patient database, Roselli *et al.* found that patients with mutations resulting in podocin being accumulated in the ER had a more severe phenotype with an early-onset form of SRNS, than patients where podocin mutants were correctly targeted to the PM [126]. Taken together, these findings suggest that podocin is intracellularly trafficked to the PM via the classical ER/Golgi pathway. However, much of the work on podocin trafficking and binding partners has been done in transfected HEK293 cells rather than in the actual cells that express podocin physiologically, ie. the kidney podocyte.

1.5 Hypothesis

Proper assembly of the slit diaphragm at the plasma membrane is crucial for the functioning of the glomerular filtration barrier. Podocin is a scaffolding protein, essential for the correct trafficking and recruitment of other proteins to lipid microdomains at the plasma membrane. Mutations, such as R138Q, which lead to mislocalization of podocin, result in disruption in the assembly of this specialized protein complex resulting in disease.

Therefore, understanding podocin trafficking and interactions could lead to new therapeutic targets for NS.

1.6 Overall Aims

The mechanism and effects of the intracellular retention of the podocin R138Q mutant have been previously studied in HEK293 cells, but not in **its bona fide cell type**, the podocyte. Furthermore, a key aim of glomerular research is to discover small molecules that correct this trafficking defect. Understanding this process, and how it is affected in the disease state is important to dissect. The overall aim of this work is to:

- Create a conditional knock-in mouse model of the R140Q mutation
- Describe the role of intracellular filaments on the ER retention of the mutant protein
- Test a novel compound c407, which has shown promise in treating protein mistrafficking diseases, both *in vitro* and *in vivo* on podocin R138Q trafficking
- Identify new genes mutated in NS
- Identify novel binding partners of podocin

Chapter 2: Materials and Methods *In Vitro*

2.1 Materials

All the laboratory reagents were of the highest quality and purity and purchased from Sigma Aldrich unless otherwise specifies in the text or Appendix 1. Appendix 1 also contains list of solutions used, cell culture and cell extraction reagents.

2.2 Cell lines

The wild-type and R138Q podocin mutant conditionally immortalized human podocyte cell lines were developed at Bristol Renal Unit by transduction with the temperature-sensitive *SV40-T* transgene as previously described [127]. These cells can proliferate at the permissive temperature of 33°C, and thereafter they can be transferred to the nonpermissive temperature of 37°C, where the cells enter growth arrest and show key characteristics of podocyte differentiation and function. The wild-type podocyte cell line is referred to as WT, while the podocin mutant podocyte cell line is called PM. The wild-type and R138Q GFP-tagged immortalized human podocyte cell lines were created using PCR-based molecular cloning approach and used in experiments, where stated (These cell lines were established during my previous MRes project).

All cells were grown and maintained in CO_2 incubators with a temperature of 33°C/37°C, 5% CO_2 concentration and 95% relative humidity. All cell work was performed in aseptic conditions in a class two biological safety hood. Cell culture media was changed every 3-4 days.

2.2.1 Podocytes

All human conditionally immortalised podocyte cell lines were grown in RPMI 1640 media with supplements as detailed in Appendix. Cells were cultured at 33°C until 70% confluent, and then switched to 37°C for 10-14 days differentiation. All podocyte cell lines were cultured under sterile conditions in tissue culture vessels including T175cm^2, T75cm^2 and T25cm^2 flasks, and 6 well plates. For immunofluorescence cells were grown as described above either on glass coverslips in 6 well plates or in 6cm^2 glass bottom dishes.

2.2.2 Human Embryonic Kidney (HEK) cells

HEK 293 cells were used predominantly for virus transfection reactions. Cells were cultured in DMEM x1 plus Glutamax with 10% FBS (see Appendix). Cells were grown at 37°C without thermoswitching and used for experimentation within 24-48 hours after seeding.

2.2.3 Cell Passage

Stock flasks of proliferating cells were maintained under an atmosphere of 5% (v/v) CO_2 and 95% air at the permissive temperature of 33°C for podocytes and at 37°C for HEK 293 cells. Cells were grown to the desired confluency (70%-90%) and sub-cultured to maintain them at a logarithmic growth rate. For sub-culturing, growth medium was removed, and the adherent cells were washed with 1ml sterile trypsin. The cells were detached from the flask by mild tryptic digestion using 0.5 ml 0.25% Trypsin-EDTA and incubation at 37°C for 3-5 mins. The cells were then resuspended in the appropriate growth medium and aliquoted into fresh tissue culture flasks or dishes. Each time the cells were split, a consecutive passage number was assigned. Passages 13 to 22 were used for experiments. Similar growth rate and cell size were observed between WT and mutant podocytes.

2.2.4 Cryopreservation

To maintain stocks, cells were periodically frozen down, especially at lower passages. Cells were frozen down in a serum rich version of the appropriate cell media containing dimethyl sulphoxide (DMSO) as detailed in Appendix. Cells were stored at a high density in cryovials (Nalgene #5100-0001) to ensure their recovery. The cryovials were placed in a Mr Frosty™ Freezing Container (Thermo Scientific #5100-0001) at -80°C, which ensures the 1°C per minute cooling rate that is essential for successful cryopreservation of cells. Cells were then placed into liquid nitrogen containers for long-term storage.

2.3 Cell Treatments

2.3.1 NSC407882 compound treatments

Compound 407882 was a kind gift from Prof. Aleksander Edelman (Paris, INSERM) and was described previously [128]. 50mM stock of 407882 was prepared in 50mM NaOH and stored for one week at 4°C. To test the effect of the drug on R138Q podocin trafficking

and function, differentiated human podocytes were treated with 10μM 407882 for 24h, 48h and 72h. The concentration was chosen based on the work done in CF field. For simplicity, compound 407882 was referred to as c407 in this manuscript.

2.4 Adhesion Assay

Cell adhesion assays are widely used to assess the adhesion properties of many cell types, for example epithelial cells to the extracellular matrix, other cells, or specially coated surfaces. In addition, this type of assay can be used to determine the effects of various treatments, such as pharmacological compounds and small molecules, on the ability of cells to adhere. An adapted cell adhesion assay protocol is detailed here for studying the adhesion characteristics of human podocytes *in vitro*. Podocytes were grown in a T75cm^2 flask and differentiated at 37^{o}C for 10-14 days. When fully differentiated, cells were trypsinised with 0.025% trypsin/EDTA for 5 min at 37^{o}C. Podocytes were then resuspended in cell culture media to stop enzyme activity and collected in a 15ml falcon. Cells were centrifuged for 5 min at 1000 g, and then gently resuspended in 1 ml of cell media. 10-15μl of cells with trypan blue were pipetted onto the disposable slide and counted with the Luna-FL™ automated cell counter. Podocytes were again resuspended to a concentration of 5x10^5/ml in cell media. Cells were allowed to recover from trypsinisation in an upright falcon tube with the lid off at 37^{o}C for 10 min. 50μl of PBS and 50μl of cells were added to each well of a 96 well plate. Three experimental wells were assigned as the 100% attachment control, to which 20%, 50% and 100% of the total volume of cells were added. Cells were left to adhere for 45 min at 37^{o}C. Control wells for 100% attachment were fixed with 100 μl 4% PFA for 20 min at room temperature. Thereafter, the plate was tapped to remove lose and non-adherent podocytes, and washed twice with 100 μl PBS, and the experimental wells were then fixed with 100 μl 4% PFA for 20 min (note that the 100% attachment wells were not washed). The PFA was then washed off three times with 100μl of distilled water, and cells were stained 100μl 0.1% crystal violet in 2% ethanol for 60 minutes at room temperature. Crystal violet was also added to three empty wells in order to measure binding of the dye to the plastic as a control. Crystal violet was removed, and wells were washed 3 times with 400μl of distilled water. 100μl of 10% acetic acid was added to each well to solubilise the dye. A 96 well plate was incubated on an orbital shaker at 150rpm for 5 minutes at room temperature. Absorbance of the plate was measured at 570nM in a plate reader. Results were

expressed as a percentage of 100% attachment and normalised against the adhesion of the human wild type podocytes cell line.

2.5 Quantitative Polymerase Chain Reaction

To determine gene expression levels in human podocytes, quantitative polymerase chain reaction (qPCR) was used, in which the quantity and quality of PCR product can be detected in real-time.

2.5.1 RNA Extraction

Podocytes were grown in 6-well plates and differentiated for 10-14 days before treatment and RNA isolation. Total RNA was also extracted from the untreated cells. The RNeasy Mini Kit (Qiagen) was used to purify high-quality RNA from cells. The manufacturer's instructions were followed throughout the entire procedure. First, media was removed from wells, and 350µl of RLT buffer was added to each well to lyse the cells. Lysates were then harvested and centrifuged for 3 min at maximum speed to fully homogenize the cells. The supernatant was carefully removed, and 350µl of 70% ethanol was added to the samples and mixed well by pipetting. 700µl of each sample was then transferred to individual RNeasy mini columns and centrifuged for 15 s at 9000 x g. The flow-through was discarded, and 700µl of RW1 buffer was added to the columns. The columns were then centrifuged for 15 s at 9000 x g, and the flow-through was discarded again. Next, 500µl of RPE buffer was added to the columns twice, followed by the centrifugation steps for 15 s or 2 min at 9000 x g. The RNeasy columns were transferred to fresh 2ml collection tubes and centrifuged for 1 min at full speed to dry the membrane. All buffers used were provided as undisclosed solutions by the manufacturer. The RNeasy spin columns were finally placed into new 1.5ml collection tubes, and 30µl of RNase-free water was added directly to the membrane of each spin column. The columns were then centrifuged for 1 min at 8000 x g to elute the total RNA. Total RNA concentration was measured using a NanoDrop Spectrophotometer, and the values, as well as 280nm/260nm and 260nm/230nm values, were noted. RNA was then stored at -80˚C until required. The same protocol was used for whole kidney samples.

2.5.2 RNA to complementary DNA

Eluted RNA was converted to single-stranded complementary DNA (cDNA) using the High Capacity RNA-to-cDNA™ Kit (ThermoFisher Scientific #4387406) as per manufacturer's protocol. Briefly, 1µg of total RNA was used per 20µl reaction. RNA sample was diluted in the appropriate volume of DNase/RNase free water and made up to 9µl. 10µl of reverse transcription (RT) buffer mix and 1µl of RT enzyme mix was added to each sample. Tubes were briefly centrifuged to spin down the contents, before being placed in the Labcycler thermocycler (Sensoquest) to start the reverse transcription reaction. The reaction consisted of the following steps: incubation at 37˚C for 1h; heating to 95˚C for 5 mins; cooling down to 4˚C. Neat cDNA was then stored at -20˚C until required.

2.5.3 96-well qPCR

Human primer sequences for qPCR were obtained from a public resource for PCR primers, called PrimerBank (see Appendix). Primers were custom ordered from Eurofins and diluted to a concentration of 10µM in nuclease-free water to use in qPCR reactions. Each primer pair used for qPCR was initially optimised by performing serial cDNA dilutions of untreated cells. A 4-point standard curve with 10-fold dilutions for every new primer pair was then created, and R^2 value was calculated (Figure 2.1). This allowed to determine the linear range of each reaction and the working concentration of cDNA template for definitive experiments.

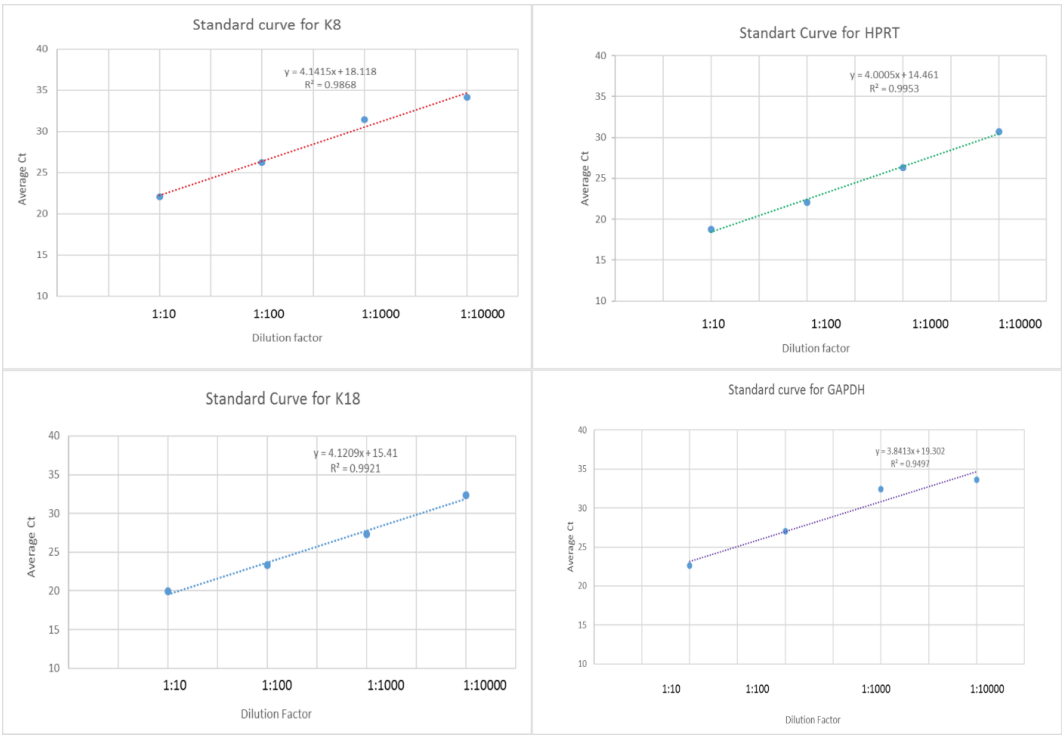

Figure 2.1 Standard Curves. Each primer pair was first optimized by performing serial cDNA dilutions of untreated cells.

QPCR was then performed using Fast SYBR® Green Real-Time PCR Master Mix as per manufacturer's instructions. Each reaction consisted of the following components: 5.5µl of SYBR Green Fast, 0.36µl of forward (F) and reverse (R) primers, and 2µl of diluted cDNA. Each cDNA sample was loaded in triplicate. GAPDH and HPRT were used as housekeeping genes, allowing samples to be compared directly. Plates were sealed with plastic plate sealers and briefly centrifuged to bring down all the contents. QPCR was performed using protocol shown in Table 2.1 on the StepOnePlus Real-Time PCR system (Applied Biosystem) with the StepOne Software v2.1. The melt curves for each PCR reaction were reviewed, and the single peaks were identified (Figure 2.2).

Stage	**Temperature (ºC)**	**Time**	**Number of Cycles**
Holding	95	10 minutes	1

Cycling	95	15 seconds	40
	60	60 seconds	
Melt curve	95	15 seconds	1
	65	60 seconds	
	95	15 seconds	

Table 2.1 QPCR reaction parameters.

Keratin 8

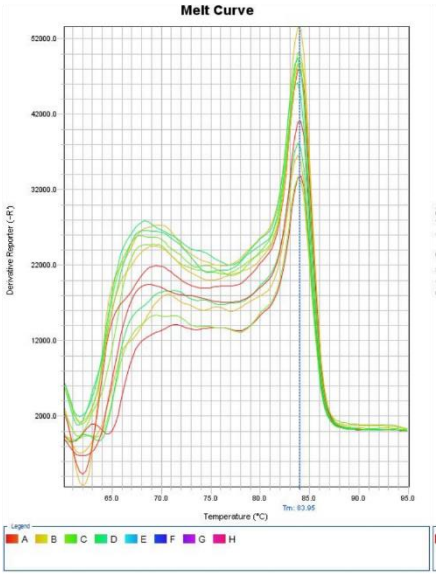

Keratin 18

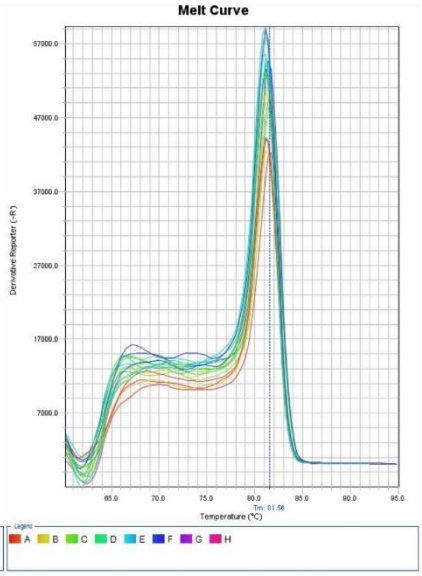

GAPDH

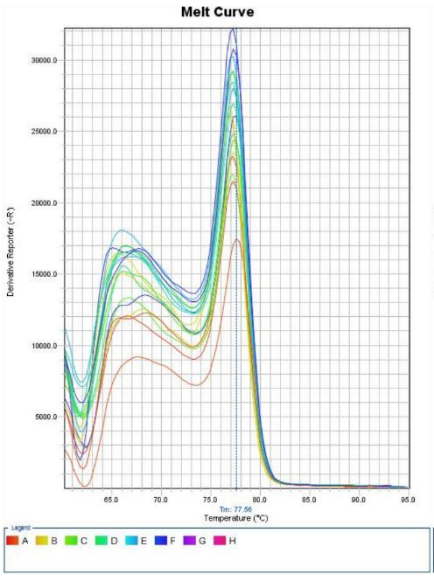

HPRT

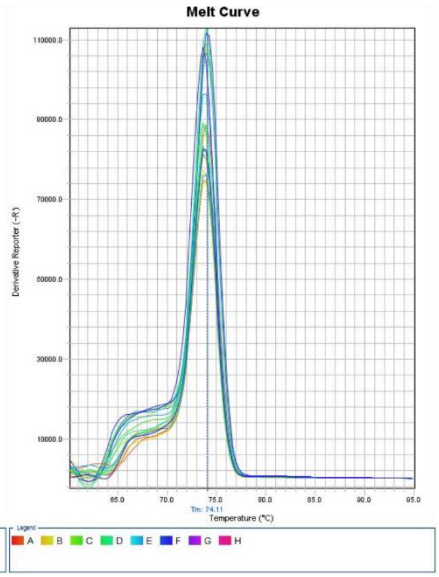

Figure 2.2 Melt curves from qPCR. The single peak indicates that the cycle thresholds are specific to the product of interest.

2.5.4 qPCR analysis

The comparative delta delta Ct method was used to analyse results from QPCR.

2.6 Protein Extraction

2.6.1 Whole Cell lysates

Cells cultured under sterile conditions were placed on ice and washed twice with ice cold phosphate buffered saline (PBS) (approximately 6 mL per T75cm^2 flask). As much PBS as possible was removed after the second wash to prevent dilution of the sample. 500µl of NP40 lysis buffer per T75cm^2 flask was then added directly to cells. The lysis buffer contains a detergent to lyse the cells and a protease inhibitor cocktail. Cells were scraped off the flasks using a cell scraper, and the cell/lysis buffer mixtures were transferred to a 1.5mL microfuge tubes and left on ice for 5 mins. Lysates were cleared by centrifugation at 13,000g (Beckman GS-15R) at 4°C for 10 mins. The supernatants containing cellular proteins were collected and transferred to fresh microfuge tubes. Samples were snap frozen in liquid nitrogen and stored at -80°C until required.

2.6.2 GFP-Trap_A for Immunoprecipitation of GFP-Fusion Proteins

For immunoprecipitation reactions podocytes stably expressing a GFP-tagged protein of interest were grown in T75 cm^2 tissue culture flasks. All steps were performed on ice, and the centrifuge was pre-cooled to 4°C. To harvest cells, growth medium was aspirated, and cells were washed twice with ice-cold PBS, and then scraped off the flask with ice-cold NP-40 lysis buffer. Cells were transferred to a 1.5 mL microfuge tubes and placed on ice for 10 mins with extensive pipetting every 5 mins. Cell lysates were then centrifuged for 10 mins at 13,000g at 4°C on a lab top centrifuge. The lysate-supernatants were transferred to fresh pre-cooled tubes, and pellets were discarded. Whole cell lysates were taken out and snap frozen at this point for long-term storage at -80°C or for use later. 25µl of GFP-Trap® _A (Chromotek) beads were added to the lysate-supernatant samples and incubated for an hour at 4°C under constant mixing. Samples were then spun down at 3,000g for 1 min at 4°C. Beads were washed three times with 500µl ice-cold wash buffer. Following washes, beads were resuspended in 4x SDS-sample buffer. Resuspended

beads were boiled for 10 mins at 95°C to dissociate the immunocomplexes from the beads. The beads were then recollected by a quick centrifugation at 3,000g, and SDS-PAGE was performed with supernatants and whole cell lysates from the step above.

2.6.3 Co-immunoprecipitation of Endogenous Protein

Podocytes were grown in T175cm^2 tissue culture flasks. 25μl of A/G PLUS-Agarose beads (Santa Cruz #sc-2003) were washed twice in 200μl of TNE buffer and centrifuged for 1 min at 3300g to equilibrate the beads. For co-immunoprecipitation, A/G PLUS-Agarose beads were combined with 5μg of the mouse K8 monoclonal antibody or mouse IgG (Santa Cruz #sc2025) and mixed with 200μl of TNE buffer, and left on a rotator wheel at 25rpm overnight at 4°C.

The following day the conjugated beads were washed in 500μl of TNE buffer and spun at 3300g for 1 min four times to remove unbound antibody and to equilibrate the beads. Cells were washed twice with ice-cold PBS and then scraped into 2ml of NP-40 immunoprecipitation buffer containing protease inhibitor cocktail. All reactions were kept on ice. Lysates were then centrifuged at 13,000g for 10 mins at 4°C. An aliquot of the whole cell lysate was taken out and kept for Western blotting. The remaining supernatants were transferred to fresh tubes, and the lysates were cleared with 20μl of agarose beads and BSA to 1% for an hour with constant mixing. The beads were then pelleted at 2000g for 1 min, and the lysates were incubated with agarose beads coupled to the K8 monoclonal antibody or IgG for 4 hours on a rotating wheel at 4°C. Samples were then washed four times with TNE buffer and resuspended in SDS sample buffer. Proteins were eluted by boiling the samples for 10 mins and stored at -80°C or used immediately in Western Blotting to be probed with podocin antibody.

2.7 SDS-PAGE and Western Blotting

2.7.1 SDS-PAGE 1D gel electrophoresis

Proteins samples were defrosted from -80˚C and separated on sodium dodecyl sulfate-polyacrylamide (SDS-PAGE) gels. Protein extraction samples mixed with 4x SDS sample buffer were first denatured to unfold the protein's tertiary structure by boiling in a hot block at 95°C for 10 mins. 20-30μl of sample per well and 3.5 μl of BLUeye prestained protein ladder (Geneflow #S6-0024) were applied to 7-15% gels, and proteins were

separated at a constant voltage of 150 V in 1 x running buffer for 70-90 mins using a BIO-RAD PowerPac, or until the visible dye front had reached the bottom of the gel. The resolving gel was prepared using the appropriate acrylamide percentage for the molecular weight of the proteins being analyzed.

2.7.2 Western Blotting

Following SDS-PAGE, proteins were electrophoretically transferred onto gel-sized polyvinylidene fluoride (PVDF) membrane using a wet transfer method with Biorad Mini Protean II blotting apparatus. Prior to transfer, the PVDF membrane was soaked in 100% methanol for 5 mins in order to remove its hydrophobic coating, so that proteins can transfer from the gel to the membrane. Proteins were transferred at a constant current of 250 mA in 1 x transfer buffer for 60-90 mins depending on the size of the protein of interest. Higher molecular weight proteins take longer to migrate from the gel to the membrane. After the transfer was complete, membranes were 'blocked' in 5% BSA made up in Tris-buffered saline with 0.1% Tween-20 (TBS-T) for 1 h at room temperature with constant agitation. Following blocking, transfer membranes were incubated with primary antibodies against the protein of interest overnight at 4°C with constant agitation. Primary antibodies were made up in 3 % BSA at suitable dilutions.

After overnight incubation, membranes were washed 5 times every 5 mins in 1x TBS-T to remove any unbound primary antibodies. Following washes, horseradish peroxidase (HRP)-conjugated secondary antibodies (1:5000 in 3% BSA) selected against the species of the primary ones were added, and membranes were incubated for 1 h at room temperature on a rocking platform. When specified by manufacture's guideline, non-milk fat powder was used instead of BSA.

2.7.3 Chemiluminescence and Imaging

Membranes were washed again 5 times every 5 mins in 1x TBS-T to remove unbound secondary antibodies. The antibody bound to the membrane was detected using SuperSignal west femto maximum sensitivity substrate. Femto peroxide is the substrate that recognizes the peroxidase linked to the secondary antibody, while the luminol enhances the signal. Images were developed using Amersham Imager 600 system.

2.7.4 Densitometry

Western blots were analyzed using ImageJ software (imagej.nih.gov/ij) that allows the protein band densities to be calculated. The protein of interest was normalized to GAPDH/total protein, which served as a loading control. All experiments were performed three times to allow for the statistical analysis.

2.8 Immunofluorescence

2.8.1 Confocal Laser Scanning Microscopy

To understand the trafficking of R138Q mutant podocin, and how this is affected by c407 treatment, a detailed analysis of the localization of GFP-tagged wild-type and mutant podocin construct was carried out. Podocytes were cultured on glass coverslips placed into the six-well plates, as described above. Media was removed, and cells were washed twice with 2mL of PBS to remove residual paraformaldehyde and fixed with 1.5mL of 4% paraformaldehyde/ Ca^{+2}/Mg^{+2} in PBS at room temperature (RT) for 20 mins. This step fixes the cells by cross-linking proteins together. The coverslips were then washed 3 times with 2mL PBS for 5 mins, before adding 60µl of 1M glycine pH 8.5 to each well during the second wash to neutralize any residual crosslinking. Cells were then permeabilized with 2mL of 0.1 % Triton X-100 in PBS for 5 mins at room temperature and washed again 3 times with 2mL PBS for 5 mins. Next, cells were blocked in 3 % BSA in PBS for 30 mins at RT to inhibit non-specific binding sites, followed by incubation with primary antibody at the appropriate dilution in 3% BSA for an hour at RT. Cells were then washed 3 times with 2mL PBS, removing as much liquid as possible after the third wash, prior to addition of secondary antibody. Species specific Alexa Fluor secondary antibody and Alexa Flour phalloidin have been applied for another hour of incubation at RT. Cells were then washed 3 times in PBS followed by a final wash in MilliQ water to remove the PBS salts, and mounted on glass microscope slides using VECTASHIELD® HardSet Mounting Medium with DAPI (Vector Laboratories #H-1500). Slides were left in darkness at RT overnight to set. Coverslips were visualized at the Wolfson Bioimaging Facility (University of Bristol) using Leica SP5-AOBS confocal laser scanning microscope attached to a Leica DM I6000 inverted epifluorescence microscope at 63x magnification.

2.8.2 TIRF Microscopy

To further understand the function of podocin at the plasma membrane, total internal reflection fluorescence microscopy (TIRFM) was used to investigate podocin trafficking/localization at or near the plasma membrane in more detail (Figure 2.3). Podocytes were grown in imaging dishes with glass bottom. Following washes, cells were fixed with 1.5mL of 4% paraformaldehyde/ Ca^{+2}/Mg^{+2} in PBS at room temperature (RT) for 20 mins, washed twice in PBS, and then permeabilized with 2mL of 0.1 % Triton X-100 in PBS at room temperature for 5 mins. Cells were then washed 3 times in PBS followed by 30-minute blocking in 3% BSA in PBS. Next cells were incubated with primary antibody at the appropriate dilution in 3% BSA for an hour at RT. Following further washes, species specific Alexa Fluor secondary antibodies were applied directly to the TIRF dish for another hour of incubation at RT. Cells were then washed 3 times in PBS, and dishes were left in PBS at 4°C. Cells were imaged at the Wolfson Bioimaging Facility (University of Bristol) using the Leica AM TIRF MC System for total reflection fluorescence microscopy. The system is linked to a Leica DMI 6000 inverted epifluorescence microscope with a Hamamatsu C9100-13 back-thinned EM-CCD camera.

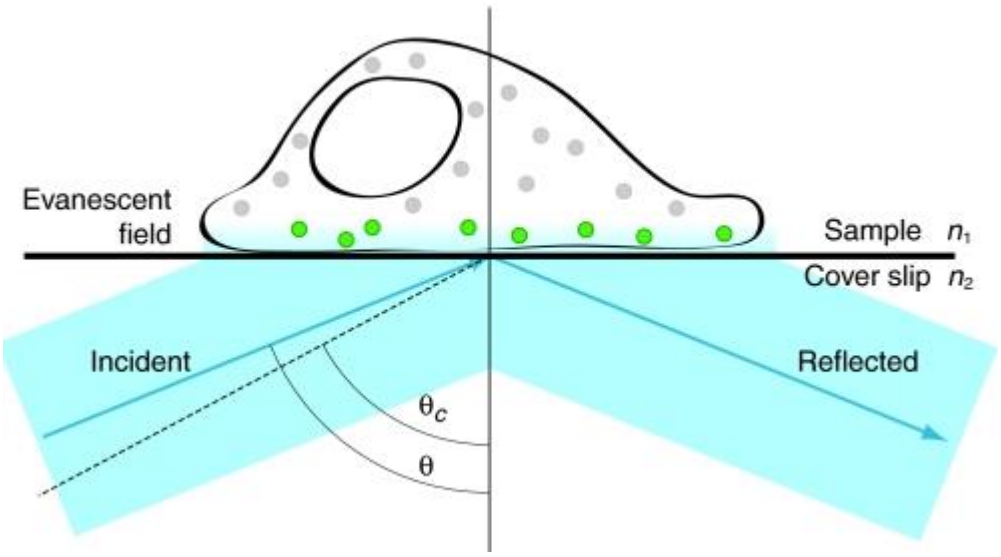

Figure 2.3 TIRF Microscopy. Schematic illustration of TIRF microscopy, where the excitation (incident) beam enters the cell surface at a greater angle than the critical angle (θ_c), causing the activation of the fluorophores at the plasma membrane. This allows imaging of the plasma membrane in more detail, when compared to traditional epifluorescence microscopy. Image taken from Mattheyses *et al* [129].

2.9 Lipid Raft Isolation

2.9.1 Detergent-resistant Membrane Isolation

Cells were cultured to 80% confluency in T175cm^2 flasks before being thermoswitched for 12-day differentiation. Differentiated cells were placed on ice, washed twice with ice-cold PBS and scraped into 2ml of TNE (150 mM NaCl, 5 mM EDTA, 10 mM Tris-HCl, pH 7.4) +0.5% Triton X-100, before being homogenized through a 21-gauge needle. Cells were left on ice for 30 mins for the lysis reaction to occur. The lysates were then brought up to 40 % sucrose by adding 2ml of 80 % (w/v) sucrose in TNE buffer in a 12ml ultracentrifuge tube and pipetting the mixture efficiently. Sucrose step gradient was then performed with samples as following: 5 ml of 35 % (w/v) sucrose in TNE buffer was layered on top followed by 1ml each of 15% sucrose, 5% sucrose and TNE. The gradients were centrifuged at 34,000 rpm in a Sorval SW-40 swing out rotor for 18 hours at 4°C.

2.9.2 TCA protein precipitation

Following the centrifugal separation, 1ml fractions were taken from the top to the bottom of the gradient solution and allocated with fraction numbers. The lipid raft fractions containing the protein of interest are in Fr. No. 1 to No. 4, while non-lipid raft fractions are in Fr. No. 5 to No. 12 (Figure 2.4). The protein was precipitated by addition of 0.25 volume of 100% Trichloroacetic acid (TCA). Samples were incubated for 10 mins at 4°C, following the centrifugation at 14,000g for 5 mins. The supernatants were removed, leaving protein pellets intact. Pellets were then washed 3 times with 200µl ice-cold acetone. Following washes pellets were dried by placing tubes in 95°C heat block for 10 mins to drive off acetone. Fractions were resuspended in SDS-Sample buffer and boiled again for 10 mins at 95°C before loading samples onto polyacrylamide gel.

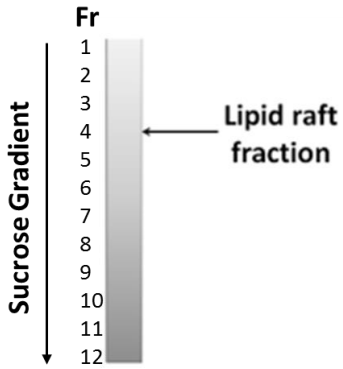

Figure 2.4 Isolation of detergent-resistant lipid rafts.

2.10 The Proximity Ligation Assay

To search for protein-protein interaction *in vitro*, the PLA was performed in podocytes using the Duolink™ kit (Eurogentec #DUO92191, Angers, France) according to manufacturer's instructions [130]. Both the number of spots and intensity were analysed.

Chapter 3: Materials and Methods *In Vivo*

3.1 Mouse model of R140Q podocin mutant

To test whether compound 407 can rescue mutant podocin localization *in vivo*, a transgenic mouse model was developed and characterized in Chapter 4. This mouse was designed to carry the R140Q mutation, the mouse analogue of human R138Q, on one allele and floxed WT *NPHS2* on the other, which can be excised upon induction with doxycycline.

3.1.1 UK Animal Care Declaration

All animals were handled in accordance with the University of Bristol and the UK Home Office guidelines and regulations. The following animal procedures were covered by Dr Becky Foster's project license (30/3048). Animals were culled according to the Home Office Code of Practice-The Humane Killing of Animals under Schedule 1 to the Animals (Scientific Procedures) Act 1986. A personal license (PIL 30/40748) was obtained in order to carry out all the regulated procedures on living animals and the following experiments described below.

3.2 Genotyping

Ear notches were received form Charles River Laboratories and digested in 100µl of 50mM NaOH at 95°C for 30-50 min to extract DNA. Prior to adding 20µl of 1M Tris-HCl (pH8) to neutralize each sample, samples were vortex and briefly centrifuged to spin down the contents. 2µl of each sample was used for the PCR reactions.

PCR was performed using PCRBIO HS Taq DNA Polymerase (PCR Biosystems Limited, London, UK) according to the manufacturer's protocol. Primers were custom ordered from Eurofins and diluted to a concentration of 10µM in nuclease-free water to use in 25µl reactions (Table 3.1). To check if the reaction had worked, 20µl of each PCR reaction was run out on a 2% agarose gel stained with SYBR™ Safe DNA Gel Stain (#S33102) (Figure 3.1).

The Pod-rtTA & TetO-Cre PCR reaction was carried out at the following parameters

Denaturation	95°C	1 minute	
Denaturation	94°C	45 seconds	
Annealing	51°C	45 seconds	38 Cycles
Extension	72°C	1 minute	
Final Extension	72°C	7 minutes	

The RG reporter PCR reaction was carried out at the following parameters

Denaturation	94°C	3 minutes	
Denaturation	94°C	30 seconds	
Annealing	61°C	1 minute	35 Cycles
Extension	72°C	1 minute	
Final Extension	72°C	2 minutes	

The NPHS2 flox PCR reaction was carried out at the following parameters

Denaturation	94°C	5 minutes	
Denaturation	94°C	30 seconds	
Annealing	62°C	45 seconds	40 Cycles
Extension	72°C	30 seconds	
Final Extension	72°C	7 minutes	

The R140Q PCR reaction was carried out at the following parameters

Denaturation	94°C	5 minutes	
Denaturation	94°C	45 seconds	
Annealing	52°C	45 seconds	35 Cycles
Extension	72°C	45 seconds	
Final Extension	72°C	10 minutes	

Gene	**Primer**	**Sequence**	**PCR product size**
NPHS2 flox	NPHS2 flox F	CCA GCA TCC CAT TAG ATA GAT GAG G	NPHS2 WT allele: 236bp NPHS2 floxed allele: 286bp
	NPHS2 flox R	GCA TCC AAA TGA TCA GAG TTC CCA GG	
Pod-rtTA	Pod-rtTA F	CGC ACT TCA GTT ACT TCA GGT CCT C	Positive band: 400bp
	Pod-rtTA R	GCT TAT GCC TGA TGT TGA TGA TGC	
TetO-Cre	TetO-Cre F	ATG TCC AAT TTA CTG ACC G	Positive band: 300bp
	TetO-Cre R	CGC CGC ATA ACC AGT GAA	
R140Q	R140Q F	TAA TTA TAG GGC CGG TTG TC	NPHS2 WT allele: 277bp
	R140Q R	TGC CTC TTC TCC CAA CTA AA	NPHS2 Ki allele: 450bp

RG reporter	RG WT F	CTC TGC TGC CTC CTG GCT TCT	Wild type allele: 330bp Mutant allele: 250bp
	RG WT R	CGA GGC GGA TCA CAA GCA ATA	
	RG Mut R	TCA ATG GGC GGG GGT CGT T	

Table 3.1 Primers used for the genotyping.

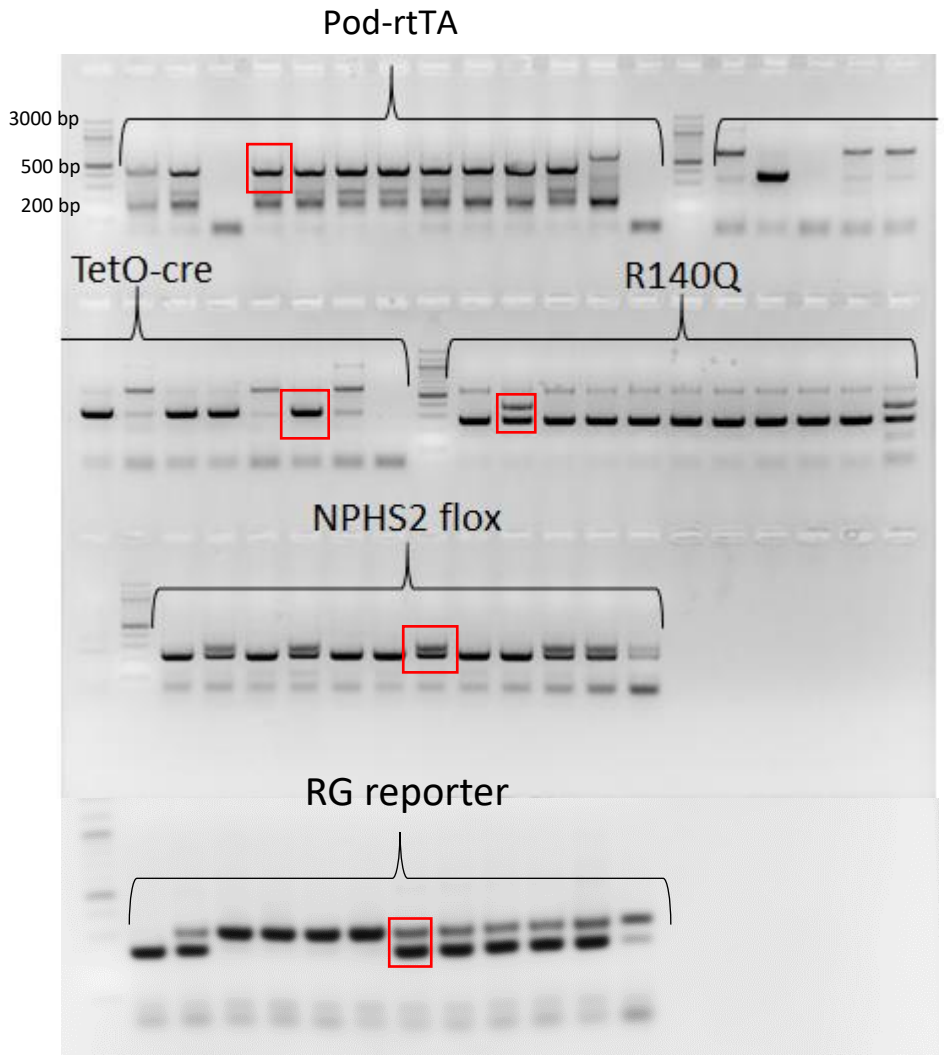

Figure 3.1 Example of genotyping results. Genotyping was carried out for 10 mice followed by positive, negative and the no template controls for Pod-rtTA and TetO-Cre. A 100bp ladder (New England Biolabs UK, Hitchin, UK) was used.

3.3 Drug delivery via ALZET osmotic pumps

Pod-rtTA$^{+/-}$*TetO-Cre*$^{+/-}$*NPHS2*$^{flox/R140Q}$*RG*$^{+/-}$ or *Pod-rtTA*$^{+/-}$*TetO-Cre*$^{+/-}$*NPHS2*$^{flox/R140Q}$*RG*$^{-/-}$ transgenic mice (*NPHS2*$^{flox/R140Q}$ mice for simplicity) were used to see whether prolonged treatment with c407 corrected the altered podocin localization and prevented proteinuria in

these mice. ALZET Osmotic Pumps 2004 were chosen to administrate c407/0.9% NaCl at a continuous and controlled rate for 28 days (Figure 3.2A). Subcutaneous pump implantation was performed to deliver c407 dissolved in 0.9% NaCl or 0.9% NaCl for 28 days as previously described (see Appendix 2) [131]. Mice were anaesthetized with 3% isoflurane (with oxygen at 1L/min), and the same level of anaesthesia was maintained during osmotic pump implantation. Directly after surgery, subcutaneous injection of rimadyl (0.1mg/kg) was administrated as analgesia. Mice were closely monitored for 24h and expected to make a rapid recovery from implantation of osmotic pumps. Wound clips were removed at day 11 post-surgery. ALZET Osmotic pumps are designed to have a fixed volume-delivery rate, therefore accurate calculations based on the volume of impermeable pump reservoir were performed to fill each pump with appropriate volume of c407 to achieve a dose of 22.3mg/month/mouse (based on the work done in CF field). It is essential to fill each ALZET pump completely with drug/saline solution under sterile conditions, avoiding any air bubbles being trapped within the reservoir. ALZET Osmotic Pumps 2004 operate based on the difference in an osmotic pressure between the osmotic layer of the pump and the subcutaneous tissue layer of the living animal (Figure 3.2B). The high osmolarity of the osmotic layer results in water being diffused into the pump through a semipermeable membrane creating an increase in pressure within the pump, which in turn displaces the contents from the pump at a controlled rate. This further results in the impermeable reservoir of the pump being compressed; thus, the pump is designed for a single use only.

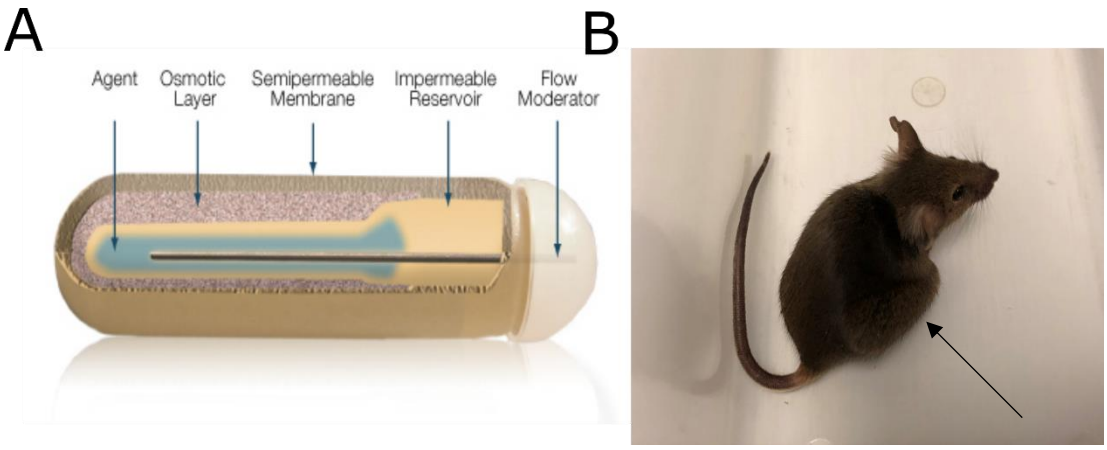

Figure 3.2 ALZET Osmotic Pump (A) in mouse (B) Alzet osmotic pump was used to deliver c407 at a constant rate and was implanted subcutaneously (A). Image of ALZET osmotic

pump was taken from http://www.alzet.com/products/ALZET_Pumps/howdoesitwork.html

3.3.1 NPHS2$^{flox/R140Q}$ mice

Homozygous *NPHS2* $^{flox/flox}$ and heterozygous *NPHS2* $^{R140Q/+}$ transgenic mice on a 129Sv/PasCrl genetic background were kindly provided by Prof. Corinne Antignac (INSERM, Paris). These mice were transported to Charles River to be used for breeding with iPod mice. *Pod-rtTA*$^{+/-}$*TetO-Cre*$^{+/-}$*NPHS2*$^{flox/R140Q}$*RG*$^{+/-}$ mice *(NPHS2*$^{flox/R140Q}$) on a mixed background were then transported from Charles River to the University of Bristol experimental housing facility at 4-weeks of age. Mice were allowed to settle for one week prior to any surgical interventions, such as implantation of the osmotic pumps.

3.4 Urine Collection

Urine samples were obtained from all mice prior to the start of any experimental procedures, such as doxycycline induction or implantation of the osmotic pumps. Beginning from the first week after doxycycline induction, weekly urine collections were performed to look for the onset and control the duration of proteinuria until the point of sacrificing (10-12 weeks) in *NPHS2*$^{flox/R140Q}$ mice. In the c407/saline osmotic pump model, urine was collected twice a week for a 28-day period. To collect samples, mice were placed individually in a clean plastic container and watched constantly. Once the mouse urinated, 50-100µl of urine was pipetted off and stored at -20˚C until analysis. Siemens Multistix Urinalysis strips were used as a basic diagnostic tool to give an estimation of proteinuria as indicated by a colour change on the protein pad.

3.4.1 Albumin Elisa

Mouse Albumin ELISA Quantitation Set (Bethyl Laboratories #E90-134) was used to detect mouse albumin in urine as per manufacturer's instructions. Frozen urine samples were defrosted, vortexed and diluted in Sample/Conjugate Diluent (50 mM Tris, 0.14 M NaCl, 1% BSA, 0.05% Tween 20) based on the expected concentration of the analyte from Multistix Urinalysis strips analysis. All samples, as well as the standards provided by the manufacturer, were assayed in duplicate each time the assay was performed. 1µl of affinity purified antibody was diluted in 100µl of ELISA Coating buffer (0.05 M Carbonate-Bicarbonate, pH 9.6) for each well to be coated. 100µl of diluted antibody was then added

to each well of the ELISA plate, which was then incubated for 1h at room temperature. Antibody solution was aspirated from each well, and the plate was washed five times in ELISA Wash solution (50 mM Tris, 0.14 M NaCl, 0.05% Tween 20, pH 8.0) before being blocked in ELISA Blocking solution (50 mM Tris, 0.14 M NaCl, 1% BSA, pH 8.0) for 30 min at room temperature. The plate was then washed again five times in Wash solution, prior to 100µl of standard or sample was transferred to each assigned well for 1h at room temperature. After incubation, the plate was washed five times in Wash solution, and 100µl of HRP detection antibody diluted in Sample/Conjugate Diluent was transferred to each assigned well for 1 hour at room temperature. Another five washes were performed, before 100µl of TMB substrate solution was added into each well. The enzymatic colour reaction was allowed to develop in the dark for 15 min at room temperature. After 15 min, the reaction was stopped by adding 100µl of ELISA Stop solution (0.18 M H2SO4). The plate was then gently tapped to mix the contents, and the absorbance was measured at 450 nm using ELISA plate reader (Opsys MR Microplate Reader, DYNEX). A standard curve was used to determine the amount of mouse albumin in urine.

3.4.2 Urine Creatinine

Urinary creatinine was measured using CREATININE (Enzymatic) kit manufactured by Thermo Scientific (#981845). All samples were processed as a single batch by Diagnostic Laboratories (Langford Veterinary Services) using a Konelab Prime 60i fully automated clinical chemistry analyzer (Thermo Scientific).

3.4.3 Albumin/Creatinine Ratio (ACR)

The mouse albumin concentration obtained from the plate reader was multiplied by the dilution factor to determine the amount of mouse albumin in the urine sample. Albumin concentrations were then converted to mg/l, while creatinine values received from Diagnostic Laboratories were in mmol/l. Albumin concentration (mg/l) was further divided by creatinine concentration (mmol/l) of the same sample to obtain albumin/creatinine ration (mg/mmol) for each urine sample.

3.5 Kidney Tissue

The kidneys harvested from the *NPHS2*$^{flox/R140Q}$ mice were processed in several ways to provide a phenotypic profile for each animal after the transgene induction and to examine the effects of c407 on the renal function.

3.5.1 Kidney Harvesting

Mice were culled in accordance with Schedule 1 humane killing methods by confirmation of permanent cessation of the circulation. Both kidneys were collected and cut in half longitudinally. Half of one kidney was fixed in 10% (v/v) formalin in PBS for four days, before being placed in 70% ethanol. Two other halves were placed in cryovials and snap frozen immediately in liquid nitrogen. The cryovials were then stored at -80˚C until required for IF, RNA and protein extraction. The last half of the kidney was cut into 1mm pieces and placed in the EM buffer for fixation and storage at 4˚C. Spleen was also harvested and snap frozen immediately from each animal to be used as a control tissue for RNA and protein.

3.5.2 Kidney Processing

Kidney tissues were fixed in 10% (v/v) formalin, further processed and paraffin embedded after ethanol dehydration. Tissues were then cut by University of Bristol histopathology staff within the Bristol Medical School histopathology laboratory to give sections 3µm thick.

3.6 Tissue Staining

3.6.1 Periodic Acid-Schiff (PAS) staining

PAS staining was performed on paraffin-embedded tissue sections to evaluate the degree of sclerosis within the glomerular tuft using PAS staining system (SIGMA-ALDRICH) as per manufacturer's protocol. Slides were immersed twice in Histo-Clear II (National Diagnostics HS-202) for 5 min to deparaffinize sections. Sections were then rehydrated by passing the slides through alcohol series (100% ethanol, 90% ethanol, 70% ethanol, 50% ethanol) to deionized water. Slides were oxidized in periodic acid solution for 5 min at room temperature, before being rinsed in several changes of distilled water. Slides were then placed in Schiff's reagent for 15 min and washed in running tap water for 5 min. The

tissue sections were counterstained in hematoxylin solution for 90 seconds and immediately washed again in running tap water. The sections were then dehydrated by being passed through alcohol series (50% ethanol, 70% ethanol, 90% ethanol, 100% ethanol), dried and mounted in DPX (Sigma #44581). The sections were then imaged using a Leica light microscope that allows to assess morphology of the kidney.

3.6.2 Masson's Trichrome staining

Masson's Trichrome staining was performed on paraffin-embedded tissue sections to evaluate the degree of glomerular fibrosis (collagen deposits) using Trichrome Stain (Masson) Kit ((SIGMA-ALDRICH) as per manufacturer's protocol. Slides were immersed twice in xylene for 5 min to deparaffinize sections. Sections were then rehydrated by passing the slides through alcohol series (100% ethanol, 90% ethanol, 70% ethanol, 50% ethanol) to deionized water. Slides were stained in Weigert's iron hematoxylin working solution for 5-10 mins and then rinsed in running warm tap water for another 10 mins, followed by the distilled water wash. The tissue sections were then stained in Biebrich scarlet-acid fuchsin solution for 10-15 mins, washed in distilled water and differentiated in phosphomolybdic-phosphotungstic acid solution for another 5-10 mins (or until collagen is not red). Sections were then transferred directly to aniline blue solution and stained for 5-10 mins, followed by a brief rinse in distilled water and differentiation in 1% acetic acid solution for 2-5 mins, followed by a brief wash in distilled water. The sections were then dehydrated by being passed through alcohol series and cleared in xylene, dried and mounted in DPX (Sigma #44581). The sections were then imaged using a Leica light microscope that allows to assess morphology of the kidney.

3.6.3 Immunohistochemistry (IHC)

IHC was performed with Wilm's tumour-1 protein (WT1) antibody (Santa Cruz) to look for the glomerular podocyte number in mice kidney sections. Slides were immersed twice in histoclear for 5 min to deparaffinize sections. Sections were then rehydrated by passing the slides through alcohol series (100% ethanol, 90% ethanol, 70% ethanol, 50% ethanol) to deionized water. Slides were next boiled in the antigen retrieval buffer (10mM Sodium citrate tribasic, pH 6) for 10 min in microwave and allowed to cool on bench top for 30 min. Sections were then washed in deionized water 3 times for 5 min each. PAP pen was used to draw around sections, which were then incubated in 3% hydrogen peroxide for 20 min in a humidified box, followed by wash in deionized water twice for 5 min each.

Sections were blocked in blocking solution (5% goat serum in TBST 0.1%) for 30 min at room temperature. Blocking solution was then removed, and sections were incubated with primary antibody (20ul/sample) overnight at 4°C. Next morning, primary antibody was removed, and sections were washed with wash buffer (TBST 0.1%) 3 times for 5 min each. Sections were then covered with 1–3 drops of SignalStain® Boost Detection Reagent and incubated in a humidified chamber for 30 min at room temperature. Meanwhile, 1 drop (30 µl) SignalStain® DAB Chromogen Concentrate was added to 1 ml SignalStain® DAB Diluent and mixed well before use (20ul/sample). Following 3 washes with wash buffer, SignalStain® DAB was applied to each section for 1 to 10 mins, or until the brown staining became apparent. Slides were then immersed in deionized water and counterstained with hematoxylin for 10 seconds. Next, slides were washed in tap water, until water became clear. The sections were then dehydrated by being passed through alcohol series and cleared in histoclear, dried and mounted in DPX (Sigma #44581). The sections were then imaged using a Leica light microscope.

3.7 Electron Microscopy (EM)

Kidney tissue preparation for immersion fixation involved rapid excision of animal tissues and immersion of small tissue pieces (1mm cubes) in fixative (2.5% glutaraldehyde in 0.1 M cacodylate at pH 7.3) in order to get the best ultrastructure. Tissues were then washed in 0.1 M cacodylate buffer 3 times for 10 minutes, followed by post fixation in 1% osmium tetroxide in 0.1M cacodylate buffer pH 7.3 at 4 - 8°C for 1 hour. Kidney tissues were washed in 0.1 M cacodylate buffer for 15 minutes, followed by 3 washes in deionised water. Tissues were then put into 1-3% Uranyl acetate *en bloc* staining overnight, followed by 15-minute deionised water wash next morning. Kidney tissues were washed twice in propylene oxide for 15 minutes and infiltrated with Epon resin mix: propylene oxide (1:1) for 2 hours. Infiltrated tissues were then embedded in fresh Epon resin mix in a silicon rubber mould and left to polymerize for >24 hours at 60°C. Note, Epon resin mix consists of resin, hardener, accelerator and plasticiser. Finally, tissues were cut into sections (70nm thick) on an Ultracut S ultramicrotome, which were then stained with 3% uranyl acetate (5mins) and Reynolds' lead citrate (2mins) with deionised water wash in between and after the lead stain. Sections of glomerulus were imaged at various magnifications in a Tecnai T12 microscope (FEI Ltd).

Chapter 4: Creation of a Conditional Knock-In Mouse Model of the R140Q Mutation

4.1 Introduction

As previously described, the podocin gene, *NPHS2*, encodes an integral membrane protein exclusively localized to the slit diaphragm of podocytes foot processes, which has been found to be mutated in both the familial autosomal recessive and sporadic forms of SRNS. Even though adult-onset cases have been identified, SRNS is most prevalent in children between 3 and 6 years of age [132]. Mutations in this protein comprise frameshift and missense changes as well as loss-of-function mutations and are spread throughout the entire length of the protein. Amongst more than 120 pathogenic mutations found to date, the most frequent variant is the *p. R138Q* mutation [120]. Furthermore, patients bearing the homozygous R138Q mutations are predicted to have a mean onset of NS before the first year of life, which rapidly leads to focal segmental glomerulosclerosis and subsequently to end-stage renal disease [124]. Effects of missense mutations of podocin have been studied in various cell culture models and some, along with the *p. R138Q* variant, have been shown to alter trafficking of podocin to the plasma membrane leading to its intracellular retention [126]. As previously established in Chapter 1, the R138Q podocin mutation results in the misfolded form of the protein, which is retained and targeted for proteasomal degradation in the ER. Several mouse models of podocin-associated glomerulopathy have been created in the last couple of years to study the function of the protein during the disease course and develop new pharmacological strategies [133],[134]. A developmental podocin knockout mouse model (*NPHS2*$^{-/-}$), for example, revealed podocin as a key player required for recruitment and assembly of nephrin at the slit diaphragm. Subsequently, a constitutive knock-in mouse model of the R140Q mutation, the mouse analogue of human R138Q mutation, was generated and demonstrated developmental arrest of podocytes and lethal renal failure within the first month of life, similar to what has been seen in the knockout model of podocin [135]. Recently, using Cre recombinase technology, an inducible podocin knockout model was created that resembled the podocin-related glomerulopathy seen in humans; however, this model still does not allow one to study pathogenesis of the R140Q podocin mutation *in vivo* and search for new therapeutic interventions aimed to restore the function of R140Q mutant protein. Therefore, one aim of this PhD was to generate a novel

doxycycline-responsive inducible Cre recombinase knock-in mouse model of the R140Q mutation.

4.1.1 Transgenic mice

Experimental animal models have been proven to play an incredible role in biomedical research. Nowadays, transgenic technology is widely used in mice, which permits the alteration of their genetic background and therefore, the manipulation of various biochemical and physiological pathways and processes in the entire animal with almost analogous specificity observed in cell culture systems [136]. However, cell culture models that are currently available in the renal field do not fully recapitulate the unique three-dimensional cytoarchitecture of podocytes or the gene expression pattern detected *in vivo.* Therefore, transgenic mouse models specifically targeting the podocyte offer new methods for studying the biology of this specialised glomerular epithelial cell and provide ways to overcome limitations seen *in vitro*. This cell specific expression of genes can be achieved using promoter elements that drive podocyte-specific expression in the kidney. In the case of the glomerulus, the slit diaphragm proteins, nephrin and podocin, have been extensively used in this way [137]. It has been previously demonstrated that nephrin is not a truly podocyte-specific protein and is detected in other organs, such as the pancreas and brain, while podocin is exclusively localized to podocytes [82]. Both NPHS1 and NPHS2 promoter constructs have been created and linked with various transgenes to activate the gene expression in a podocyte-specific manner. There are circumstances, when researchers want to switch off gene expression in some cells. In this occasion, Cre recombinase will excise any piece of DNA/gene of interest flanked by loxP sites under the control of the cell specific promoter.

Developmental gene knockout (KO) or knock-in (KI) systems are not always powerful enough to study podocyte-specific genes, such as *NPHS1 and NPHS2*, because up- or down-regulation of these genes leads to lethal renal failure at neonatal age [138]. Therefore, it is essential to generate mouse models that allow the inducible expression or knockout of genes specifically in the podocyte at any age. In glomerular research, a transgenic mouse model has been generated that expressed the mouse NPHS2 (podocin) promoter linked to a reverse tetracycline-controlled transcriptional activator (rtTA), which is made of a mutant tetracycline repressor protein and VP16 [134]. These mice can be further bred with other transgenic mice, which have genetically modified gene of interest. This gene of interest is linked to a tetracycline-responsive promoter element

(Tet-O) and the transcription of the target gene is activated by rtTA in the presence of tetracycline, so-called Tet-off system (Figure 4.1) [134]. Thus, the level of transgene expression can be controlled by administration of the drug, such as doxycycline, in a dose- and time- dependent fashion. This system can be further associated with Cre recombinase technology to induce the deletion of the target gene that is flanked by two loxP sites in the adult mouse [138]. In general, the tetracycline-controlled systems have been invaluable in evaluating the podocyte as a key player in glomerular function. However, this technology could be less than 100% effective, thus there is need to check gene expression in every mouse model.

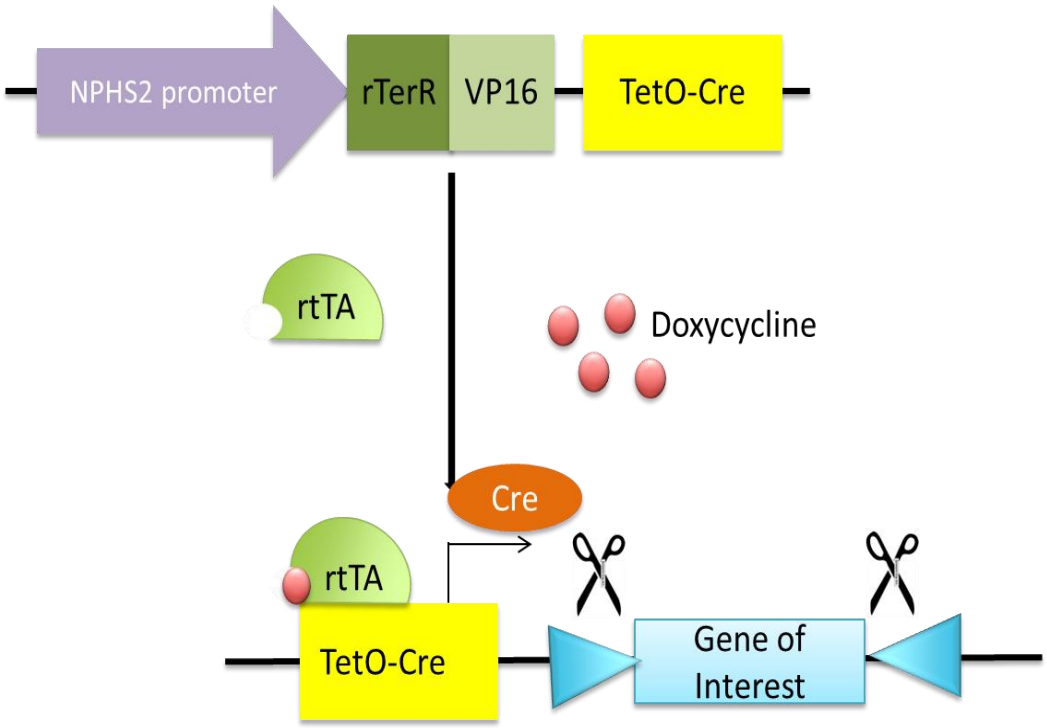

Figure 4.1 Tet-off System. A 2.5 kb fragment of the NPHS2 promoter element drives the expression of rtTA in podocytes. In the presence of doxycycline, rtTA binds to TetO, which is associated with Cre recombinase technology, and activates the deletion of the gene of interest, flanked by two loxP sites, in the adult mouse.

4.1.2 Targeting of the murine *NPHS2* allele results in expression of the R140Q podocin variant

Podocin is encoded by the *NPHS2* gene, which is composed of eight exons, and situated on chromosome 1q25-q31. When transcribed, the mouse *NPHS2* gene produces a 3.1 kb

mRNA that encodes a 385-amino-acid protein, which shares 92% similarity with human podocin [111]. A mouse model carrying R140Q podocin mutation, which is analogous to human p.R138Q variant, was generated using a 6.6 kb targeting construct [135]. Using site-directed mutagenesis, the c.505G>A, c.506A>G mutations were introduced into exon 3 of the *NPHS2* gene of the targeting vector, while a *phosphoglycerate kinase–hygromycin* cassette flanked by flox sites was inserted into intron 3 to select positive embryonic stem (ES) cell clones [135]. Following successful homologous recombination, two ES cell clones were selected and injected into the murine blastocyst of C57BL/6 mice [135]. Several rounds of breeding were undertaken to generate a mouse with germline incorporation of the mutant allele, which was further mated with mice constitutively expressing Cre recombinase that aids the removal of the floxed hygromycin insert. Using this model, the group of C. Antignac have demonstrated that homozygous *NPHS2* $^{R140Q/R140Q}$ mice die within the first week of life with some mice dying during embryogenesis, while heterozygous *NPHS2* $^{R140Q/+}$ mice did not develop albuminuria or any renal anomalies [135]. The above models are characterized either by severe renal phenotype resulting in early death or by insufficient expression of the mutated protein. Therefore, the conditional inactivation of wild-type protein is essential to elucidate the role of podocin in health and disease in mice at postnatal age.

4.2 Methods

4.2.1 Breeding of a conditional knock-in mouse model of R140Q mutation

Homozygous *NPHS2* $^{flox/flox}$ and heterozygous *NPHS2* $^{R140Q/+}$ transgenic mice on a 129Sv/PasCrl genetic background were a kind gift from Prof. Corinne Antignac (INSERM, Paris). Homozygous *NPHS2* $^{flox/flox}$ mice were generated to carry a floxed *NPHS2* exon 2 alleles, which can be excised, when Cre recombinase is expressed leading to a conditional podocin inactivation in mature kidneys (Figure 4.2) [139].

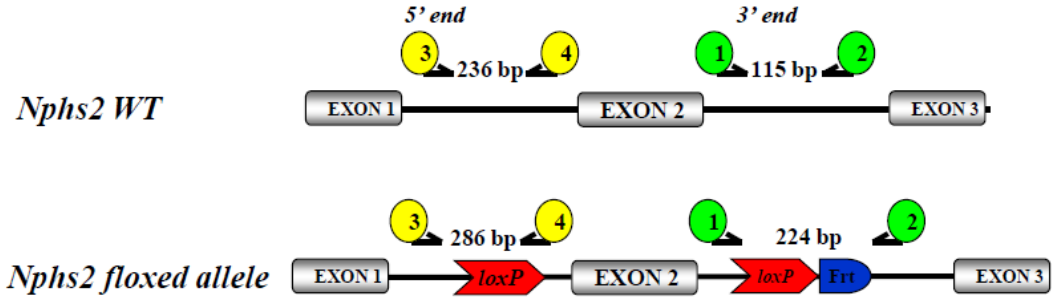

Figure 4.2 *NPHS2* floxed allele. Mice were created to carry a floxed *NPHS2* exon 2 alleles, which can be excised using Cre recombinase.

Initially, two lines *NPHS2* $^{flox/flox}$ and *NPHS2* $^{R140Q/+}$ were crossed to generate heterozygous *NPHS2* $^{flox/R140Q}$ offspring mice, which were used for further breeding (Figure 4.3). Subsequently, the *NPHS2* $^{flox/R140Q}$ mice were crossed with a transgenic iPod male mouse model of a mixed genetic background (a kind gift from Prof. Richard Coward) for generation of the inducible mice line. The iPod male mouse model is composed of three genes: 1) rtTA that is under the control of a 2.5 kb *NPHS2* promoter driving podocyte-specific expression of rtTA [134]; 2) TetO-Cre that is under the control of a tetO, to which the rtTA protein binds in the presence of tetracycline or analog, such as doxycycline, thus allowing Cre recombinase expression; 3) RG reporter, also known as mT/mG, that is a red green fluorescent reporter under the control of a CMV enhancer/chicken beta actin core promoter that regulates the expression of a loxP-flanked tdTomato reporter element followed by a polyadenylation signal and EGFP reporter element. Mouse podocyte cells initially express red fluorescence, and then green fluorescence in the presence of Cre recombinase, which can excise floxed tdTomato reporter, suggesting that the R140Q allele is in the heterozygous state. Succeeding multiple rounds of breeding, the resulting

transgenic mice had the specified cassette of genes (*Pod-rtTA*$^{+/-}$*TetO-Cre*$^{+/-}$*NPHS2*$^{flox/R140Q}$*RG*$^{+/-}$ or *Pod-rtTA*$^{+/-}$*TetO-Cre*$^{+/-}$*NPHS2*$^{flox/R140Q}$*RG*$^{-/-}$) and were used for the final experiments. For simplicity, the mice were called *NPHS2*$^{flox/R140Q}$ in this document.

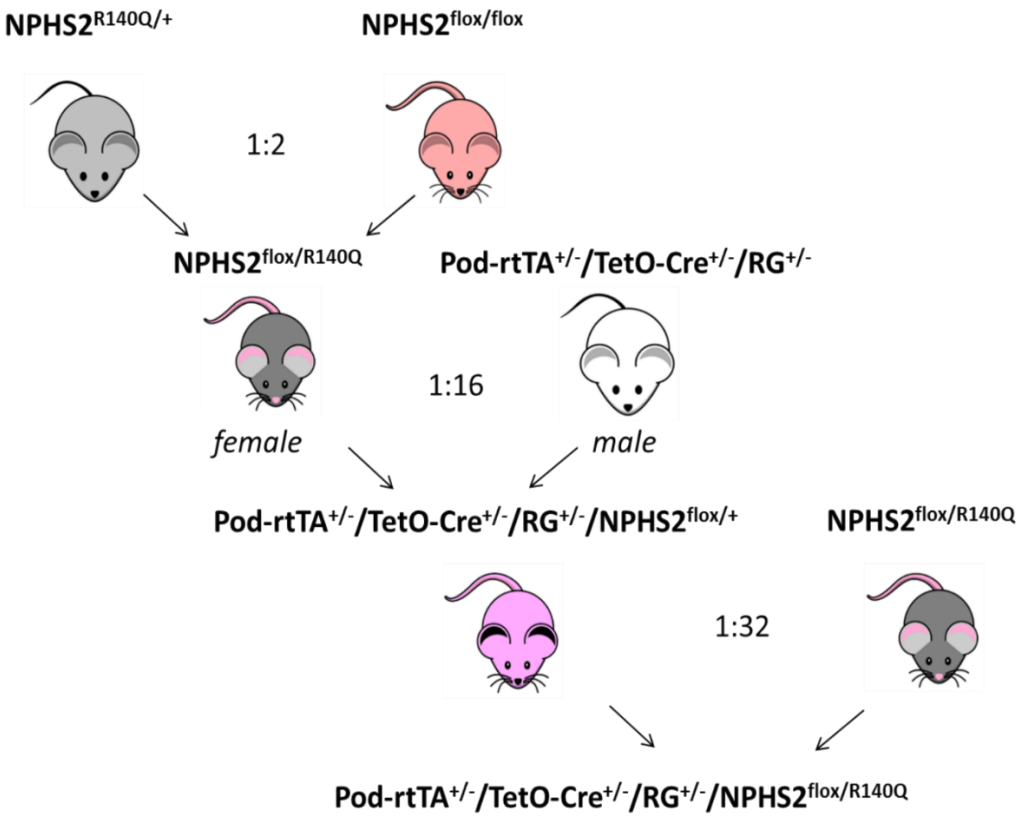

Figure 4.3 An example of breeding strategy used to generate a Conditional Knock-In Mouse Model of the R140Q Mutation. Only male mice had *TetO-Cre* and were used for further breeding, as *TetO-Cre* was shown to be leaky in females.

4.2.2 Experimental design for phenotypic characterization

Postnatal induction of R140Q hemizygosity in *NPHS2*$^{flox/R140Q}$ mice was achieved by administration of doxycycline at 2 mg/ml in 5% sucrose dissolved in drinking water for three weeks. Doxycycline, a tetracycline derivative, binds with high affinity to rtTA, thus inducing a Tet-off system in transgenic mice. Doxycycline was shown to have an excellent medical safety record and deep tissue penetration with relatively low toxicity in eukaryotic cells [140]. Doxycycline was made fresh every 4 days and administered in black bottles to protect from light. Control mice with the same genotype (*NPHS2*$^{flox/R140Q}$) were

given the same volume of drinking water without doxycycline. Other control groups of mice, which lacked either *Pod-rtTA* or *TetO-Cre* or both, received the equivalent volume of drinking water with doxycycline at the same concentration as used for the experimental mice. The rationale for having mice without the *Pod-rtTA* gene, for example, is that the induction efficiency of the floxed wild-type podocin can be monitored. Mice were maintained and managed by skilled animal technicians in the pathogen-free conditions of ASU unit, University of Bristol.

Beginning from the first week after doxycycline induction, weekly urine collections were performed to look for the onset and control the duration of proteinuria until the point of sacrificing. Animals were sacrificed at weeks 10-12 after doxycycline administration. In case of weight loss (over 10%), the affected animal was culled immediately. At designated experimental time points mice were maintained under general anaesthesia with isoflurane, and 1 ml of blood was withdrawn by cardiac puncture. Animals were subsequently sacrificed by Schedule 1, and both kidneys were removed (flash frozen, put in PFA or EM buffer). Samples were collected and used for RNA and protein extraction, immunofluorescence studies, immunohistochemistry and electron microscopy. Urine albumin concentration was analysed using human albumin ELISA kit (Bethyl Laboratories). Whole blood samples were sent to Diagnostic Laboratories (Langford Vets, University of Bristol) to measure serum creatinine, albumin and urea. Urine samples were also sent to Diagnostic Laboratories (Langford Vets) to analyse creatinine in the urine.

4.3 Results

4.3.1 *NPHS2*$^{flox/R140Q}$ mice develop NS and end-stage kidney disease

Doxycycline induction of a hemizygous state in the *NPHS2*$^{flox/R140Q}$ mice led to severe proteinuria detectable within few days, which peaked to a maximum at 2-4 weeks after induction of *NPHS2*$^{null/R140Q}$ and was maintained at week 12 (Figure 4.4a). Consequently, there was a continuous decrease in proteinuria observed from week 6 in experimental animals, but it still stayed elevated compared to controls until the point of sacrificing at 12 weeks. This is due to the deformation of the kidney structure. Furthermore, proteinuric animals had a significantly reduced weight gain from week 8 onward, when compared to healthy controls (Figure 4.4c). The *NPHS2*$^{null/R140Q}$ animals presented with hypoalbuminemia (g/L), hypercholesterolemia (mmol/L), uremia (mmol/L) and abnormally high plasma creatinine levels (µmol/L) at the point of sacrifice (Figure 4.4b).

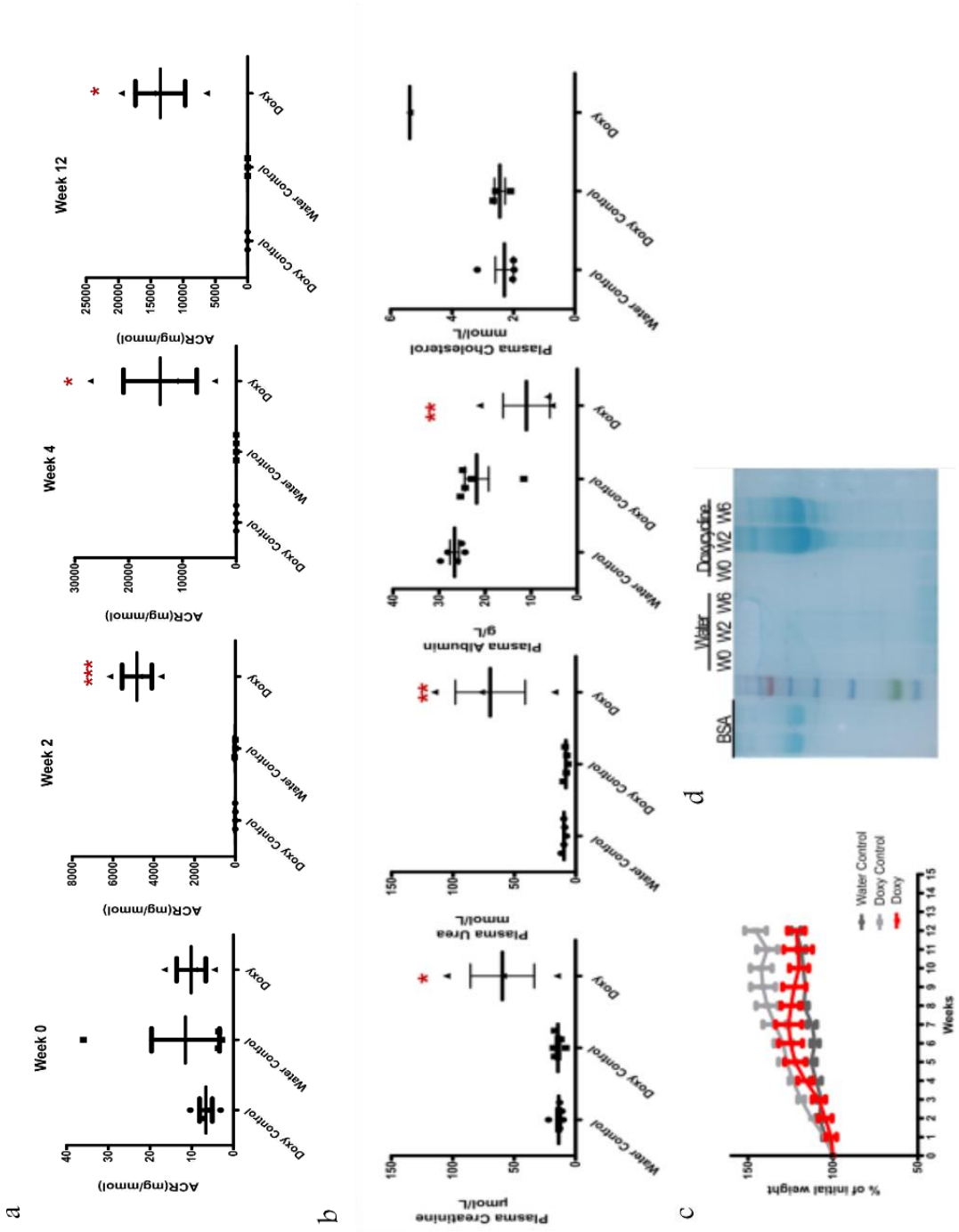

Figure 4.4 NPHS2$^{flox/R140Q}$ mice develop NS. (a) Doxycycline induced mice develop massive proteinuria from week 2 onward. One-way ANOVA (p≤0.05). (b) NPHS2$^{null/R140Q}$ mice demonstrate significantly diminished creatinine clearance, uremia, hypoalbuminemia and hypercholesterolemia at 12 weeks (One-way ANOVA (p≤0.05) vs. controls at the same time point). (c) Weight loss is observed in experimental animals from week 8 onward. (d) SDS-PAGE urine protein analysis. Coomassie staining displays albuminuria in doxycycline-induced animals at weeks 2 and 6. ACR=Albumin-to-Creatinine Ratio.

4.3.2 Loss of podocin mRNA expression by 12 weeks

QPCR analysis was performed to look for total, floxed WT and R140Q *NPHS2* expressions at 4 and 12 weeks, in order to check the doxycycline efficiency. Interestingly, R140Q podocin mRNA expression was similar to healthy controls at 4 weeks, but then dropped significantly at 12 weeks after induction (Figure 4.5a, b). The expression of WT podocin mRNA decreased at 4 weeks after doxycycline induction of the heterozygous state, as anticipated (Figure 4.5a). Furthermore, total loss of podocin mRNA expression was observed at 12 weeks, suggesting that mice had lost all the podocytes and gone into renal failure.

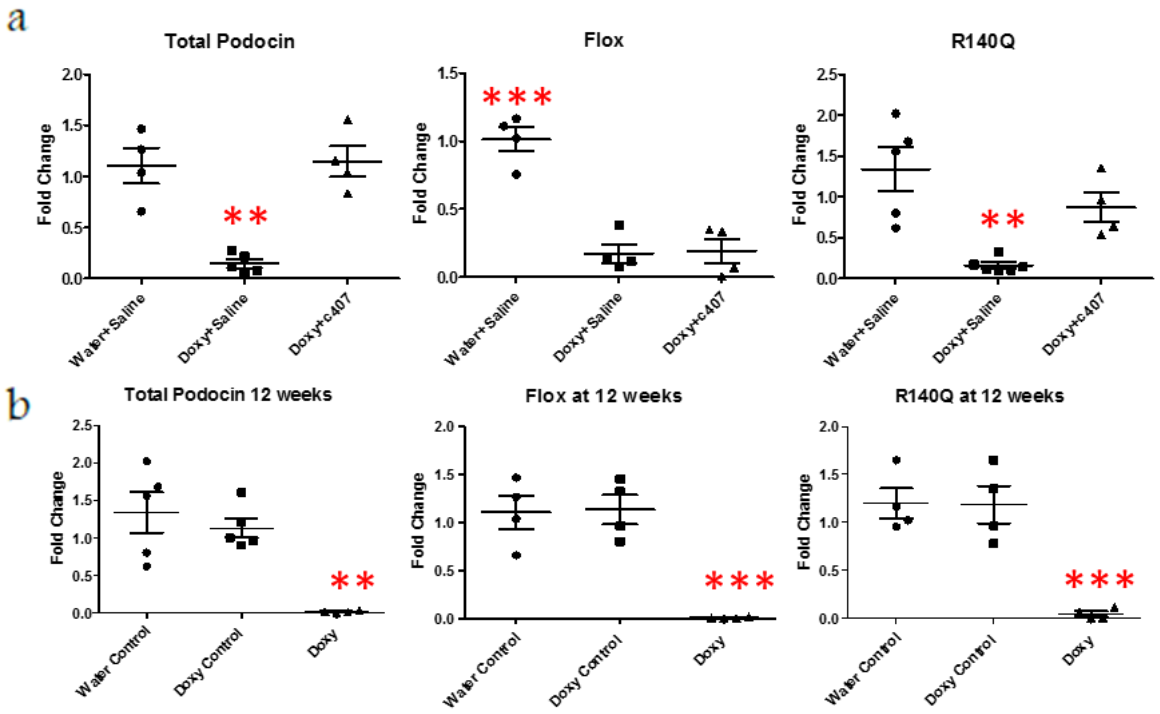

Figure 4.5 mRNA expression analysis. (a) Diseased mice displayed a loss of total, floxed WT and R140Q podocin mRNA expressions at week 4. One-way ANOVA ($p \leq 0.05$) (b) Total loss of total, floxed WT and R140Q podocin mRNA expressions was observed at week 12 in the induced animals. One-way ANOVA ($p \leq 0.05$). ** $P \leq 0.01$; *** $P \leq 0.001$

4.3.3 Total podocin loss associated with the loss of podocytes in *NPHS2*$^{flox/R140Q}$ mice

Immunofluorescence studies were performed to detect the level of total podocin protein in glomeruli of healthy and *NPHS2*$^{null/R140Q}$ animals at the point of sacrificing. The loss of podocin expression in *NPHS2*$^{null/R140Q}$ mice was observed at 12 weeks after doxycycline induction compared to healthy controls (Figure 4.6). The loss of podocin was associated with the reduction in number of podocytes in the induced animals during the course of the disease. Furthermore, the nephrin expression was also reduced in proteinuric animals.

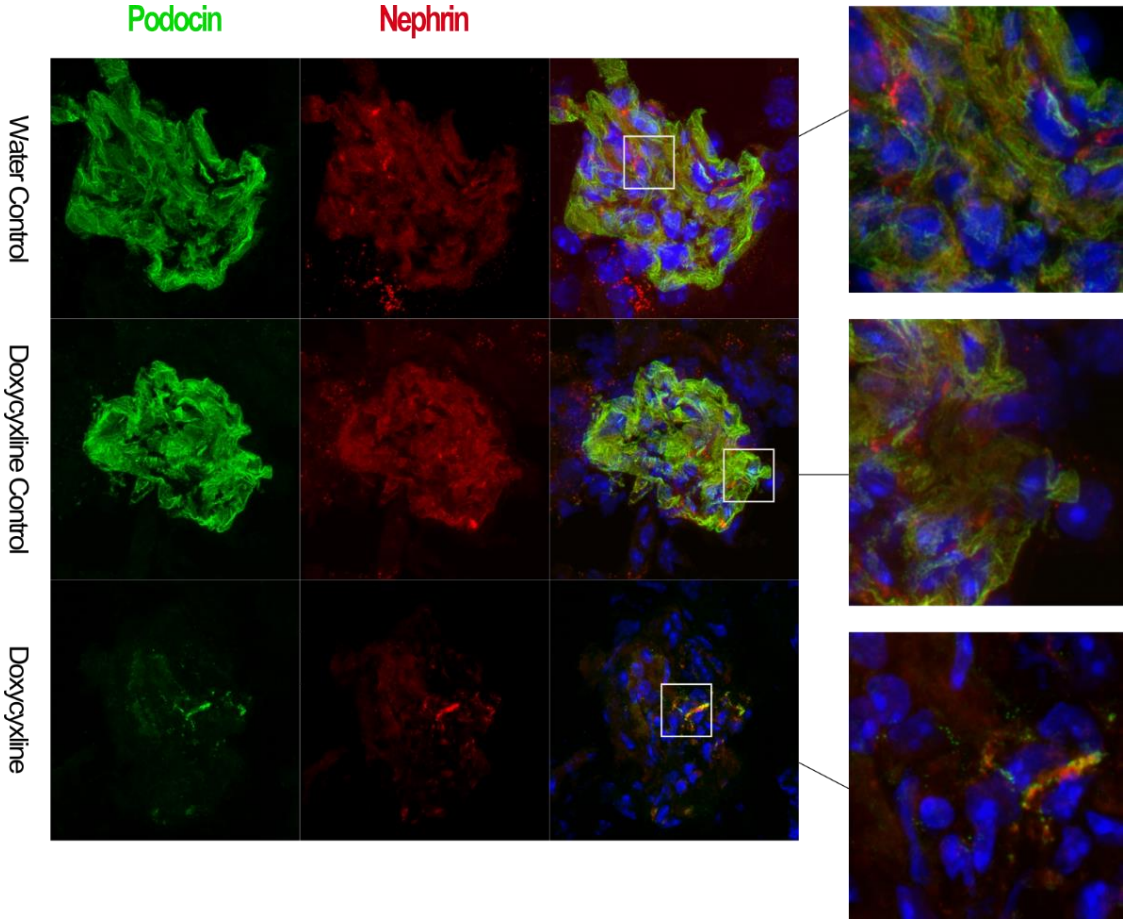

Figure 4.6 Loss of podocin is observed in NPHS2$^{flox/R140Q}$ mice. Podocin (green), nephrin (red) and nucleus (blue) staining of glomeruli of healthy and NPHS2$^{null/R140Q}$ animals at the point of sacrificing (12 weeks). Water and doxycycline control groups show normal expression of podocin and nephrin in glomerulus. Doxycycline induced animals demonstrate podocin and nephrin loss at the point of end stage renal disease. Magnification, X63; zoom, x8.

4.3.4 Proteinuric animals develop global glomerulosclerosis

Control healthy animals had normal glomeruli on PAS stain without GBM thickening and mesangial cell deposits. Bowman's space and proximal tubules were well-defined (Figure 4.7). The *NPHS2*$^{flox/R140Q}$ mice displayed 100% of globally sclerosed glomeruli with collapsed Bowman's capsules space at 12 weeks after induction. In addition, the proteinuric mice demonstrated podocyte loss and developed tubulointerstitial fibrosis with prominent proteinaceous casts. Electron microscopy further revealed podocyte foot process effacement and global fusion with GBM thickening in induced animals relative to two control groups (Figure 4.7).

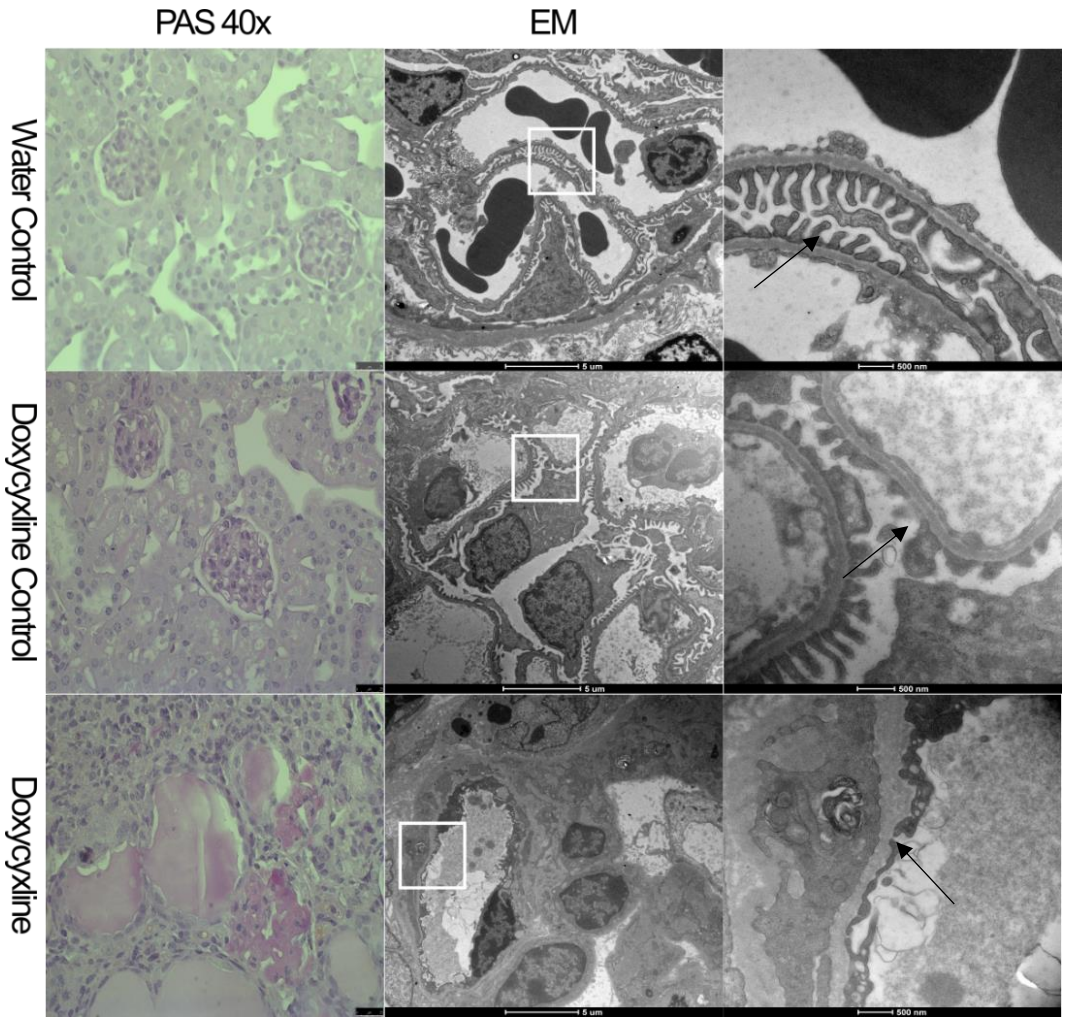

Figure 4.7 NPHS2flox/R140Q mice present with global glomerulosclerosis at 12 weeks. PAS staining was performed to look for glomerular lesions in induced animals. Magnification, x40. Scale bar, 25 µm. Ultrastructural studies demonstrated podocyte foot processes effacement in NPHS2$^{null/R140Q}$ mice compared to regular foot processes seen in healthy control animals on the opposite side of endothelial cells (indicated by arrows). Scale bars, 5 µm; 500 nm.

4.4 Discussion

Previous hereditary podocytopathy mouse models, such as *NPHS2* KO mice, *Nphs2*$^{R140Q/R140Q}$ KI mice and *laminin beta2* mutant mice, develop severe renal phenotype and have an average survival time of 4-23 days depending on the genetic background [141]. This results in insufficient characterization of the disease course because of the incomplete nephrogenesis with the mouse models not being suitable for preclinical testing of novel pharmacological strategies, such as antiproteinuric therapies, due to early demise. To investigate the pathogenesis of podocin mutation related to NS at postnatal life, a transgenic mouse line was generated using a doxycycline-inducible Cre recombinase technology that results in conditional inactivation of wild-type protein expression [138]. Postnatal induction of R140Q hemizygosity in the *NPHS2*$^{flox/R140Q}$ mice results in massive proteinuria within the first few days, which is maximal at 3-4 weeks. Moreover, other biochemical aspects of NS, such as hypoalbuminemia (low albumin level in the blood), uremia and insufficient creatinine clearance, were observed in proteinuric animals, suggesting that the animals progressed to end-stage renal disease (ESRD). The progression to ESRD is closely correlated with the development of focal segmental glomerulosclerosis (FSGS), which is largely detected in renal biopsies of patients bearing *NPHS2* mutations, such as R138Q [132]. Based on the work done by the group of C. Antignac, it was concluded that the *NPHS2*$^{flox/R140Q}$ mice initially developed FSGS, where only some of the glomeruli were affected, that quickly progressed to almost all glomeruli being scarred and sclerosed at 12 weeks. At the point of sacrificing, kidneys of the *NPHS2*$^{flox/R140Q}$ mice showed global glomerulosclerosis and severe interstitial fibrosis, as indicated by significant PAS staining (Figure 4.7). Furthermore, capsular adhesion and collapse of the glomerular tip was observed in some variants along with podocyte loss. In support of this notion, the link between podocyte depletion and glomerulosclerosis has been previously described in a transgenic rat stain expressing human diphtheria toxin (DT) receptor transgene [142]. Wharram *et al.* have identified three stages of podocyte depletion from glomeruli, when DT was injected into transgenic but not wild-type rats in a dose-dependent manner, supporting the theory that podocyte depletion may be a major driver for glomerulosclerosis in humans [142]. In addition, tubulointerstitial fibrosis was observed in induced animals at the end stage of the disease. The degree of tubulointerstitial damage is in parallel with the severity of proteinuria, as it has been previously shown that nephrotic range albuminuria is toxic to tubular and interstitial structures [143]. The described phenotype strongly corelates with that of the tamoxifen-

inducible R140Q-podocin mouse model recently generated by the group of C. Antignac, with almost same time course of proteinuria and uremia [133].

It still remains unclear what mechanisms cause podocytes to detach and, specifically, whether this loss is prompted by podocyte cell death, such as apoptosis, or due to the loss of adhesive characteristics of the cells [144]. Further ultrastructural assessment using electron microscopy was performed to evaluate for probable foot process fusion and effacement as a result of disease. Electron microscopy findings demonstrated that the development of high-grade proteinuria is closely associated with widespread podocyte foot process effacement and global fusion (Figure 4.7). These findings are in agreement with previously published mouse models of hereditary podocytopathies, such as the inducible podocin knockout model, where foot process effacement evolved with the inactivation of podocin in the mature kidneys [139]. Podocyte loss in the mouse model described is most likely caused by podocin being misfolded and retained in the ER, therefore it cannot maintain podocyte foot processes structure and function.

Finally, immunofluorescence staining, and qPCR analysis were undertaken to establish the degree of podocin loss on the molecular level following postnatal induction of R140Q hemizygosity in *NPHS2*$^{flox/R140Q}$ mice. When global glomerulosclerosis was fully established at 12 weeks, a loss of podocin protein was observed compared to control animals. Due to the excision of the floxed wild-type allele in *NPHS2*$^{null/R140Q}$ mice, the expression of wild-type podocin mRNA was reduced, resulting in the diminished expression of podocin protein. Interestingly, R140Q mRNA expression remained elevated at this stage of the disease, suggesting the decreased podocin protein is a definite consequence of the mutant protein intracellular retention and proteasomal degradation as previously observed *in vitro* for the R138Q podocin mutation [145].

In conclusion, the inducible *NPHS2*$^{flox/R140Q}$ mouse model described here closely recapitulates the commonest human mutation. Furthermore, this novel model of nephrotic syndrome highlights some significant phenotypic differences observed in previous inducible knockout mouse models of podocin, such as the inducible podocin knockout model. Therefore, the ability to produce a mutant podocin protein with defective folding and subsequent retention in the ER provides the model ideal for pharmacological screening of chaperone compounds *in vivo* that could correct trafficking defect of the mutant protein.

Chapter 5: Disruption of cytokeratin-8 interaction with R138Q podocin corrects its functional defect both *in vitro* and *in vivo*

5.1 Introduction

5.1.1 Keratin 8 (K8) – a novel candidate for targeting and degradation of misfolded proteins

As highlighted in Chapter 1, NS is the most prevalent kidney disease in children, which is caused by altered function of the GFB resulting in proteinuria, edema and hypoalbuminemia. Even though primary causes of NS vary, steroid therapy is used clinically to descriptively classify NS as SSNS and SRNS. Amongst SRNS genes discovered to date, mutations in the *NPHS2* gene encoding podocin represent the major and the most frequent cause of the disease. This integral protein with a membrane domain forms a hairpin like structure with both the C- and N-terminal tails facing the cytoplasm. The R138Q podocin mutation in exon 3 was found to be present in 57.5% of families carrying two disease-causing mutations, confirming the role of R138Q as a founder mutation [125]. The R138Q mutation produces a folded form of the protein that is retained in the endoplasmic reticulum (ER). Consequently, this has prompted an intensive search for a possible strategy that might recover defects in cell sorting of podocin mutant.

Studies performed by Colas *et al*. identified an interaction between the major disease causing mutant of the cystic fibrosis transmembrane conductance regulator (CFTR) with the cytokeratin network [130]. This 1480-amino acid protein is a PKA-activated chloride channel, which shares structural similarities with members of the ATP-binding cassette transporters family and is made of two transmembrane domains (MSDs), two nucleotide-binding domains (NBDs) and one regulatory domain (R-domain) (Figure 5.1) [146]. Gating function of the channel is highly dependent on the phosphorylation of the R-domain by PKA and is further controlled by the binding and hydrolysis of the ATP molecules to the NBDs [147]. Cystic fibrosis (CF) is a fatal autosomal recessive genetic disorder affecting mostly the lungs, caused by mutations in the gene encoding the chloride channel CFTR [148]. In particular, the F508del mutation of CFTR was found to be present in more than 70% of mutated alleles according to Cystic Fibrosis Mutation Database [130]. The deletion

of phenylalanine 508 in NBD1 domain of CFTR results in a more severe form of CF [148]. Similar to the R138Q mutation, F508del mutation generates an improperly folded form of the CFTR, which is mostly retained and targeted for proteasomal degradation in the ER, however, when it reaches the plasma membrane, the function is moderately restored [149]. Therefore, due to the defective trafficking or folding, there is a significant reduction of functional CFTR at the apical plasma membrane, moreover, the amount of F508del-CFTR that in some cases is targeted to its destination displays a dysfunction, known as a gating defect [150],[151]. Apart from having effects on epithelial cell function, CFTR mutations can have an impact on bone homeostasis, as CF patients in some cases present with low bone mineral density [152]. The study by Colas *et al*. provided a new insight into a previously unknown mechanism that plays a role in the retention of F508del-CFTR. Using an immunoprecipitation approach, a physical interaction between K8 and F508del-CFTR has been demonstrated in cultured cells, suggesting a critical role of K8 in the mutant CFTR retention [130]. Furthermore, inhibition of this interaction is able to recover the function of the mutant at the cell surface [130].

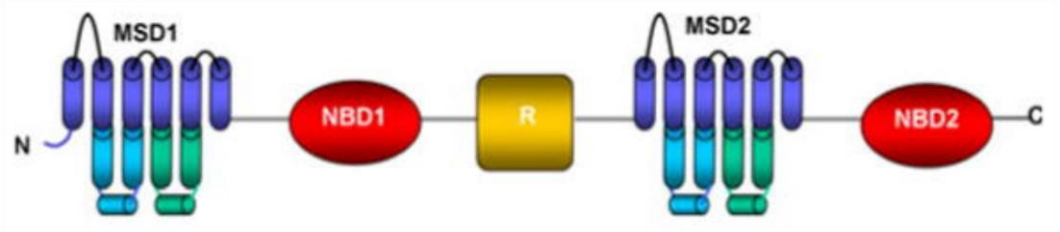

Figure 5.1 Schematic representation of CFTR. CFTR is made up of two transmembrane domains (MSDs), two nucleotide binding domains (NBDs) and a regulatory domain (R-domain). Adapted from Kalid *et al* [153].

Since the discovery of mutations in podocin as the cause of NS, further studies are required to elucidate potential pharmacological advancements to rectify the dysfunction of the mutated proteins. For missense mutations, such as F508del-CFTR and R138Q podocin, small correctors (molecules) have to be discovered/created to target the mutant proteins back to the plasma membrane and to improve their function, also known as potentiators [154]. One of the successful potentiators developed for CF patients bearing the G551D mutation is a VX-770/Ivacaftor, which demonstrates a clinical benefit with no major side effects [155]. Nevertheless, protein folding and targeting are complex intracellular processes, which makes it difficult to develop correctors. Indeed, such molecules are in the minority among the established CFTR modulators and non-existent

for podocytopathies. Recently, using virtual screening approach together with molecular dynamic simulation methods Wieczorek and Zielenkiewicz discovered four novel effective molecules, which are able to rescue trafficking defect of F508del-CFTR, resulting in correction of CFTR function both in CF human cells and mice [156], [157]. One of the most promising chemical molecules identified is 407882 (c407 in this document) that has two phenylphosphinic acid moieties and is able to inhibit K8-F508del-CFTR interaction [157]. Furthermore, 407882 is a water-soluble molecule, which makes it beneficial for drug administration, and was shown to target mutant CFTR back to the plasma membrane [157].

Based on the work done by Colas *et al.* that proposed a potential dominant role for cytokeratin network in mutant CFTR misprocessing, it was suggested that K8 and/or K18 might also interact with the R138Q podocin mutant. Therefore, the aim of the present work was to confirm and study the molecular basis of this interaction on R138Q podocin localization and function, and to examine whether the disruption of this interaction with K8 silencing or compound c407 rescues R138Q podocin localization back to the plasma membrane and corrects its functional defect both *in vitro* and *in vivo*.

5.1.2 Cytoplasmic intermediate filaments

The major structural feature of all eukaryotic cells is their well-developed cytoskeletal systems, which predict cell shape and perform a variety of cellular roles. As previously underlined in Chapter 1, two major ubiquitously expressed cytoskeletal polymers (F-actin and microtubules) are present in the cytoplasm of eukaryotic cells, however a third fibrous polymer of the cell, called intermediate filaments (IFs), was more recently discovered [158]. A minimum of 67 genes have been revealed to date through molecular cloning to encode various IF proteins, which are able to self-assemble into the distinctive 10-12-nm-wide cytoskeletal filaments as seen by electron microscopy [159]. Analogously to microtubules and microfilaments, IFs are dynamically regulated in cells, where they participate in the cytoskeletal network assembly of the cytoplasm and interact with a variety of cellular proteins [160]. These flexible fibrous polymers can also be found in the nuclear lamina meshwork, where they are recognized as nuclear lamins [160]. Nonetheless, there are a number of characteristics that are unique to intermediate filaments and apart from their shared conserved substructure and sequence, these features include: a lack of the intrinsic polarity that is fundamental for actin filaments and microtubules; their association with other proteins and structures; and their control of

filament dynamics is independent of ATP binding and hydrolysis [161],[162],[163]. Therefore, IFs are predicted to carry out functions that are distinct from those of other cytoskeletal polymers. At the protein level, IFs can be classified into five groups according to polymerization properties. Type I and Type II groups consist of proteins that correspond to cytokeratins (CKs), while Type III group includes proteins, such as vimentins and desmin, which are produced by mesenchyme derived cells [160]. Type IV group includes proteins, such as internexin, which are mainly found in neuronal cells, while Type V is defined by proteins located in the nuclear envelope [160].

All IF proteins show a characteristic ternary domain architecture with a centrally located domain being of a fixed length, either 310 or 352 amino acid residues [158]. However, the main universal feature of these proteins is the presence of a common motif composed of four alpha-helical segments found in the central domain, which is flanked by nonhelical linker parts, head and tail (Figure 5.2) [160]. Both head and tail domains can vary in length and primary structure adding to the heterogeneity found within the family of IFs [158]. The alpha helix displays a specific distribution of hydrophobic/apolar amino acid residues, thus allowing helices to connect in a coiled coil rod, the foundation block of the IF proteins [164]. This rod domain further contains highly conserved signature motifs located at the N- and C-termini. Moreover, IF proteins can associate with other IF-associated proteins to form macrofibrils in secondary structure, which are connected by disulfide bonds in the case of hair for example [160]. These proteins are also known to undergo several post-translational modifications (PTMs), such as phosphorylation and glycosylation [160]. The interactions with other proteins and these PTMs together are essential in establishing the function and dynamics of IFs in various cell types, some of which will be outlined in the next section.

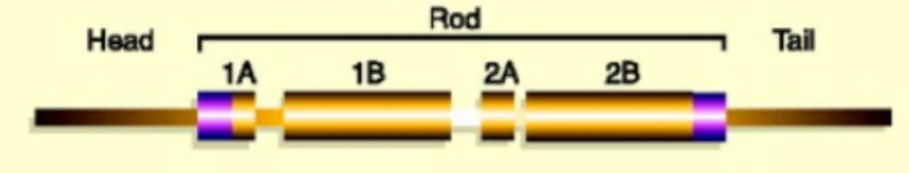

Figure 5.2 Secondary structure of IF proteins. A centrally located domain is composed of 4 alpha-helical segments (subdomains 1A, 1B, 2A and 2B) forming a rod in secondary structure, which features highly conserved signature motifs at its N- and C-termini (magenta coloured boxes). This rod domain is further flanked by non-helical head and tail domains. Reproduced from Coulombe *et al* [158].

5.1.3 Keratins - versatile structures

Keratins (Ks), the distinctive IF proteins produced by epithelial cells, represent the largest class of cytoskeletal proteins, which are subdivided into Type I 'acidic' (K9–K28) and Type II ' neutral-basic' (K1–K8 and K71–K80) subgroups [165]. Keratin IFs are typically arranged into bundles, called tonofibrils, which are able to form cage-like structures surrounding the nucleus and expanding from the perinuclear space towards the cell periphery, where they make contacts with adhesive structures [160]. Keratin IFs form non-covalent heteropolymers of members of Type I and Type II subgroups by antiparallel binding, which are expressed as pairs in a highly differentiation-specific way, suggesting functional diversity [163]. The pairs formed can be further classified into two or three expression subgroups: simple keratins, keratinocytes and structural keratins [160]. The keratin K8/K18 pair represents the first IFs expressed during embryogenesis, and is present in all simple epithelial linings, such as kidney and liver, in the adult [163]. When an impaired pairing of individual keratins occurs, the mispaired keratin either enters a degradation pathway or associates with proteins involved in apoptosis and signalling events, thus opening a window into a new field of CKs functions [160].

Considering their mechanical roles, keratin IFs have been recognized as stable cytoskeletal elements, however, it is now well known that they are highly dynamic scaffolds *in vivo* [160]. These proteins participate in the variety of cellular events, including migration and proliferation, and particularly, IFs aid the positioning of intracellular organelles [160]. Nevertheless, the discovery of cytokeratin mutations and their study in mice allowed to determine some non-structural functions of these proteins, some of which are highlighted below [166]. These proteins show selective localization in epithelial cells, where they protect epithelia against multiple kinds of stresses and perform a number of additional roles [165]. Other additional functions include their involvement in cell signalling and apoptosis, along with unique properties emerging, which are keratin specific and tissue specific (Figure 5.3). The keratin IFs are able to protect cells against mechanical stress by forming a 3-D complex that interacts with desmosomes and hemidesmosomes [160]. The work done on hepatocytes isolated from mice synthesizing keratins that have mutated phosphorylation sites has revealed that these cells were able to cope with mechanical stress subsequent to liver perfusion [167]. Therefore it has been suggested that, during stress, K8 and possibly other keratins might act as a 'sponge' for stress-activated phosphate kinases, and in doing so provide a protective mechanism [166]. A role of

keratins in cell cycle regulation has been recently acknowledged from the work on hepatocytes of K8- and K18-deficient mice, where an elevated accumulation of the signalling 14-3-3σ protein was observed [168]. Enlarged nuclei with a doubled DNA content have been found in these cells, suggesting that absence of keratin filaments results in cells entering the S-G2 cell cycle phase, which further causes abnormal cytokinesis [168]. Keratins have been also seen to play a role in the attenuation of apoptosis both at the death receptor and cellular levels [160]. The evidence comes from the work done on the keratin 8-deprived hepatocytes isolated from K8-null mice, which are more resistant to Fas (tumour necrosis factor alpha receptor)-mediated apoptosis in comparison to wild-type cells [169]. IFs are implicated in the trafficking of proteins to their intracellular compartments in polarized epithelia, while they also participate in the regulation of ion transporters, such as CFTR (cystic fibrosis transmembrane conductance regulator) [160]. The latter is based on the evidence that CFTR is mistargeted in K8-null small intestine villi [170]. Here, most of the work will be focused on the IF-related protein-targeting functions.

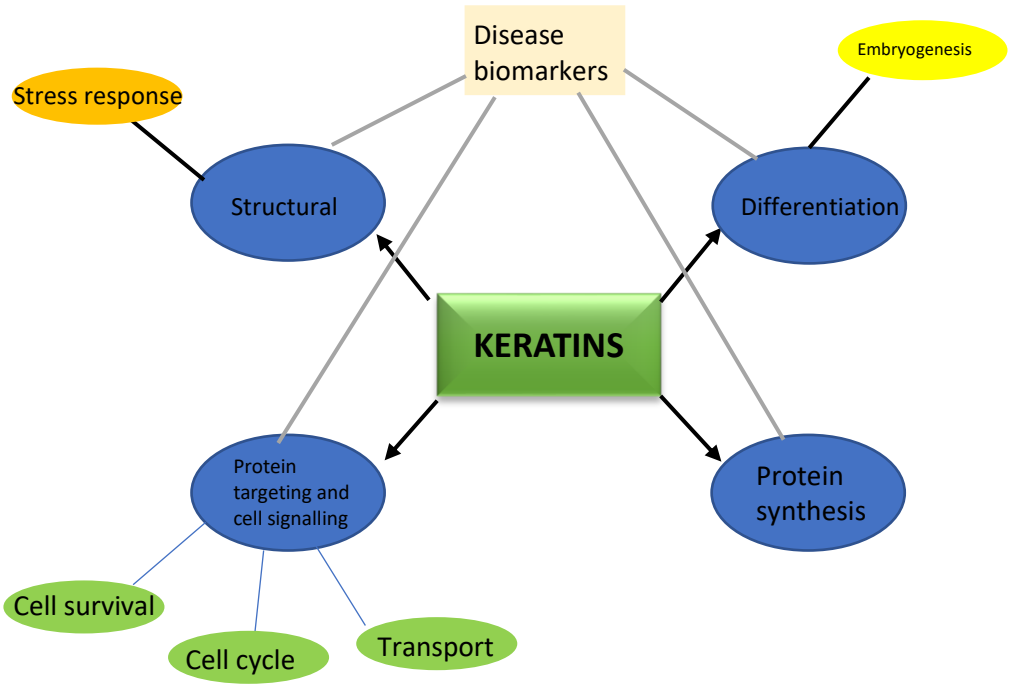

Figure 5.3 A schematic diagram demonstrating the main functions of keratins. Four main roles, namely structural, differentiation, protein targeting and synthesis, are in agreement with the rest of functional aspects. The role of keratins as disease biomarkers is connected to the main functions by grey lines. Modified from Brouillard *et al* [160].

5.2 Results

5.2.1 Intracellular localization of R138Q podocin

In this work, the consequence of the R138Q mutation of podocin was studied by expressing the GFP-tagged wild-type and R138Q mutant podocins in human podocytes. As shown in Figure 5.4a, wild-type podocin displayed a localization consisting of a plasma membrane staining and an intracellular vesicular labelling. On the other hand, the R138Q podocin mutant was strongly retained in the ER as seen by complete colocalization with calnexin, an ER marker. Furthermore, TIRF microscopy was used to access podocin's localization at or near the plasma membrane in human podocytes. The fluorescence signal obtained by TIRF imaging represents podocin within 100 nm of the coverslip, i.e., in or in close proximity to the plasma membrane. As anticipated, the mutant podocin displayed no plasma membrane labelling, while wild-type podocin localized with F-Actin at the plasma membrane (Figure 5.4b). Next, flotation gradient centrifugation was used to determine whether the disease-causing mutation of podocin interfered with its ability to associate with lipid rafts. In flotation gradients of Triton X-100 extracts, detergent-insoluble raft-associated proteins represent the first 4 fractions, while detergent-soluble protein/protein complexes are identified as fractions 5-8, 9-12. The quality and purity of the fractions were examined using Flotillin-1, as a lipid raft marker. As expected, the R138Q podocin was not able to associate with lipid rafts due to its ER retention, causing lipid raft composition to be altered, while wild-type podocin reached the plasma membrane and associated with detergent-resistant membranes (Figure 5.4c).

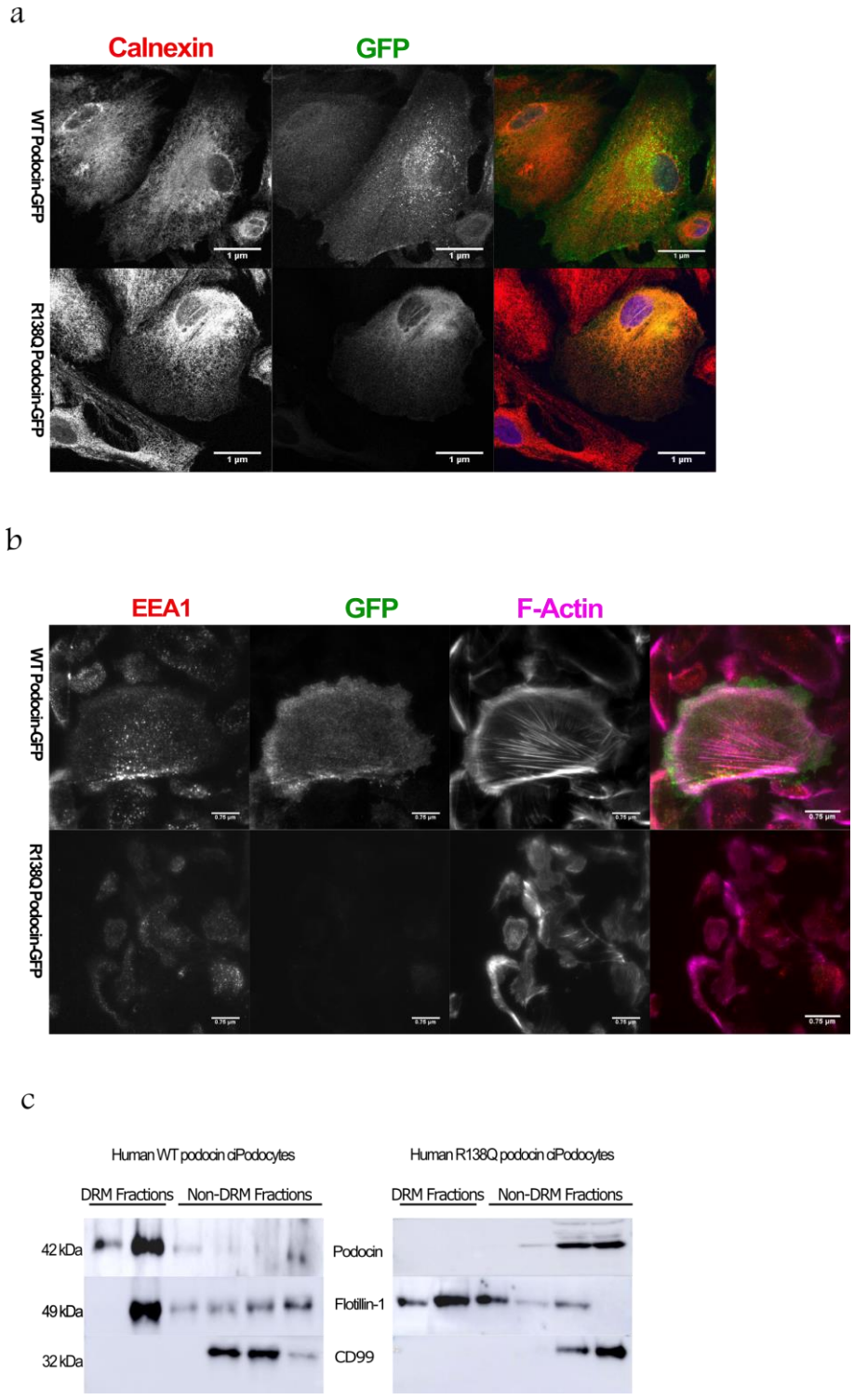

Figure 5.4 Effect of disease-causing podocin mutation. (a) Confocal images showing immunofluorescence staining of GFP-tagged podocin constructs and the ER protein calnexin in conditionally immortalized human podocytes. Scale bar=1 µm. (b) TIRF images of GFP-tagged podocin constructs and an early endosomal marker-1 (EEA1) with F-actin. Scale bar=0.75 µm. (c) Lipid raft isolation experiment of either the endogenous wild-type or mutant podocins. The quality and purity of the fractions were examined using Flotillin-1, as a lipid raft marker, and absence of CD99, as a plasma membrane marker.

5.2.2 Keratin 8/18 and podocin

In the next set of experiments, the intracellular distribution of keratin 8/18 was analysed in human podocytes expressing either the GFP-tagged wild-type or R138Q mutant podocins using confocal microscopy. Localization of keratin 8 and WT podocin was shown by immunofluorescence at the cytosol level, while localization of keratin 8 was seen in the perinuclear area in close vicinity of R138Q podocin (Figure 5.5a). Here, the keratin 8 expression was elevated, and the keratin 8 network reorganized itself to form the meshwork like structure, further trapping the mutant protein in the ER. The same was observed for Keratin 18 (Figure 5.5b). Next, an immunoblot and qPCR analyses were performed to verify the expression of K8 and K18 on both the protein and RNA levels in human podocytes. The results confirmed the observation of the immunofluorescence analysis, both K8/K18 protein and RNA expression levels were significantly higher in human podocytes derived from the patient bearing R138Q mutation (Figure 5.5c, d).

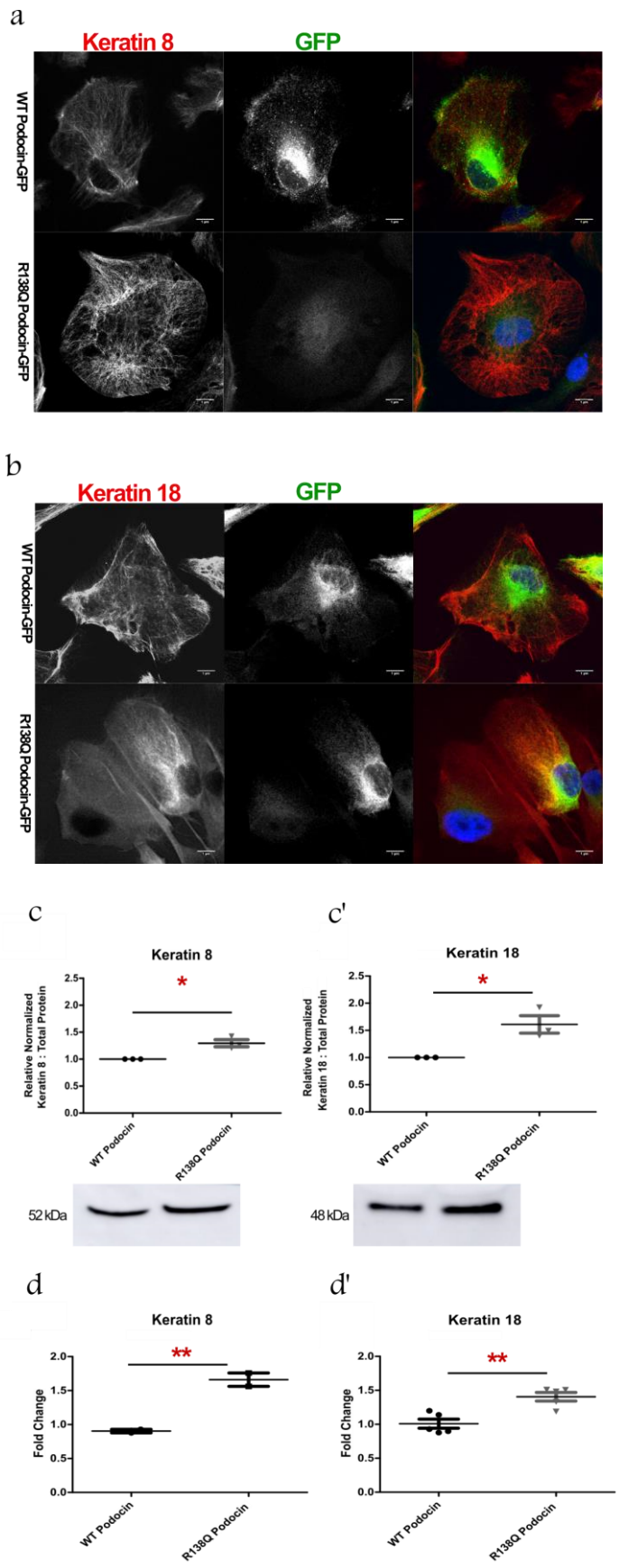

Figure 5.5 Analysis of Keratin 8/18 expression levels using Immunofluorescence, Western Blotting and qPCR. (a, b) Colocalization of K8/K18 and GFP-tagged podocins in

human podocytes. Scale bar=1 µm. (c, c') Immunoblot analysis showing that K8 and K18 protein expression levels are significantly increased in mutant podocytes compared to wild-type cells. The expression profiles were normalized to the total protein. Differentiated ciPod n=3, two-tailed T-test *≤0.05. (d, d') RNA expression profiles of keratin 8 and keratin 18, two-tailed T-test *≤0.05

5.2.3 Keratin 8-R138Q podocin interaction

Co-immunoprecipitation (Co-IP) assay of endogenous proteins was then conducted to see whether keratin 8 and podocin interact directly in human podocytes. Co-immunoprecipitation experiments demonstrated that endogenous keratin 8 preferably interacts with R138Q podocin over its wild-type counterpart (Figure 5.6a). To further search for K8-Podocin interaction *in vitro*, the Proximity Ligation Assay (PLA) was performed using the Duolink™ kit (Eurogentec, Angers, France) according to manufacturer's instructions in human podocytes derived from either a healthy patient or a patient with R138Q mutation [130]. The PLA is a highly sensitive and specific approach that can directly detect proteins and protein interactions within 40 nm proximity in unmodified cells. A <40 nm proximity between K8 and R138Q podocin was identified in human podocytes (Figure 5.6b). This strongly suggests that detectable physical interaction between K8 and podocin only prevails for the R138Q mutation.

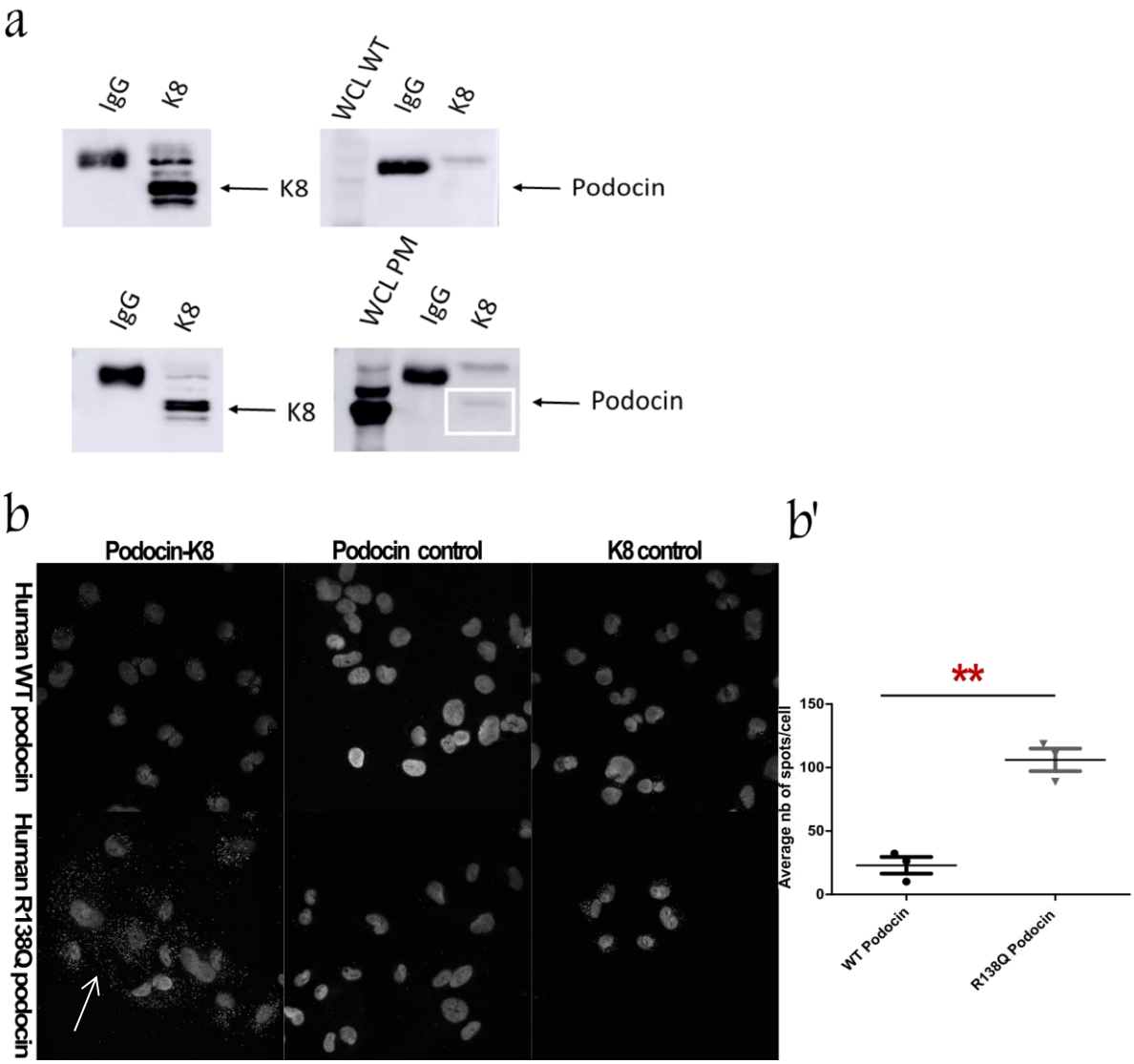

Figure 5.6 Keratin 8-R138Q podocin interaction. (a) Anti-keratin 8 antibody precipitated keratin 8 and co-precipitated podocin in human podocytes derived from the patient with R138Q mutation. Mouse-IgG was used as a control. (b) Molecular proximity of K8 and wild-type/R138Q podocin in human podocytes. No primary antibody was used as a negative control. Scale bar=20 µm. (b') Results are representative of 3 independent experiments, two-tailed T-test *≤0.05.

5.2.4 Silencing of keratin 8 restores R138Q podocin's localization and function in patient's cells

In this study, we hypothesized that inhibiting the keratin 8-R138Q podocin interaction by keratin 8 silencing might rescue the lipid raft association of the mutant protein and restore its functional defect. All K8-shRNA sequences considerably decreased K8 expression in both human podocyte cell lines (Figure 5.7a). The effect of keratin 8-shRNA on lipid raft association of mutant podocin was studied in patient's cells. Knockdown of keratin 8 in

mutant podocytes restored the association of the R138Q podocin with lipid rafts, while non-coding shRNA had no effect (Figure 5.7b). Finally, to evaluate the functional impact of keratin 8 silencing, human K8 shRNA podocyte cells were further analysed for their adhesive capacity in an *in vitro* adhesive assay. There was a significant decrease in adhesion observed in GAPDH shRNA mutant podocyte cell line, when compared to the wild-type control. This adhesive defect of the mutant podocyte cell line was rescued by knock-out of K8 (Figure 5.7c).

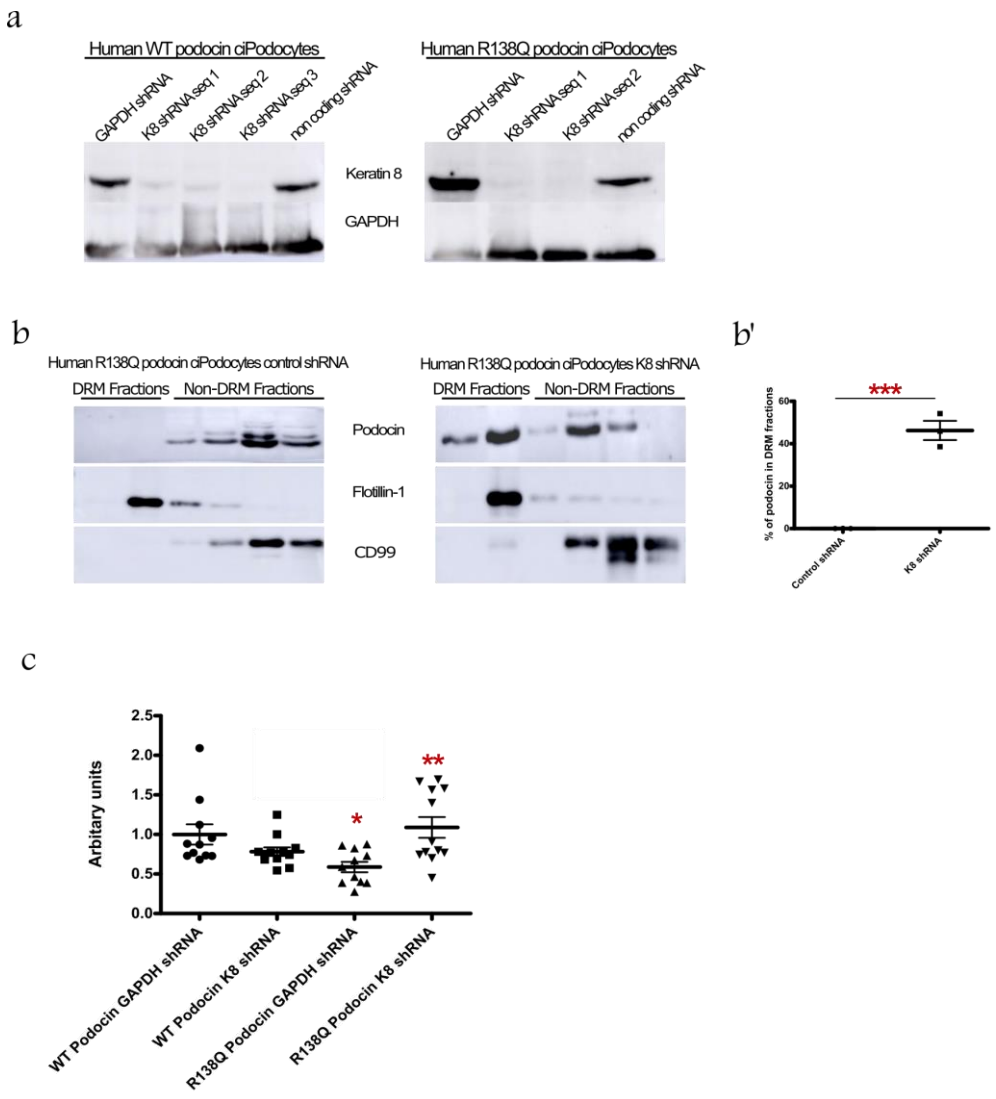

Figure 5.7 Effects of Keratin 8 silencing. (a) Western blots of protein lysates showing the effect of shRNA treatment on keratin 8 expression in human podocytes derived either from a healthy patient or a patient with the R138Q mutation. Cells were treated either with non-coding shRNA, GAPDH shRNA or with Seq. 1/2/3 of K8 KO shRNA. (b, b') Seq.1 of K8 KO shRNA restored the association of R138Q podocin with lipid rats. The quality and purity of the fractions were examined using Flotillin-1 as lipid raft marker and the exclusion of CD99 as a marker for non-raft associated proteins. Two-tailed T-test *≤0.05. (c) The adhesive defect of the cells was rescued using K8 shRNA sequence, while GAPDH shRNA had no effect. One-way ANOVA p≤0.05. n=3 with 4 biological repeats in each.

5.2.5 Molecular modelling

To create the computer model of podocin and to study the effect of R138Q mutation on podocin structure, the podocin amino acid sequence was submitted to the HHPred server (Protein homology detection and structure prediction server). The best matching structure found was the stomatin core domain from *Pyrococcus horikoshii* (PDB 3BK6) providing a gapless alignment between residues 158-316 with a 37% sequence identity in this region. The model shows that R138 is in a sequence of hydrophobic amino acids (IFRL; 136-139) located on the tip of a reverse turn in the middle of a β-sheet, flanked on either side by loops bearing mostly hydrophobic residues (Figure 5.8a). Consequently, the R138Q mutation, replacing the positively charged arginine with the neutral residue glutamine, will essentially merge these regions into a larger hydrophobic patch. This is illustrated in Figure 5.8b, where the protein surface is coloured by amino acid hydrophobicity. Computer modelling was used to see if the c407 ligand could bind adjacent to the hydrophobic patch on the R138Q surface. Some molecular dynamic simulations were further performed to see if the c407 remains bound under more realistic conditions. It was predicted that c407 fits into the hydrophobic pocket of R138Q podocin (Figure 5.8c). This work was performed by Dr. Richard Sessions, University of Bristol.

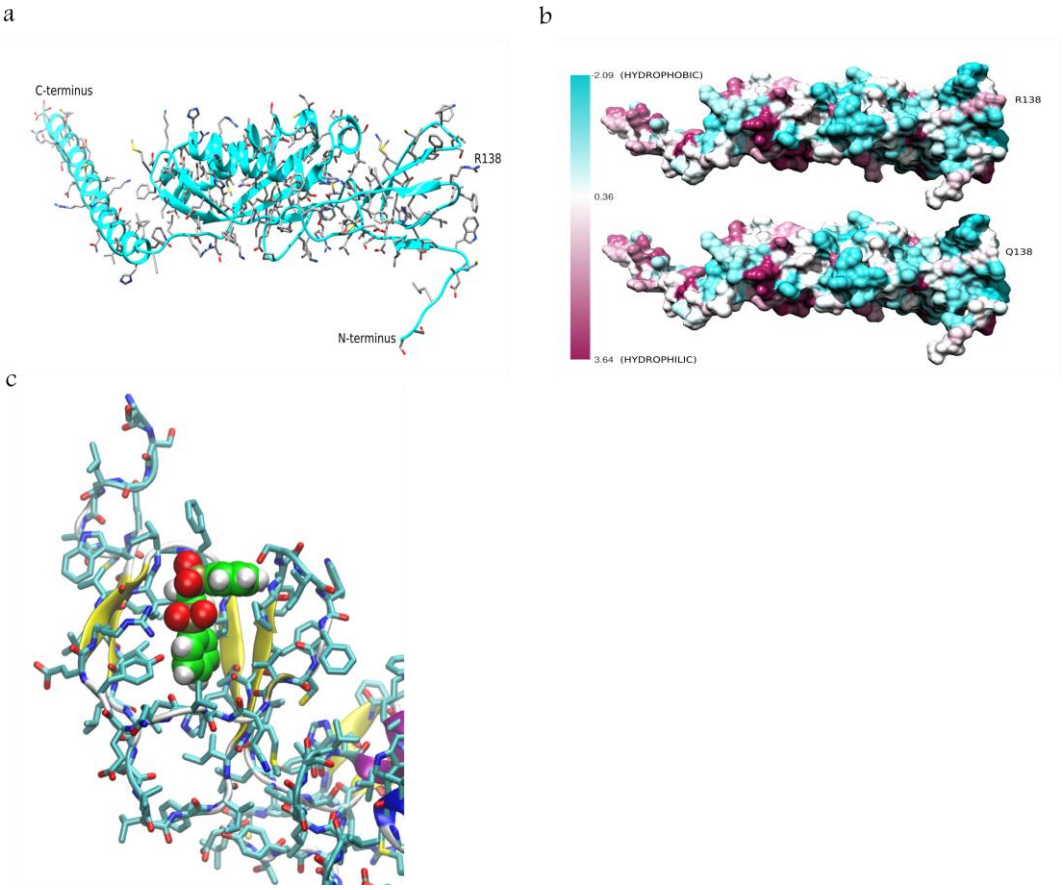

Figure 5.8 Molecular modelling. (a) A ribbon diagram of the podocin model (residues 95-314) showing the amino acid side chains as sticks and coloured by atom type. Arginine 138 is labelled. (b) Surface representations of the wild type podocin model (upper) and the R138Q mutant (lower) coloured by hydrophobicity. The scale on the left is the experimental free energy of transfer from water to octanol in kcal/mol. (c) The c407 ligand is able to fit into the hydrophobic pocket created by the replacement of arginine residue at position 138.

5.2.6 Novel compound c407 disrupts Keratin 8-R138Q podocin interaction

Since c407 disrupts the F508del-CFTR interaction, immunofluorescence studies were performed to see whether treatment with c407 for 24 hours rescued mutant podocin localization back to the plasma membrane. Figure 5.9a shows immunofluorescence images of Podocin (green) and Keratin 8 (red) in human podocytes stably expressing either GFP-tagged WT podocin or R138Q podocin mutant in control conditions and after treatment with c407. Treatment with c407 rescued the localization of mutant podocin back to the plasma membrane by decreasing the keratin 8 expression, as anticipated. Furthermore, c407 treatment decreased both keratin 8 and 18 protein expression levels detected by Western Blotting (Figure 5.9b). Next, to test the theory human podocytes

derived from the patient with the R138Q mutation were treated with c407 to see whether it caused the targeted disruption of the protein-protein interaction *in vitro*. As expected, c407 interrupted the K8-R138Q podocin interaction, while treatment with NaOH had no effect, where the K8-R138Q podocin interaction was observed using Co-IP (Figure 5.9c).

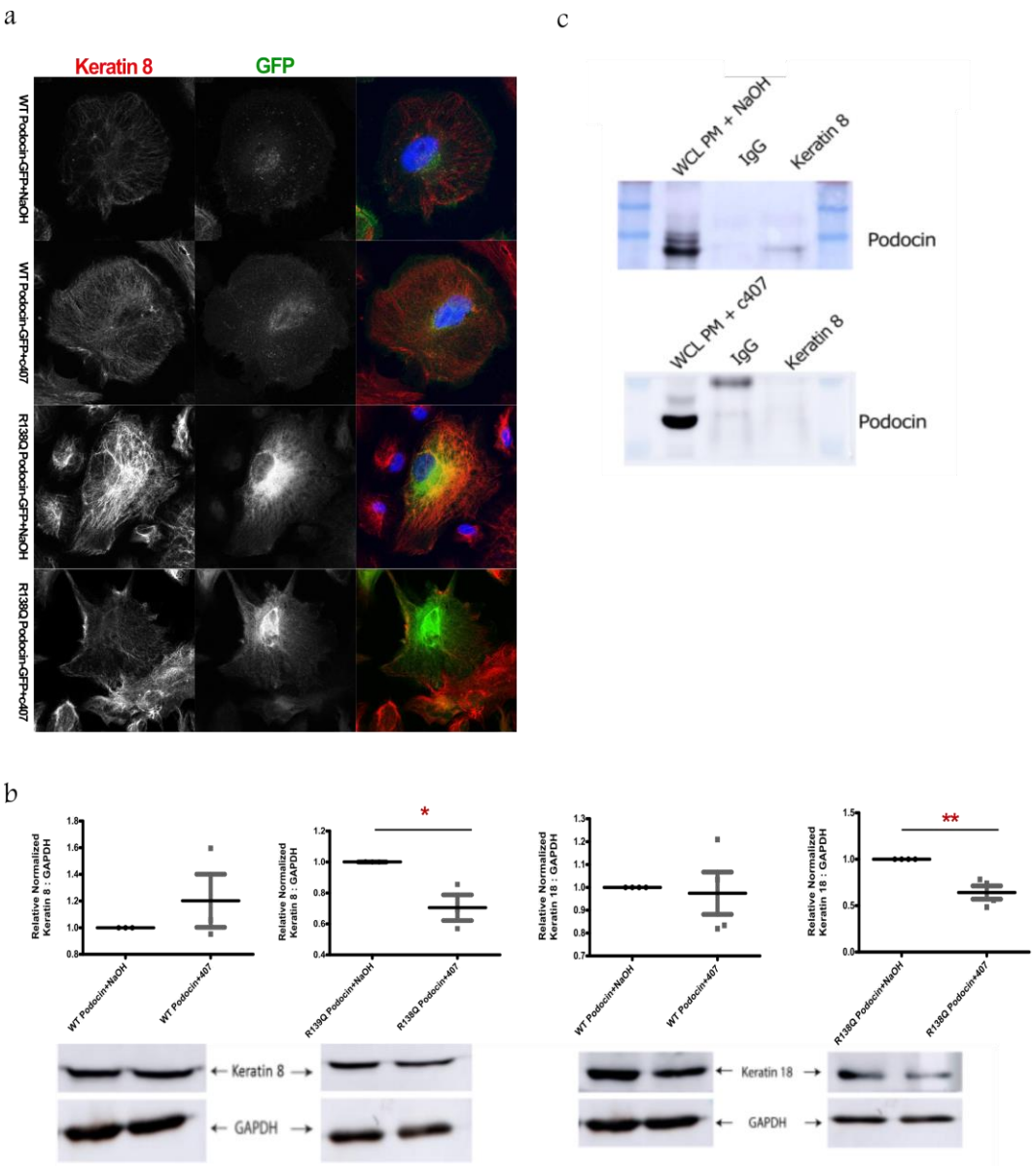

Figure 5.9 Treatment with c407 rescues R138Q podocin localization. *(a) Podocytes stably expressing either WT podocin or R138Q podocin mutant were subjected to GFP and K8 immunodetection and analysed by confocal microscopy. (b) Effect of c407 treatment on the K8/18 protein expression levels in human podocytes derived from either a healthy patient or a patient with R138Q mutation. Results are representative of 3 independent experiments, two-tailed T-test *≤0.05. (c) Co-IP was performed to see whether treatment with c407 disrupts K8-R138Q podocin interaction in human mutant podocytes.*

5.2.7 Inhibition of K8-R138Q podocin interaction by c407 restores function of the mutant protein

To test whether compound c407 interrupts the direct protein-protein interaction, a series of proximity ligation experiments were performed on human podocytes derived either from a healthy patient or patient with the R138Q mutation. Figure 5.10a demonstrates that there is a significant decrease in K8-R138Q podocin interaction, indicated by green fluorescent spots, after treating cells with c407. Furthermore, that disruption of interaction results in functional correction of the mutant protein as seen by two sets of experiments: (a) lipid raft isolation in human mutant podocytes and (b) an adhesion assay. Subsequent treatment with c407 allowed the association of mutant podocin with specialized lipid raft microdomains of the plasma membrane, while also restored the lipid raft composition (Figure 5.10b). Finally, the adhesive defect of the mutant cells was corrected with c407, while treatment with NaOH had no effect (Figure 5.10c).

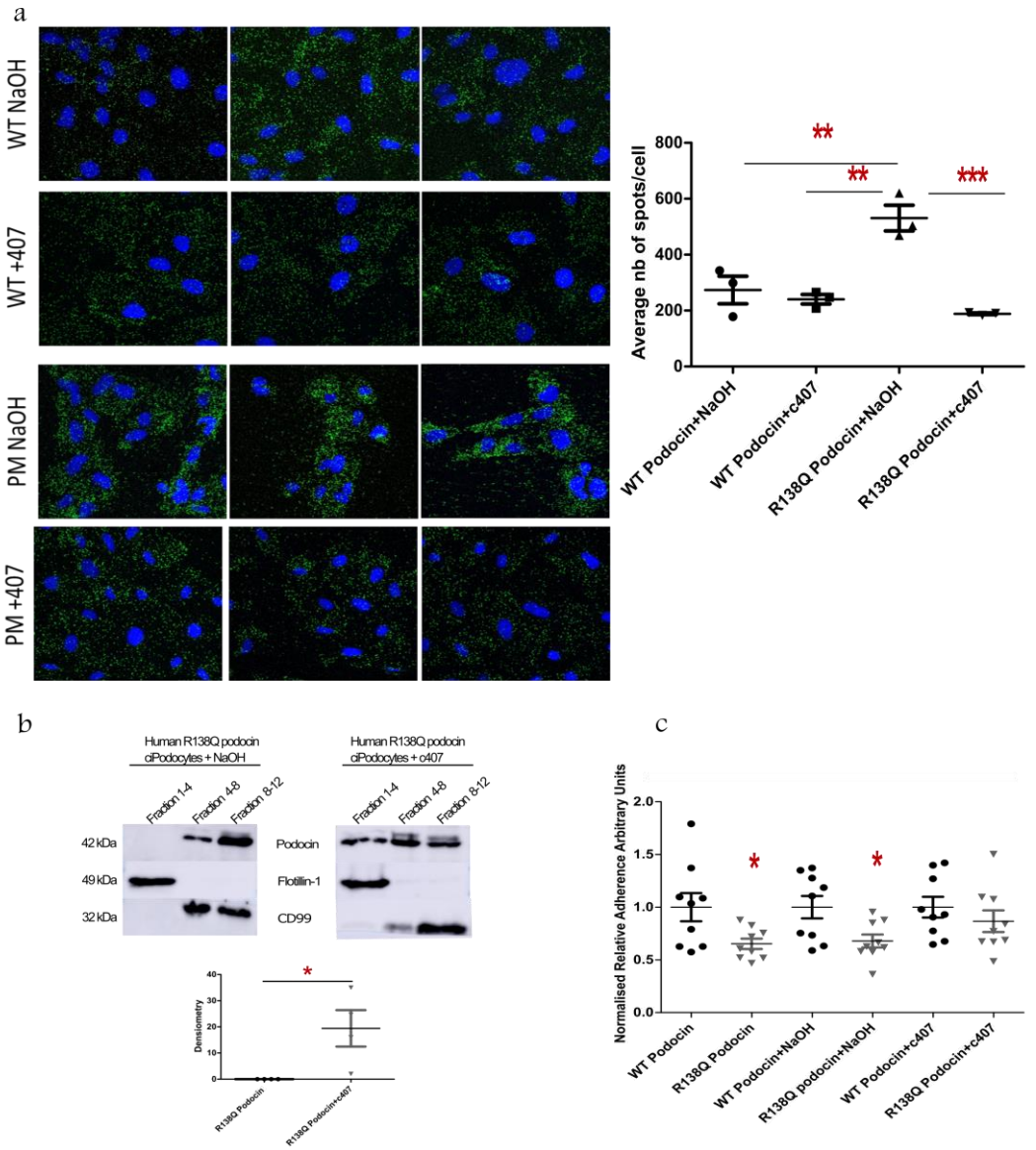

Figure 5.10 Effect of c407 on the R138Q podocin's function and interaction. (a) Proximity ligation assay of K8 and WT/R138Q podocin in human podocytes derived either from a healthy patient or a patient with the R138Q mutation. Green spots correspond to K8/Podocin interaction (proximity of less than 40nm). Nuclei (DAPI) is stained blue. Results are representative of at least three independent experiments; one-way ANOVA $p \leq 0.05$. (b) R138Q podocin is found in the DRM fraction (fraction 1-4) after c407 treatment. Flotillin-1, raft marker, was used to confirm the purity of the fractions. Two-tailed T-test *≤0.05. (c) Cell adhesion assay to see the effect of c407 on the adhesion of both cell types. Differentiated ciPod n=3, Two-tailed T-test *≤0.05.

5.2.8 C407 treatment prevents the development of NS in the transgenic mouse model of the R140Q mutation

To understand whether c407 could prevent the development of NS in *NPHS2*$^{flox/R140Q}$ mice, doxycycline was administrated for 3 weeks, at the same time as one group was treated with c407 and another group was treated with vehicle (0.9% NaCl) for 4 weeks via osmotic mini pumps. A third group with vehicle pumps served as no disease controls and was administrated drinking water for the duration of the study. Doxycycline animals treated with vehicle, developed proteinuria within the first two weeks of R140Q hemizygosity induction, which peaked at Week 4 as anticipated (Figure 5.11a). On the other hand, c407 treatment significantly prevented the development of proteinuria in R140Q mice starting from Week 2, and also reversed podocytes loss associated with NS induced by doxycycline (Figure 5.11 a, c). Furthermore, experimental mice displayed hypercholesterolemia, hypoalbuminemia and high blood urea levels, all of which were prevented upon administration of c407 (Figure 5.11b). Finally, the Cre/LoxP system was used to excise podocin on both alleles in NPHS2 $^{flox/flox}$ mice leading to total podocin knockout in these animals. These mice were used as controls to prove the theory that c407 only targets misfolded proteins. These mice displayed no change in proteinuria levels upon administration of c407 at disease induction via osmotic mini pumps, as anticipated (Figure 5.11d).

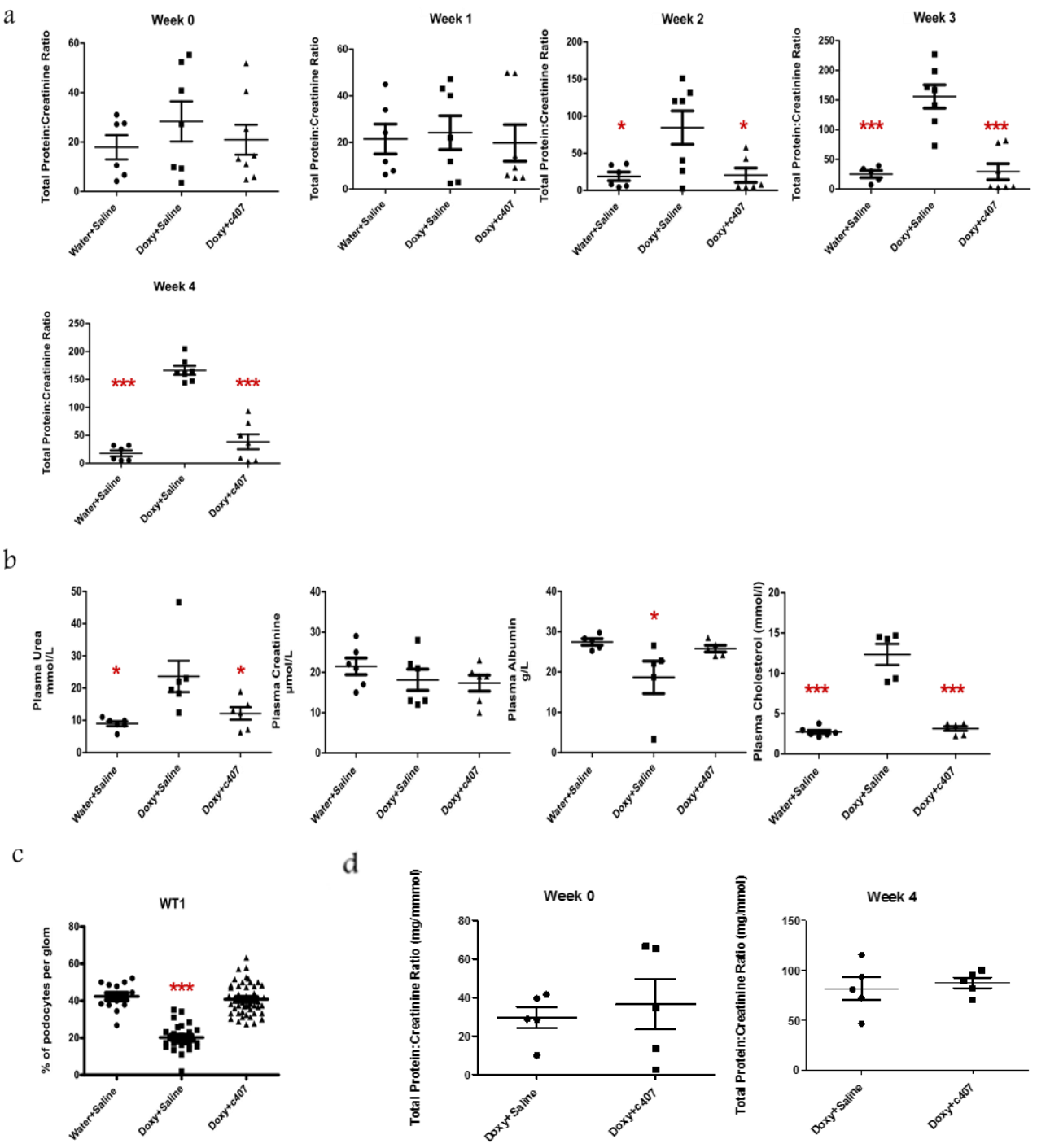

Figure 5.11 In vivo treatment with c407. (a) Induced control mice developed severe proteinuria at 4 weeks after doxycycline induction, which was prevented in c407 mice. One-way ANOVA p≤0.05. (b) Control mice display hypercholesterolemia, hypoalbuminemia and high blood urea levels, all of which is prevented upon administration of c407. One-way ANOVA p≤0.05. (c) Treatment with c407 prevented podocyte loss in R140Q mice. One-way ANOVA p≤0.05. (d) c407 treatment had no effect on the proteinuria levels of the NPHS2 $^{flox/flox}$ mice. All mice were between 4-6 weeks old.

5.2.9 Immunofluorescence and histological analysis

Decreased podocin protein expression was observed at week 4 in in *NPHS2*$^{flox/R140Q}$ mice, which were given doxycycline for 3 weeks compared to that of healthy controls. *In vivo* c407 treatment restored mutant podocin localization back to the plasma membrane as seen by immunofluorescence on mice kidney sections (Figure 5.12a). By contrast, Keratin 8 was seen to be upregulated in glomeruli of mutant mice, and treatment with c407 resulted in restoration of minimal keratin 8 expression in glomeruli (Figure 5.12b). Furthermore, foot process effacement, FSGS and glomerulosclerosis with protein casts were observed in those animals, as seen on kidney histology and EM, which were prevented with c407 treatment, as anticipated (Figure 5.12c).

a

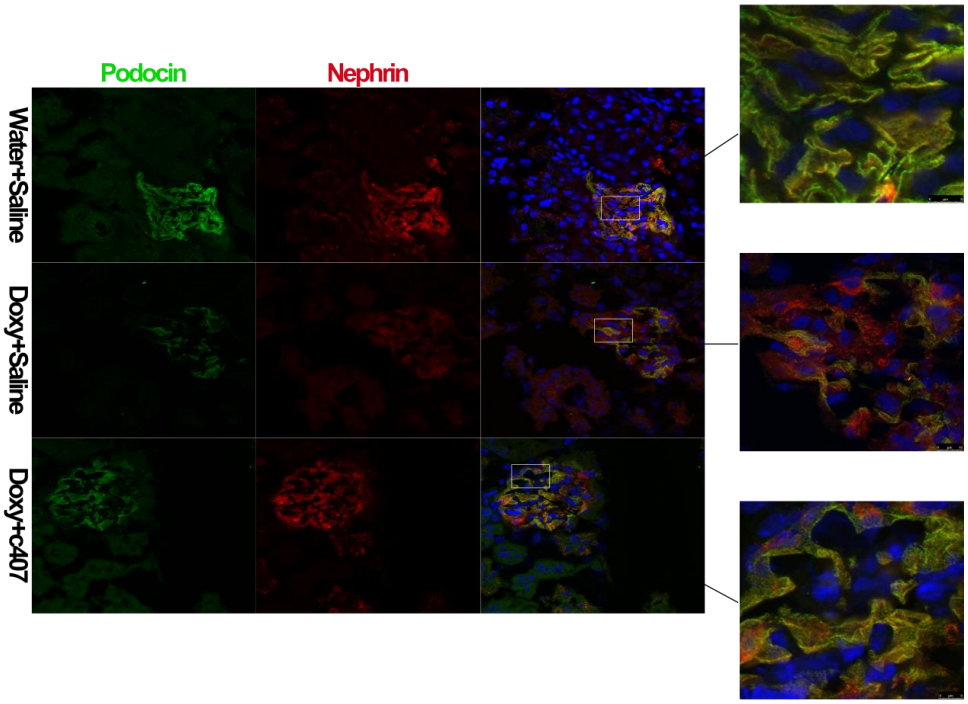
Podocin
Nephrin
Water+Saline
Doxy+Saline
Doxy+c407

b

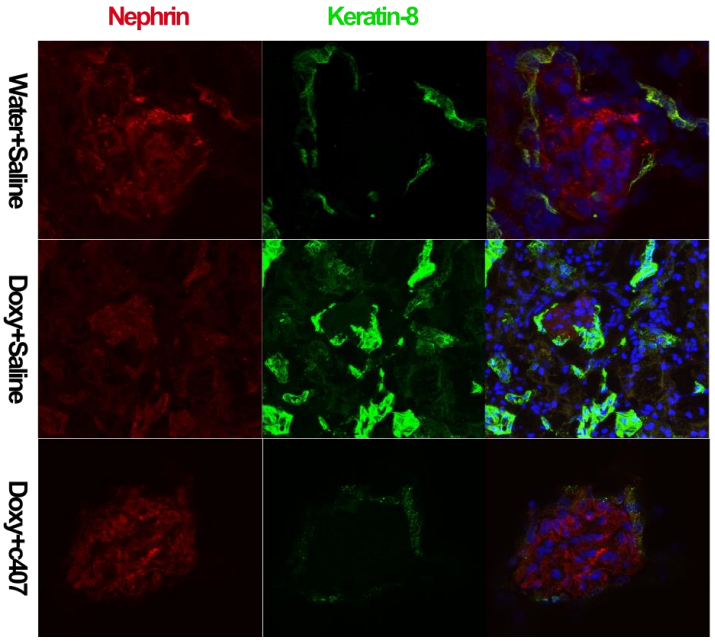
Nephrin
Keratin-8
Water+Saline
Doxy+Saline
Doxy+c407

c

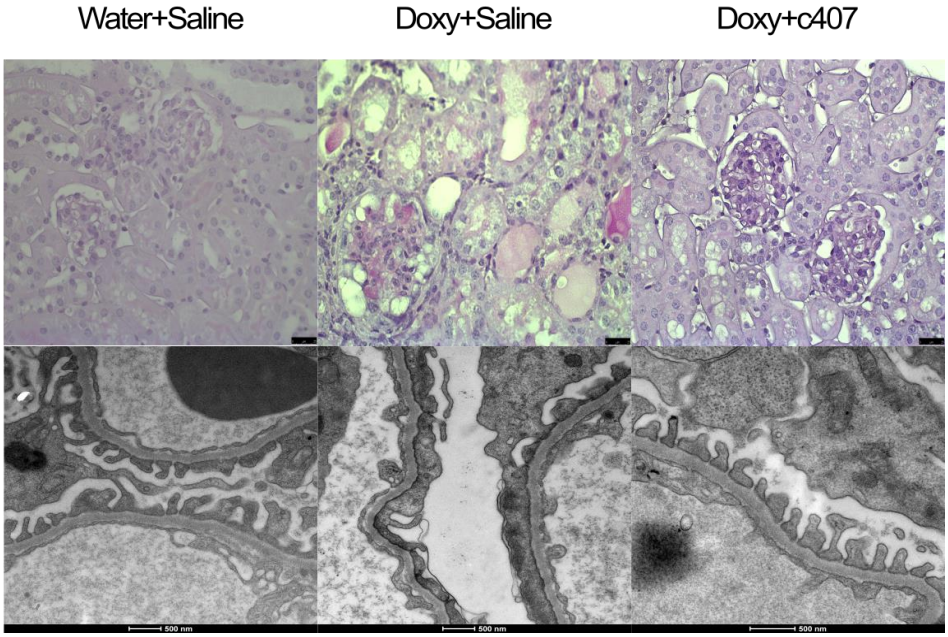

Figure 5.12 Immunofluorescence and histological analysis. (a) Confocal images of podocin and nephrin performed on the NPHS2$^{flox/R140Q}$ mice kidney sections. Treatment with c407 rescued the mutant podocin localization in mice. Magnification, X63; zoom, x8. (b) Keratin 8 expression was elevated in glomeruli of diseased animals, which was brought back to normal upon treatment with c407, as seen by immunofluorescence. Magnification, X63; zoom, x8. (c) These mice developed FSGS with the large percentage of glomeruli affected by sclerosis. Mice that were given the c407 compound demonstrated normal histology. Magnification, x40. Podocytes loss and effacement was observed in doxy+saline mice. Scale bar=500 nm.

5.3 Discussion

As mentioned in Chapter 1, NS is a common renal disease identified in children of a wide range of ages and characterized as a triad of proteinuria, hypoalbuminemia and edema. Although a lot of work has been previously done to identify molecular mechanisms underlying the nature of the disease, NS is still categorised as steroid-sensitive NS (SSNS) and steroid-resistant NS (SRNS) based on the patient's response to steroid therapy [125]. Using a positional cloning approach, a number of genes mutated in SRNS patients have been revealed, amongst which mutations in *NPHS2* gene represented the most common cause [171]. Histologically, patients bearing *NPHS2* mutations initially present with minimal glomerular changes observed on renal biopsies, which at later stages develop into FSGS and in the majority of clinical cases rapidly progress to ESRD [69].

The majority of the functional studies addressing the link between cytoskeleton and proteins, such as podocin, have been mainly focused so far on proteins that are involved in the actin network assembly. The mode of action of both microtubules and actin filaments in protein sorting and trafficking is well described; while no significant information is present that reveals the role of IFs in this process. However, a number of recent studies have identified new functions of IFs, specifically of keratins, filament-forming proteins of epithelial cells. Indeed, a novel function of IFs in vesicular trafficking and protein sorting was first reported in the studies showing altered trafficking of membrane proteins, such as CFTR [130].

The present work describes previously unknown machinery that plays role in the R138Q podocin intracellular retention and firmly suggests that keratin 8-R138Q podocin association facilitates the ER retention of the mutant protein. Keratins have been previously reported to be up-regulated in different disease models, such as animal models of pancreas and liver injury [172], while keratin 8 and 18 have been recently described to be novel markers of renal epithelial cell injury [173]. The current study reports an increased expression of keratin 8 in R138Q mutant human podocytes for the first time. There is also an increased interaction of keratin 8 and podocin in close vicinity of the ER in R138Q mutant cells, which is reversed by treating cells with c407, resulting in the rescue of the mutant protein localization. When addressing the localization of R138Q podocin at the plasma membrane, the crucial question to ask is whether the mutant protein is functioning correctly. Nephrotic Syndrome podocytes are known to display changes in actin cytoskeleton organization associated with defects in adhesion and migration [174].

Excitingly, a full rescue of adhesion function of mutant cells was achieved upon treatment with c407. Furthermore, computer modelling of protein folding revealed that R138Q mutation creates a large hydrophobic region, which becomes exposed for interaction with other proteins or small molecules, such as c407. Therefore, it is tempting to hypothesize that K8-R138Q interaction occurs as a result of the appearance of this hydrophobic pocket, and that c407 is able to bind to this pocket blocking the interaction with K8 and thus allowing for the correction of the R138Q podocin processing defect.

The importance of the keratin 8 network in the mutant protein misprocessing is supported in the context of the cell response to keratin 8 silencing. Various gene-ablation techniques have been widely used therapeutically to target lipopolysaccharide-induced proteinuria [175] or renal fibrosis [176] for example. Furthermore, keratin 8 mRNA silencing has been studied experimentally; K8 knockdown in the cancer cell line MCF-7 resulted in loss of cell adhesion and collective migration, and an abolition of multidrug-resistant phenotype of these cells [177],[178]. To date, to our knowledge, keratin 8 expression was modified for the first time in the kidney field in the current study. Here, we demonstrate that keratin 8 shRNA results in the correct localization of the R138Q mutant protein and the recovery of its function. The fact that silencing of keratin 8 recovers the function of the mutant protein further suggests that keratin 8 network can act as a potential therapeutic target. This agrees with the study showing that the specific modification of the K18 expression by RNA silencing led to the regulated transport of F508del-CFTR to the plasma membrane in transfected HeLa cells [179].

Finally, we demonstrate the cellular effects of the small molecule c407 *in vitro* translated into a therapeutic benefit *in vivo*. Indeed, 28-day treatment with c407 in *NPHS2*$^{flox/R140Q}$ mice resulted in the prevention and treatment of proteinuria with normal kidney histology observed. Control mice were treated with saline for the same period of time; these mice underwent a gradual increase in proteinuria, which was associated with high plasma urea level and hypoalbuminemia. Furthermore, histological analysis revealed that c407 prohibited the development of glomerulosclerosis, which was observed in control mice at the point of sacrificing. Next, electron microscopy was employed to visualize podocyte foot processes and to see whether c407 can prevented podocyte foot process effacement, as this biological process is characteristic of many renal diseases. Similar therapeutic effect was seen in F508del-Cftr mice, where short-term administration of c407 resulted in the correction of bone growth rate and osteoblast activity [180].

This work suggests that keratin 8, and potentially keratin 18, inhibit the transport of the mutant protein to the plasma membrane. Although there are yet questions that remain unanswered regarding the precise mechanism of this interaction, this work demonstrated physical interaction between K8 and R138Q mutant, suggesting that keratin 8 forms a complex with the R138Q-podocin. Furthermore, the disruption of this interaction with c407 lead to the localization of the functional protein back to the plasma membrane, and that R138Q podocin delocalization was associated with the keratin 8 network reconstitution. However, both the wild-type and mutant proteins must be purified to identify the direct site of the interaction with keratin 8 using Biocore or an equivalent chemical assay. Moreover, it has previously been shown that interaction of the mutant protein with the keratin network leads to it being degraded via the ubiquitin-mediated degradation pathway. Therefore, it would be interesting to determine whether the K8-R138Q podocin interaction targets mutant protein towards the proteasomal machinery [181]. Another important aspect that must be addressed in the future is to study the expression of K8 in kidney biopsies of patients with the R138Q mutation. Finally, the eventual aim for this project is to further develop the c407 compound within an industry partnership leading to clinical trial in patients with R138Q mutation.

In summary, our study provides direct evidence that keratin 8 is involved in the podocyte dysfunction associated with the most common R138Q podocin mutation in NS. This work further demonstrates that pharmacological targeting of keratin 8 with c407 *in vivo* leads to prevention and correction of proteinuria in *NPHS2*$^{flox/R140Q}$ mice. Moreover, this study provides a solid foundation for developing other pharmacological compounds targeting the keratin 8-R138Q podocin interaction, which can be used in NS patients bearing R138Q mutation.

Chapter 6: *TBC1D8B* Loss-of-Function Mutations Lead to X-Linked Nephrotic Syndrome via Defective Trafficking Pathways

6.1 Introduction

In the past 20 years, advances in genetic testing and techniques have increased our understanding of the pathogenesis of genetic SRNS. To date, various genetic mutations of structural and functional molecules of podocytes are known to result in serious abnormalities of the podocytes themselves, but also of neighbouring structures, leading to, for example, sclerotic lesions, such as FSGS, and, importantly, more remain to be identified [70]. These mutations have been found in a number of intracellular compartments of the podocyte, and play an important role in actin cytoskeleton dynamics, podocyte integrity and Golgi/mitochondrial function [182]. Furthermore, more details continue to emerge on the defects in intracellular protein trafficking, that result in the accumulation and aggregation of proteins in various subcellular compartments, and appear to be a prevalent causative factor in the development of numerous human diseases, such as NS [183]. In most cases, this disruption in protein trafficking occurs due to mutations, which give rise to abnormal protein structures as a result of protein malfunction [184]. Therefore, this study was undertaken in collaboration with Dr. Guillaume Dorval (Laboratory of Hereditary Kidney Diseases, Imagine Institute, INSERM U1163, Paris Descartes University, 75015 Paris, France) to identify a novel gene mutated in X-linked NS and study the effects of the mutation on the podocyte structure and function both *in vitro* and *in vivo.*

6.1.1 New gene mutated in SRNS identified by exome sequencing

Through studies aiming at identifying new genes mutated in SRNS in two families, we identified a potential actor of endosomal trafficking. The first family (family A) was from Ecuador and presented with isolated congenital SRNS consistent with an X-linked inheritance. Pedigree and clinical features are described in Figure 6.1A. Briefly, affected females (I-2 and II-2) exhibited non-nephrotic proteinuria, while affected boys (II-1, II-3, and II-4) developed congenital or early-onset NS. All pregnancies were marked by pre-eclampsia, when carrying a male boy. In the proband (II-4) and her sister (II-2), kidney

biopsy revealed FSGS lesions and electron microscopy (EM) showed FP effacement, a hallmark of NS [185]. The pro-band (II-4) reached ESKD by the age of 2.8 years and did not exhibit recurrence after kidney transplantation. By exome sequencing (ES), we identified a c.738G>C variant in TBC1D8B (GenBank: NM_198881.1; HGNC:24715) localized on chromosome X (Figure 6.1B). This missense variant (p.Gln246His) was defined as probably damaging by pathogenicity prediction software. Through a European collaborative network (Eurenomics), we identified another sporadic SRNS-affected individual (II-2) in a family (family B) originated from the UK Renal Rare Disease Registry (RaDaR #425), with a missense c.872T>C (p.Phe291Ser) variant in the same gene (Figures 6.1C and 6.1D). This variant also displayed highly pathogenic scores. The affected individual (II-2), a male from European ancestry presenting with early-onset SRNS at the age of 2 years, had no other systemic features. Kidney biopsy revealed global sclerosis on light microscopy and FP effacement on EM (Figure 6.1E). He reached ESKD by the age of 9 years and underwent kidney transplantation a year later. Both mutations segregated with the affected status in the respective families and were, respectively, present in 1/27, 314 (with no hemizygous) and absent from gnomAD database in the population-matched control subjects. Both mutations involved residues conserved from C. elegans to H. sapiens. Based on the information above, it was concluded that the *TBC1D8B* is novel gene associated with X-Linked NS. TBC1D8B, encoded by the *TBC1D8B* gene, is an uncharacterized Rab-GTPase-activating protein likely involved in endocytic and recycling pathways (discussed in more details below).

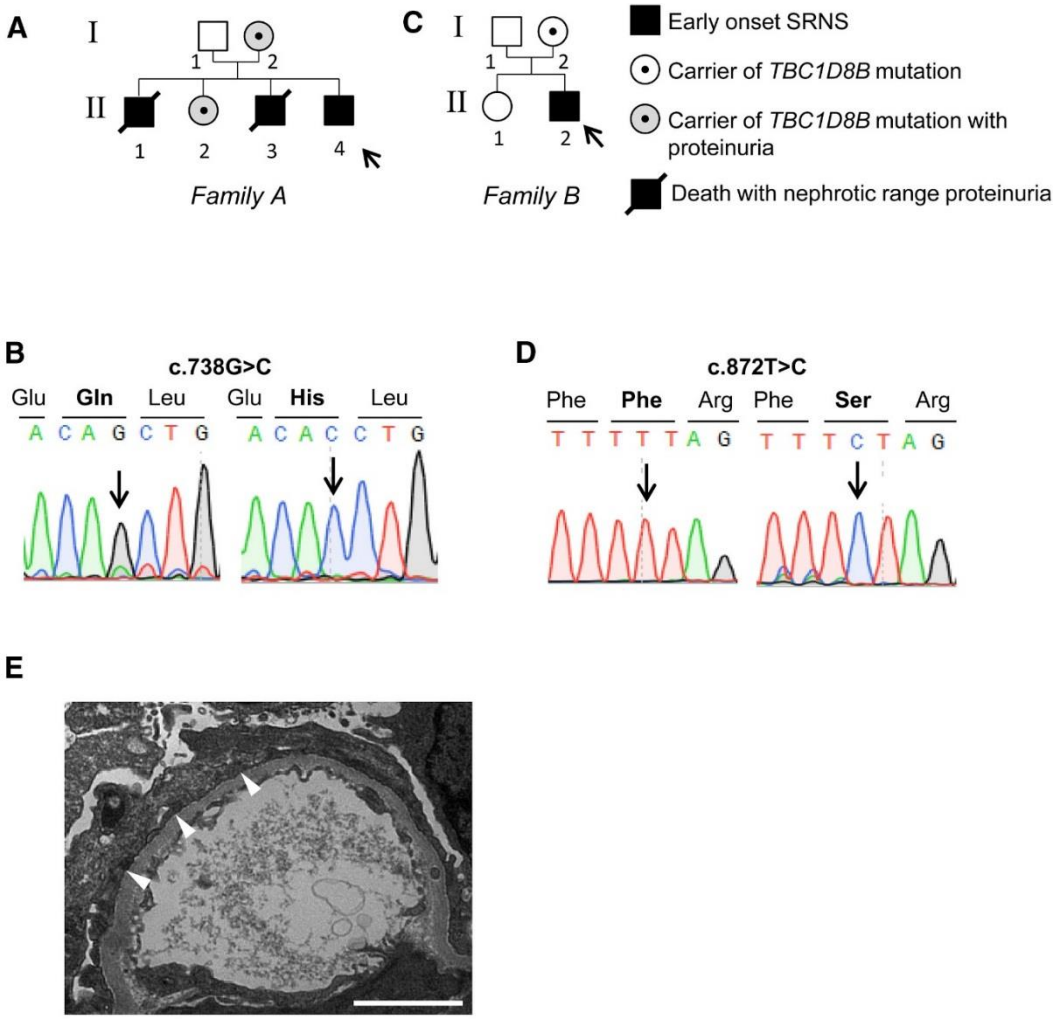

Figure 6.1 Clinical and genetic information for Families A and B. (A and C) Family pedigrees for families A (A) and B (C). In family A, the proband (II-4) and his brothers (II-1 and II-3) developed congenital nephrotic syndrome, while the individual from family B (II-2) developed an early-onset nephrotic syndrome. Arrows indicate probands. *TBC1D8B* mutations c.738G>C and c.872T>C were detected in affected subjects and carriers of families A and B, respectively. (B and D) Exome sequencing revealed two distinct missense variants in *TBC1D8B* (c.738G>C and c.872T>C). Segregation of variants was confirmed by Sanger sequencing in both families. (E) Electron microscopy image from affected individual from family B (II-2) harbouring the p.Phe291Ser mutation revealed foot processes effacement (white arrowheads) (scale bar, 2µm).

6.1.2 Link between Rab and TBC (Tre-2/Bub2/Cdc16)

Rab proteins are small GTPases that represent evolutionarily conserved family of membrane proteins, which regulate and participate in a variety of membrane trafficking pathways, such as formation, transport, tethering and fusion of vesicles with the target plasma membrane, thus acting as molecular switches [186], [187]. Principally, Rabs switch between two nucleotide-bound states, an active GTP (guanosine triphosphate) state and

an inactive GDP (guanosine diphosphate) state, where the active form is the one that allows vesicles/organelles trafficking through interaction with a Rab partner, also known as Rab effector [188]. Furthermore, that Rab cycle is controlled by two activating enzymes, GEF (guanine-nucleotide-exchange factor) and GAP (GTPase-activating protein) (Figure 6.2) [188]. Accordingly, recognition and characterization of these GEFs and GAPs at the molecular level are essential in order to understand Rab-mediated trafficking events at the plasma membrane of eukaryotic cells.

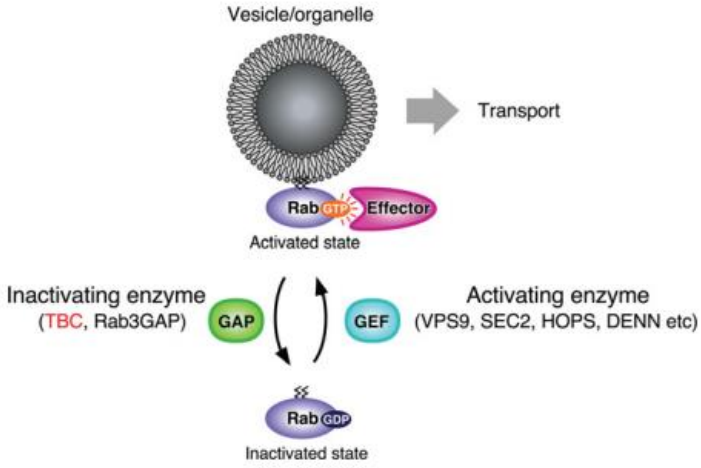

Figure 6.2 Cartoon illustration of a Rab cycle. The active GTP form of Rab is targeted to a designated vesicle/organelle and facilitates its transport through interaction with Rab effector molecule. Adapted from Fukuda [188].

Recently developed tools, such as Rab panels, allowed for the systemic identification of the mammalian Rab proteins and their isoforms [189], while also made it possible to comprehensively validate a variety of Rab effector molecules [190]. Apart from Rab3-GAP and Rab3-GEF, majority of the mammalian GEFs and GAPs have been so far identified based on the sequence homology to budding yeast GEFs and GAPs [191]. Furthermore, there is only a small number of mammal-specific GEFs verified on the basis of the sequence homology to yeast GEFs [188]. Contrarily, Rab-GAPs identified so far in mammals, excluding Rab3-GAP, have a TBC domain, which is made of approximately 200 amino acids [188]. Interestingly, there are more than 40 different TBC proteins described in humans and mice, which runs in parallel with the number of proteins in Rab superfamily, for example Rab1-43 in humans [188]. Recent studies have demonstrated that some TBC proteins have the Rab-GTPase (Rab-GAP) activity, thus believed to be involved in numerous membrane trafficking processes [188].

One such protein is TBC1D8B, a member of the TBC domain protein family (Tre-2/Bub2/CDC16). Like other TBC proteins, TBC1D8B may function as a Rab-Gap by binding to specific Rab proteins and stimulating their GTPase activity [188]. Interestingly, in addition to its Rab-GAP (TBC) domain, TBC1D8B contains one GRAM domain repeated two times, which allows binding to lipid rafts, critical elements of SD signalling in podocytes [105],[192]. The two mutations described above are localized within each GRAM domain (Figure 6.3). TBC1D8B also possesses an EF-Hand domain localized at the C-terminal extremity. EF-hand domain has been previously described in other proteins as a calcium-binding regulation site, which may downregulate the protein activity, when bound to Ca^{2+} [192]. A second isoform of TBC1D8B results from alternative splicing events in intron 11 and leads to a shorter 632-amino acid protein, lacking the C-terminal extremity of the Rab-GAP domain and the entire EF-like domain. However, the catalytic residues (Arg534 and Glu574) are present in both protein isoforms. Interestingly, the role of TBC1D8B has never been explored either in cell lines or animal models. To our knowledge, results obtained in the current work reveal the role of TBC1D8B in the kidney or more precisely, the podocyte, for the first time.

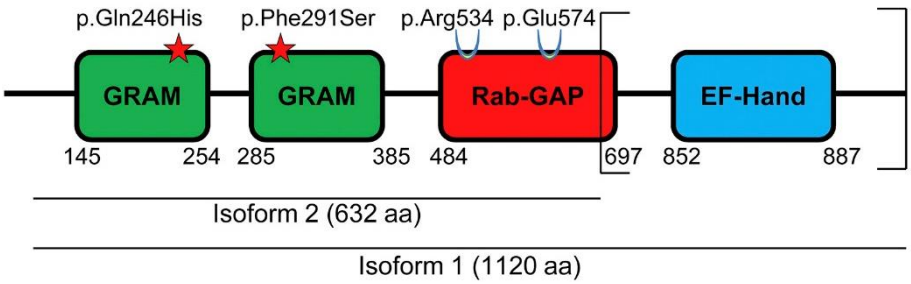

Figure 6.3 Cartoon illustrating the structure of the TBC1D8B protein. Mutations are localized in GRAM domains at the N-terminus. Catalytic residues on the Rab-GAP domain are maintained. C-terminal EF-hand domain is not conserved in isoform 2.

6.2 Materials and Methods

6.2.1 Cell culture

Conditionally immortalized human podocytes [127] were routinely cultured at 33°C in RPMI-1640 (Gibco® , Life Technologies), supplemented with 10% FBS, 1% insulin/transferrin/selenium, glutamine and penicillin/streptomycin (all from Life

Technologies), and then, for experiments, cells were thermoswitched to 37°C for 10-14 days differentiation. Cells used in this study were tested mycoplasma-free.

6.2.2 Antibodies, reagents and chemical compounds

The following antibodies were used in this study: mouse monoclonal antibodies (mAb) against GFP (Roche, Cat. No. 118144600001), c-myc epitope (Thermo Fisher, MS-139-P), synaptopodin (Progen, Cat. No. 65194), and rabbit polyclonal antibodies against TBC1D8B (Abcam, ab121780) and Rab11b (Atlas Antibodies HPA054396). Alexa-fluor 647 Phalloidin from ThermoFischer was used for IF (catA22287). For IF, Alexa Fluor-conjugated secondary antibodies (donkey anti-rabbit Alexa Fluor 488 and anti-mouse Alexa Fluor 546) were obtained from Life Technologies (ThermoFischer). Alexa-Fluor 555- or 546-conjugated transferrin (Life Technologies, Cat.No T35352 and T23364, respectively, used at 25µg/mL) was used for trafficking experiments.

6.2.3 Immunofluorescence and vesicular trafficking studies

Podocytes were grown on type I collagen-coated coverslips and either used to study the subcellular localization of endogenous TBC1D8B, or transiently transfected the next day using FuGENE® HD Transfection Reagent (Promega) or used for endocytosis and recycling experiments. Cells were fixed in 4% paraformaldehyde (PFA) for 20 min at room temperature and alternatively permeabilized with 0.3% Triton TX-100 (Sigma) in 1X PBS for 4 min (for endogenous TBC1D8B) or directly incubated in blocking buffer containing 5% bovine serum albumin (BSA, Sigma) for 1h at room temperature. Cells were then incubated in the appropriate primary and secondary antibodies for 1h each at room temperature. Nuclei were stained with Hoechst (#33342, Sigma) at room temperature for 8 min.

For transferrin endocytosis (uptake) / recycling (chase), we performed two different analyses:

For endocytosis study (transferrin uptake), fibroblasts were starved at 37°C for 60 min in transferrin- free OptiMEM medium supplemented with 1% Bovine Serum Albumin (BSA) and podocytes were starved in Serum-Free-Medium devoid of transferrin (SFM, Gibco® , Life Technologies) with 1% Bovine Serum Albumin (BSA) for 60 min. Cells were then incubated on ice at 4°C in the same ice-cold medium enriched with Alexa-Fluor (AF-555)-conjugated transferrin at a final concentration of 25µg/mL. This step allows transferrin to

bind its receptor but inhibit internalization. After 30 min incubation, cells were washed in cold 1X PBS. Cells were then incubated at 37°C in their respective medium (with transferrin) to allow transferrin internalization and blocked in 4% PFA at different time points. Mutated cells were compared to control cells for each time point.

For recycling study (chase study), cells were incubated in Alexa-conjugated transferring-enriched appropriate medium (25µg/mL) supplemented with 1% BSA for 60min at room temperature for fibroblasts and 120 min for podocytes. Cells were then washed with 1X PBS, incubated in transferrin-free medium and then fixed in 4% PFA at different time points. For endocytosis and recycling, all time points' results were normalized to T0.

As transferrin endocytosis/recycling kinetics are dependent on cell types, the use of different time points for transferrin endocytosis and chase in podocytes vs fibroblasts were based on the manufacturer instructions (30 to 60 min for endocytosis) and literature when available [127],[193][194], and empirically on our personal lab experience. Experiments were repeated 3 times and at least 20 cells were analysed in each time point experiment. Microscope settings were the same within each independent experiment. The integrated fluorescence intensity in each independent cell was measured and the background fluorescence intensity was subtracted to calculate corrected total cell fluorescence (CTCF) using the following equation CTCF=integrated density − (area of selected cell × mean background fluorescence per unit area). All time point values were normalized to T0 (maximum intensity). Whereas microscope settings allow to easily detect a 50% decrease of fluorescence in cells, they were imprecise for lower values. Thus, recycling assay was stopped, when the fluorescence intensity in WT cells reached 50% of the intensity measured at T0.

Immunofluorescence studies of endogenous TBC1D8B were performed as described above on 10 µm-frozen sections of human embryonic kidney biopsies obtained from The Department of Pathology of Necker-Enfants Malades Hospital (Paris, France).

6.2.4 Scratch assay and adhesion assay

This was performed as previously described by Vollenbroker *et al*. [193]. In brief, confluent differentiated human podocytes were cultured in six-well plates and scratched with two lines at 90° angle with a sterile 0.4-mm 200-µl Gilson style extension length tip. Images of the same field were captured at 0 and 12 hours.

Medium was removed, and cells were trypsinised until all cells were suspended, which was optically controlled. Cells were plated into 96-well plates and three experimental wells were assigned as the 100% attachment control, to which 20%, 50% and 100% of the total volume of cells were added. Cells were left to adhere for 45 min at 37 ^{o}C. Control wells for 100% attachment were fixed with 100 µl 4% PFA for 20 min at room temperature. Thereafter, the plate was tapped to remove lose and non-adherent podocytes, and washed twice with 100 µl PBS, and the experimental wells were then fixed with 100 µl 4% PFA for 20 min. Cells were stained with 100µl of 0.1% crystal violet in 2% ethanol for 60 minutes at room temperature. Absorbance on the plate was measured at 570nM in a plate reader. Results were depicted as a percentage of 100% adherent cells and normalized against the adhesion of the human wild type podocytes.

6.2.5 Zebrafish experiments

All results obtained from Zebrafish were performed by Dr. Guillaume Dorval (Laboratory of Hereditary Kidney Diseases, Imagine Institute, INSERM U1163, Paris Descartes University, 75015 Paris, France)

6.3 Results

6.3.1 Localization and phenotype studies of TBC1D8B in human kidney and podocytes

Immunofluorescence studies in human kidneys revealed the presence of TBC1D8B both in glomerular podocytes and tubules at early stages (25 weeks) and in mature kidney. In glomeruli, TBC1D8B colocalized with synaptopodin a specific cytosolic protein (Figure 6.4A). To further comprehend the role of TBC1D8B, we undertook functional studies in human podocytes. Podocytes from individual B (harbouring the p. Phe291Ser variant) were conditionally immortalized from the affected individual's nephrectomy specimen using the published methodology [127]. Podocytes from affected individual B exhibited alterations in actin cytoskeleton organization, and TBC1D8B displayed an intracellular vesicular localization as shown in Figure 6.4B. Furthermore, mutated podocytes presented with an increased adhesion and a decreased migration (Figure 6.4C and D).

Podocytes from individual A were not available, since he underwent bilateral nephrectomy several years before.

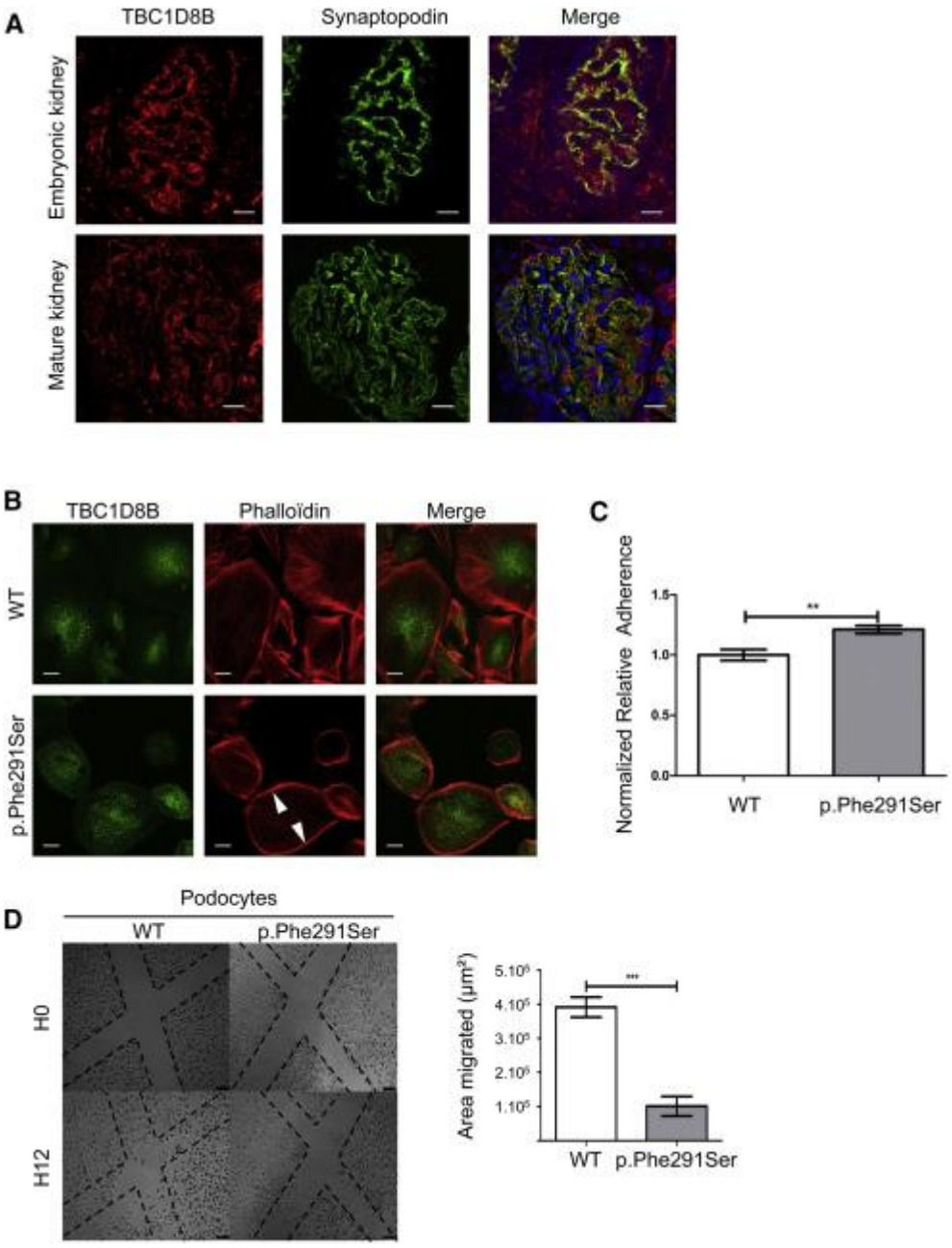

Figure 6.4 TBC1D8B localization and phenotype observed in mutated podocytes. (A) Immunofluorescence studies were performed on human fetal kidney at 25 gestational weeks (top) and in mature kidney in a healthy 7-year-old male (bottom). TBC1D8B displayed a glomerular localization with partial colocalization with synaptopodin, a cytosolic podocyte protein (scale bar, 20 µm). (B) In immunofluorescence experiments in immortalized podocytes, TBC1D8B displayed an intracellular vesicular expression. F-actin cytoskeleton was detected by immunofluorescence with phalloidin staining. p. Phe291Ser human mutant podocytes cortically (arrowhead) reorganized their F-actin

cytoskeleton. Original magnification ×63. (C) Cell adhesion was measured with a spectrophotometer at 570 nm optical density (n = 3, **p < 0.01, mean ± SEM). (D) Human podocyte cell motility and migration were measured by scratch assays. Number of cells per unit was significantly higher in the WT group 12 hr after the scratch, as shown on the graph on right (n = 3, ***p < 0.0001, mean ± SEM).

6.3.2 Zebrafish studies

In zebrafish, pericardial oedema was observed in >95% of both MO^{SPLICE} and MO^{ATG} morphants at 96 hpf, whereas it was found in fewer than 2% of control MO fish at 96 hpf (Figure 6.5A and B). Furthermore, an identical phenotype was obtained in the *tbc1d8b*$^{-/-}$ fish with the expected Mendelian ratio (n = 261; 22.9% phenotype in *tbcd8b*$^{+/-}$offspring; Figure 6.5C). histological analysis showed a retracted glomerulus in an enlarged Bowman's capsule in *tbc1d8b*$^{-/-}$ fish compared to controls (Figure 6.5D). EM revealed significant FP effacement and disappearance of SD in *tbc1d8b*$^{-/-}$ KO fish compared to controls (Figure 6.5E). The following results were obtained by Dr. Guillaume Dorval (Paris, France).

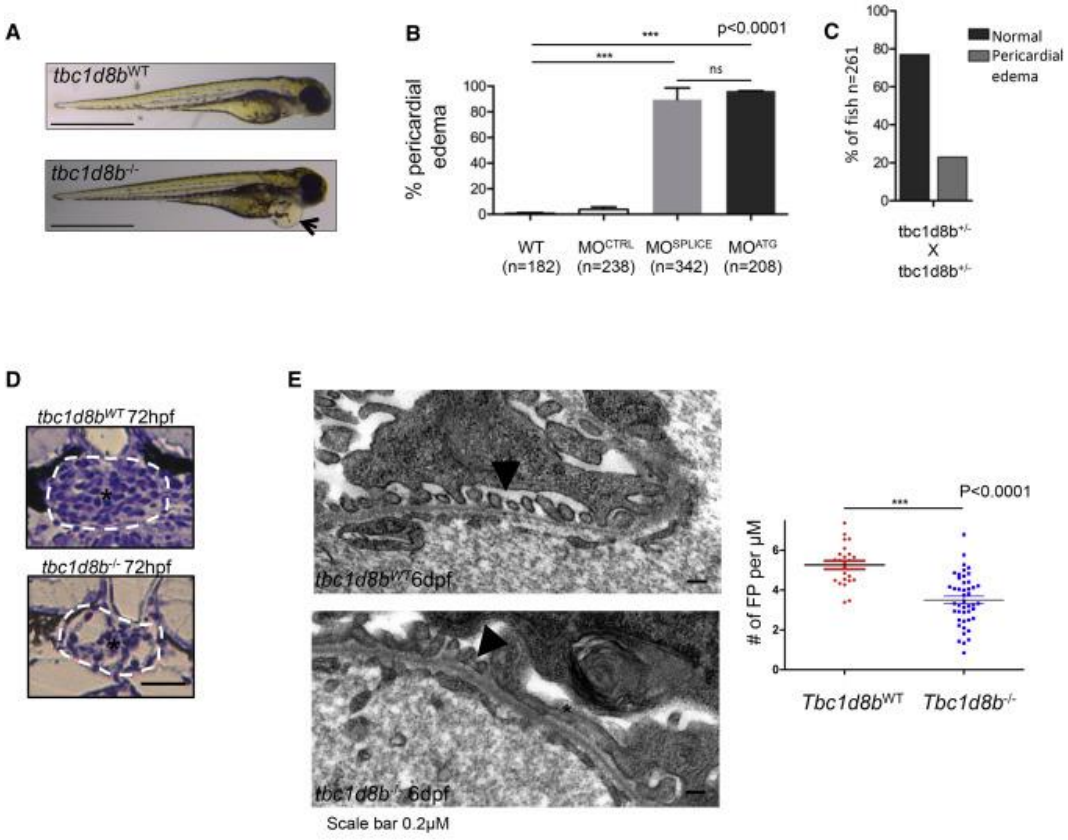

Figure 6.5 Phenotype observed in *TBC1D8B* KO and KD Zebrafish. (A) KO fish displayed pericardial edema at 48 hpf on mutant fish (black arrow). Scale bar, 1 mm. (B) Both

MO^{ATG} and MO^{SPLICE} also exhibited pericardial edema in more than 95% fish whereas $MO^{CONTROL}$ did not ($n > 200$, $^{***}p < 0.0001$, mean ± SEM). (C) *tbc1d8b*$^{+/-}$ offspring displayed pericardial edema with a Mendelian ratio. (D) Regular optical microscopy revealed a retracted glomerulus (*) in an enlarged Bowman's capsule (white circle) in mutated *tbc1d8b*$^{-/-}$ fish compared to control (scale bar, 15 µm). (D) Electron Microscopy findings showed a mixture of foot processes (FP) effacement (*) with regular FP (black arrowheads). Graph on the right shows a significantly lower rate of FP per uM in tbc1d8b$^{-/-}$ fish compared to control ($n = 3$ fish per condition, $^{***}p < 0.001$, mean ± SEM).

6.3.3 TBC1D8B interaction and trafficking

Transferrin endocytosis and recycling assays were performed in wild type and affected individuals' podocytes. Fluorescence intensity progressively increased in control podocytes, whereas it increased much more slowly in mutated podocytes harbouring the p.Phe291Ser mutation, suggesting an endocytosis defect (Figure 6.6A,B). Measuring recycling of fluorescently labelled transferrin in WT and mutant podocytes revealed persistence of fluorescence 45 min after internalization in mutant cells, while it reached 50% of T0 intensity in control podocytes, indicating a delay in recycling processes in mutant cells (Figure 6.6C,D). Next, co-IP studies were done in HEK293T cells, where the Rab-binding domain (RBD) of TBC1D8B was seen to interact with a dominant active, GTP-bound, mutant of Rab11b (DA-Rab11b), but not with DA-Rab11a (Figure 6.6F). Moreover, endogenous IP was performed to look for the interaction between TBC1D8B and DA-Rab11a (Figure 6.6G).

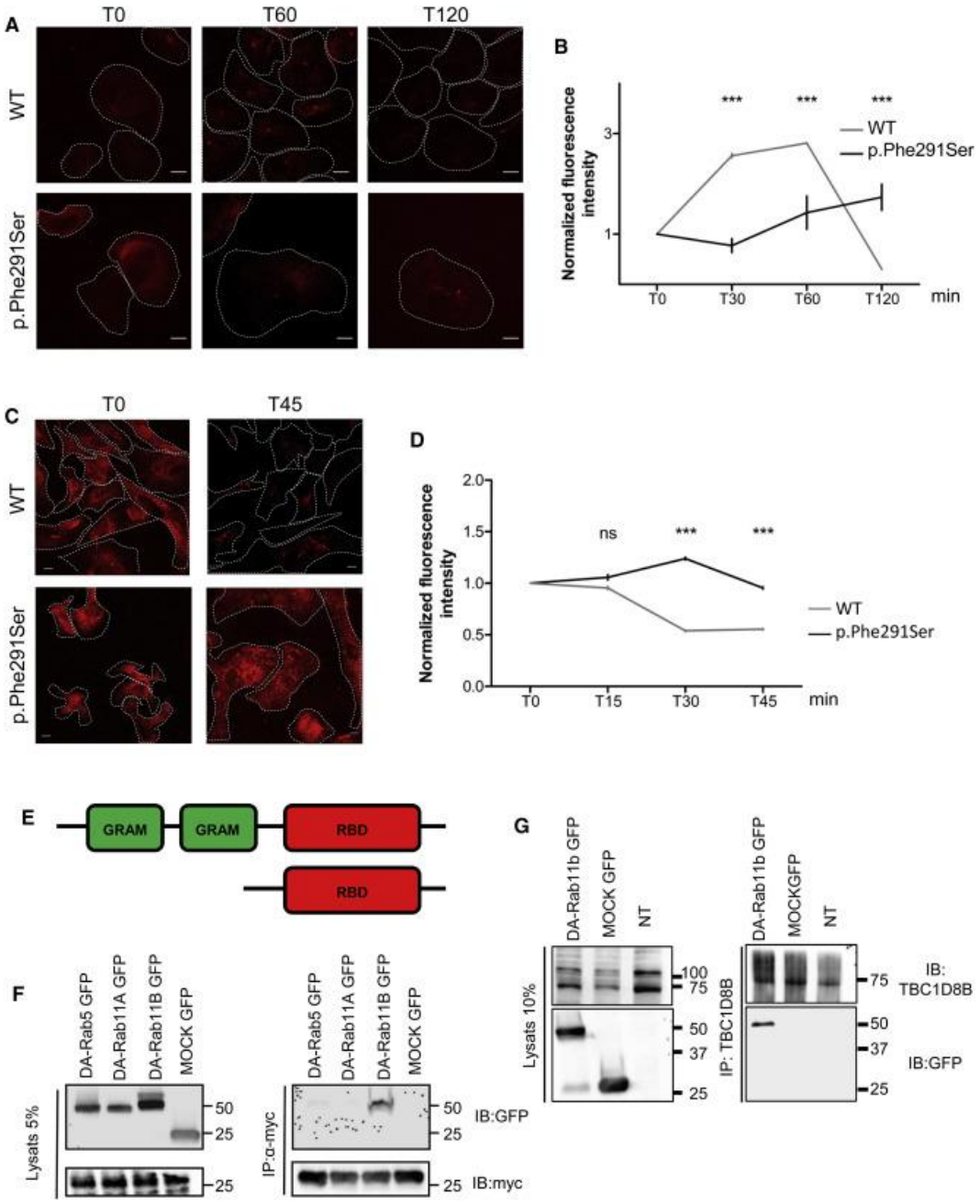

Figure 6.6 TBC1D8B interaction and effect of mutations of vesicular trafficking. (A and B) Transferrin uptake is evaluated by incubation with fluorescently labelled transferrin. Graph B represents the quantification of normalized fluorescence in both mutated and control cells (***p < 0.001, mean ± SEM; scale bar, 25 µm). (C and D) Transferrin chase evaluates the recycling process in podocytes. Graph D represents the quantification of normalized fluorescence in both mutated and control cells (***p < 0.001 at 45 min, mean ± SEM; scale bar, 25 µm). (E) Construct used for to perform co-immunoprecipitation with a specific plasmid harbouring only the TBC1D8B Rab-binding domain (RBD) tagged with the myc epitope, and under the CMV promoter. (F) In co-transfected HEK293T, the (myc-)RBD of TBC1D8B is able to interact with Dominant Active (DA)-Rab11b but not DA-Rab11A nor DA-Rab5. (G) The endogenous TBC1D8B protein interacts with transfected DA-Rab11b-GFP in HEK cells.

6.4 Discussion

As described in Chapter 1, SRNS is a glomerular disease characterized by massive proteinuria, most often associated with FSGS [185]. SRNS is responsible for chronic kidney disease and accounts for 15% of ESKD cases in individuals under 25 years of age [195]. Identification of monogenic causes of SRNS involving more than 40 genes has helped decipher podocyte physiology [196], [197]. By exome sequencing, we identified missense mutations in *TBC1D8B* in two families with an X-linked early-onset SRNS with FSGS. Many studies have reported a strong relationship between the SD and the actin cytoskeleton [197], and the role of vesicular trafficking has been well established in the maintenance of SD complexes [198],[199]. Nevertheless, intracellular transport defects have rarely been related to monogenic SRNS [200].

As mentioned above, TBC1D8B may act as Rab-GAP, promoting GTP hydrolysis in specific Rab proteins [201]. In mammalian cells including podocytes, Rab-GTPases are mostly involved in vesicular trafficking [202],[203]. To further analyse the role of TBC1D8B in this process, transferrin endocytosis and recycling assays were performed in affected individuals' podocytes and fibroblasts harbouring p.Phe291Ser and p.Gln246His variants, respectively. Transferrin is a widely used marker for both clathrin-mediated internalization and recycling pathways in most cell types [204]. After internalization from the plasma membrane and before being recycled back to cell surface, transferrin and its receptor accumulate in the PNRC [205],[206]. Here, a delay in transferrin uptake in affected individuals' cells compared to control subjects was detected. However, endocytosis was significantly slower in mutant fibroblasts and podocytes. In addition, analysis of transferrin recycling revealed a significant decrease of normalized fluorescence intensity 45 min after transferrin loading in WT podocytes, whereas it was maintained in the PNRC in affected individuals' cells. Altogether, these results strongly suggest that both endocytosis and vesicular recycling are altered in affected podocytes.

In cells, PNRC dynamics and recycling are mostly regulated by Rab11. We then hypothesized that TBC1D8B might be a crucial GAP for Rab11 that displays at least two isoforms (Rab11a and Rab11b) both present in mouse podocytes [206], [207]. By co-immunoprecipitation experiments in HEK293T cells, we showed that the Rab-binding domain (RBD) of TBC1D8B was able to interact with a dominant active, GTP-bound, mutant of Rab11b (DA-Rab11b), but not with DA-Rab11a. We also observed a specific

interaction between endogenous TBC1D8B and DA-Rab11b. In addition, we showed that DA-Rab11b and TBC1D8B Rab-binding domain colocalized at the PNRC when co-expressed in podocytes, but interestingly, the widespread Rab11b signal in WT cells shifted to a very restricted localization to the PNRC in mutant podocytes, which suggests that GTP-bound Rab11b is trapped in the PNRC in cells from affected individuals. Altogether, these data strongly suggest that TBC1D8B is a specific Rab11b-GTPase activating protein.

Numerous proteins are subject to Rab11-dependent recycling in various cell types, especially in neurons [208]. However, although it has been shown that some proteins are recycled in a Rab11b-dependent manner, only a few studies explored the role of Rab11b on vesicular trafficking [209]. In 2016, Grimsey *et al.* reported the crucial role of Rab11b GTP hydrolysis for the initiation of transferrin recycling from the PNRC to the plasma membrane [210]. In podocytes SD integrity is of utmost importance and several SD proteins are subjected to endocytic and recycling events to maintain their regulation [211]. Very recently, mutations in *GAPVD1*, a Rab5 effector showed to be involved in nephrin regulation at the SD, were reported as disease causing [200]. In our study, we did not find any interaction between TBC1D8B and Rab5, suggesting that Rab5 is not a target of TBC1D8B. Thus, our results highly suggest that some podocyte-specific proteins could specifically use the Rab11b-dependent recycling pathway, as it has been shown for some SD proteins and the use of the Rab5-dependent pathway [200]. By this means, alterations in Rab11b activation would lead to SD dysregulation, implying that not only endocytosis but also recycling are of fundamental importance for SD integrity. Indeed, it is likely that mutations in *TBC1D8B* lead to strong defect in recycling processes in podocytes, which could also induce a defect in transferrin uptake linked to decrease number of receptors at the plasma membrane at steady state.

Altogether, our results confirmed that mutations in *TBC1D8B* gene are involved in the development of early SRNS in rare affected individuals. We show herein that vesicular trafficking plays a fundamental role in podocyte disease, especially in SRNS, through a Rab11-dependent recycling process. Recent discoveries in monogenic SRNS and especially in SD regulation during disease through endocytic and recycling pathways would certainly help to develop targeted therapy for affected individuals.

Chapter 7: CDCP1 is a Novel Binding Partner of Podocin

7.1 Introduction

Although podocin has been the subject of much research, the majority of this has been done in transfected human embryonic kidney cells (HEK293) and not in podocin's bona fide cell type, the kidney podocyte. As a further step in understanding podocin biology, identification of novel binding partners of podocin in podocytes is required to provide new insights into the functions of this protein. As mentioned in Chapter 1, podocin plays an important role in establishing a lipid-enriched signalling platform by which numerous proteins, such as nephrin and TRPC6, are recruited to the slit diaphragm of podocytes [212]. It is currently well understood that podocin acts as a scaffold for the recruitment of proteins for correct function of the slit diaphragm complex [213]. Although, it is known that the unique structure of this multiprotein complex requires a tight regulation of the local protein environment, the exact make up of this complex in health and disease is still unclear [214]. Therefore, there is a need for identification of novel proteins interacting with podocin that could provide more information about its cellular roles and functions. In the current study, wild-type podocin was subjected to a targeted proteomic approach in order to identify and characterize novel interacting partners. This system provides an accurate mass data that identifies and quantifies the proteins, even those of low abundance, within complex mixtures in a single experiment [215]. An analysis of proteomic data revealed several proteins linked to major pathways associated with variety of cellular processes, such as intracellular transport and autophagy. CD2AP, a known podocin interactor, was identified, therefore validating the screen. The interactome also contained several signalling molecules and receptors. To further validate the interactome, it was compared to the recently performed proteomic screen of FLAG-tagged podocin expressed in podocytes [214]. Here, a significant number of proteins and receptors, such as podocin, ephrin type-A receptor 2 and receptor-type tyrosine-protein phosphatase F, were found to match.

Here, most of the work is focused on the characterization of the processes that lead to the adhesive defect of the mutant podocytes derived from the patients bearing the R138Q mutation. Cell migration is a dynamic process of leading edge protrusion, focal adhesion turnover and generation of retraction/detachment forces that is not only involved in a variety of biological processes like embryogenesis, but also in various disease states, such

as cancer as seen with metastasis [216], [217]. The major players during these events are the integrin family of cell adhesion receptors, which can control cellular migration as well as other intracellular functions via their interaction with a variety of cytoskeletal and signaling molecules [218]. Indeed, interaction between focal adhesion kinase (FAK) and Src family kinases (SFKs) is the main driving force of cellular migration and attachment [219].

7.2 Methods

7.2.1 CDCP1 antibody uptake

CDCP1 antibody (ThermoFisher, #PA5-17245) uptake was performed as previously described in section 6.2.3. The same protocol was followed as for the transferrin assay.

7.3 Results

7.3.1 CDCP1 is a novel podocin interactor

Figure 7.2A shows the proteomics data from 2 independent experiments using two different extraction buffers demonstrating that CUB domain containing protein 1 (CDCP1) was identified as an interacting protein for podocin. Western Blot of a GFP TRAP with Podocin GFP and CDCP1 confirms the proteomic screen (Figure 7.2B). Next, immunofluorescence studies were performed to show colocalization between podocin GFP (steady state) and trafficking CDCP1 (antibody uptake for 20 mins). We also show TIRF images of FAKpY397 – a marker for focal adhesions and CDCP1 in WT cells. The CDCP1 lines up along F-actin filaments and FAK around the periphery of the cell with a few filaments in the centre (Figure 7.2C). The CDCP1, F-actin and FAKpY397 in the PM cells is localised throughout the cell, implying that focal adhesion dynamics are dysregulated in PM cells (Figure 7.2C). TIRF images also display an increased FAKpY397 expression in PM cells, when compared to WT cells.

A

IP Buffer	Protein ID	Score	Coverage	Peptides	Total	AA	MW (Kda)
2% NP40	CDCP1	28.17865	14.47	9	12	836	92.81436
1% Triton	CDCP1	71.7518	15.31	9	22	836	92.87237

B

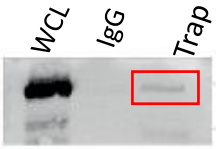

C

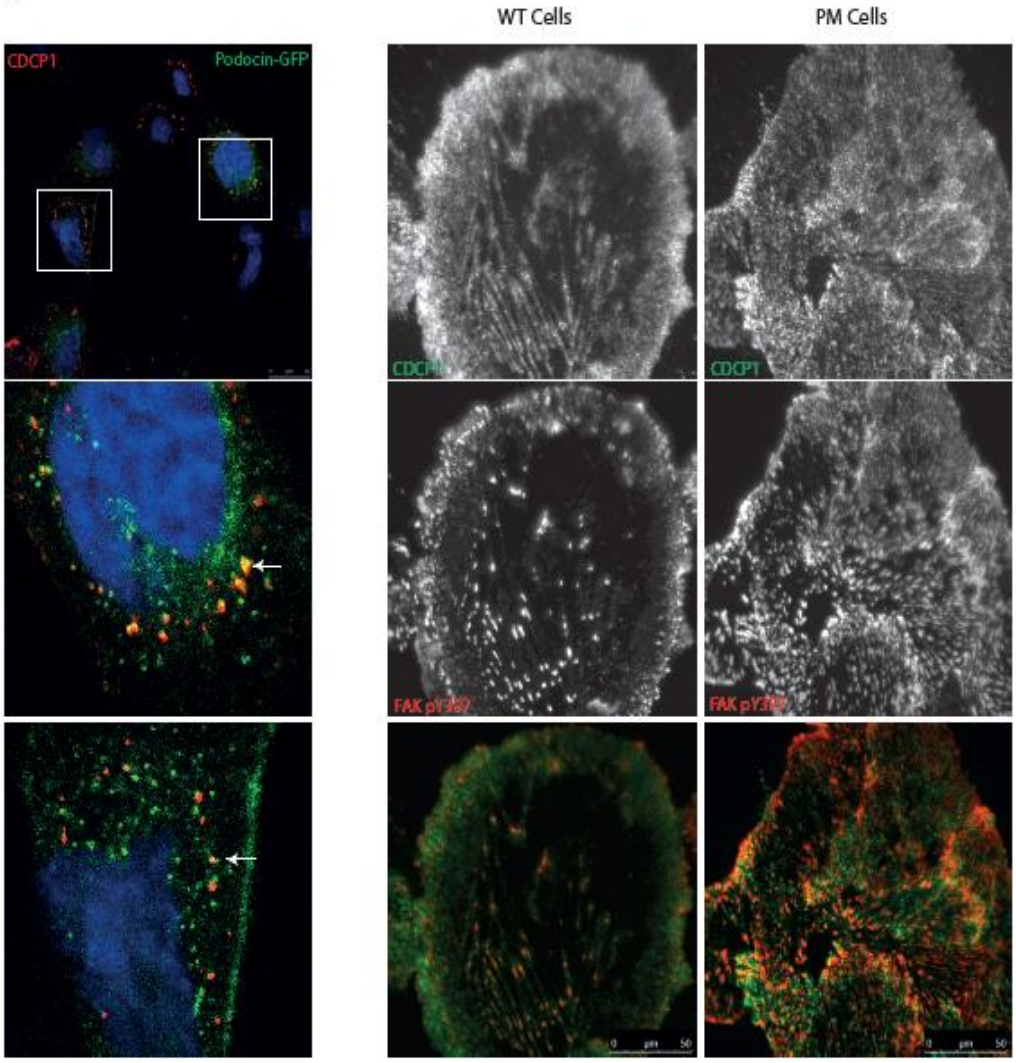

Figure 7.1 CDCP1 and Podocin. (A) Results from proteomics using different immunoprecipitation buffers from WT Human ciPodocytes stably expressing WT podocin GFP differentiated for 10 days. (B) Co-immunoprecipitation between over expressed WT podocin GFP and endogenous CDCP1. (C) Co-localisation studies between steady state WT podocin GFP and CDCP1 after 20 minutes antibody uptake in differentiated Human ciPods. TIRF images of CDCP1 and FAK pY397 in differentiated WT and PM ciPods. Scale bar=50 µm.

7.3.2 Western Blotting analysis of FAK and CDCP1 protein levels

To further confirm immunofluorescence studies, western blotting was performed to look at FAK and CDCP1 protein levels in human podocytes derived either form a healthy individual (WT) or a patient with the R138Q mutation (PM). Similar to IF, there is a significant increase in FAK y397 phosphorylation in PM cells, while an increase in FAK y925 phosphorylation was also observed in these cells (Figure 7.2A). There was no change in CDCP1 expression detected between the cell lines, however, the 70 kDa cleaved form of CDCP1 was observed in PM cells (Figure 7.2B).

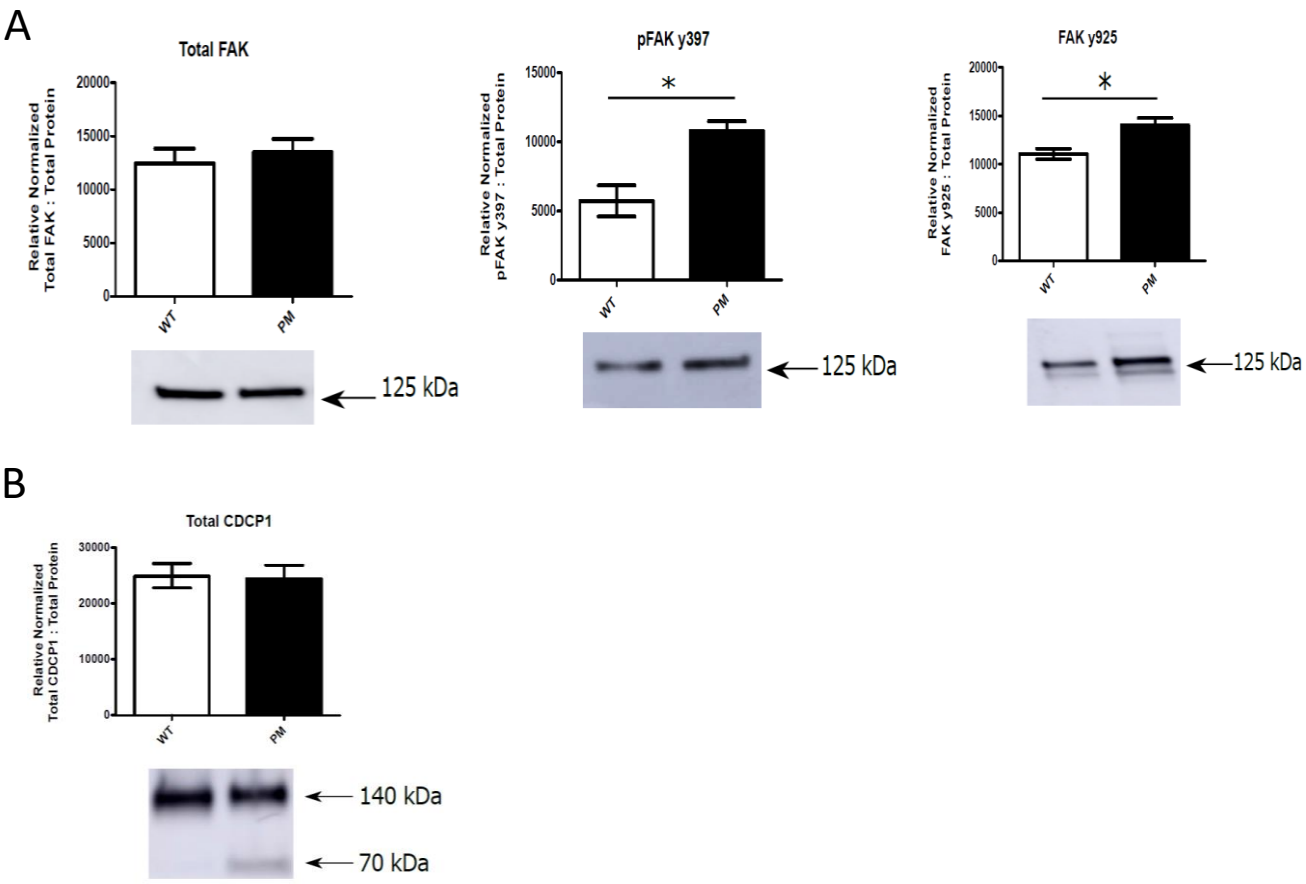

Figure 7.2 Western Blotting analysis. (A) Relative protein levels of FAK, FAKpY925 and FAKpY397 in differentiated WT and PM cells. Results from three independent experiments. Two-tailed T-test, * P≤0.05. (B) Relative protein levels of CDCP1 in differentiated WT and PM cells.

7.3.3 CDCP1 interacts with total beta integrin 1

Literature reports suggest that CDCP1 and beta integrin 1 interact, and that CDCP1 has a regulatory effect on FA turnover/activity. This interaction is observed both in WT and PM cells, but the interaction is much reduced/abolished in the PM cells, and is rescued in PM cells expressing WT Podocin GFP (Figure 7.3A). There's no difference in levels of active beta integrin 1, and active beta integrin 1 does not interact with full length or cleaved CDCP1 (Figure 7.3B).

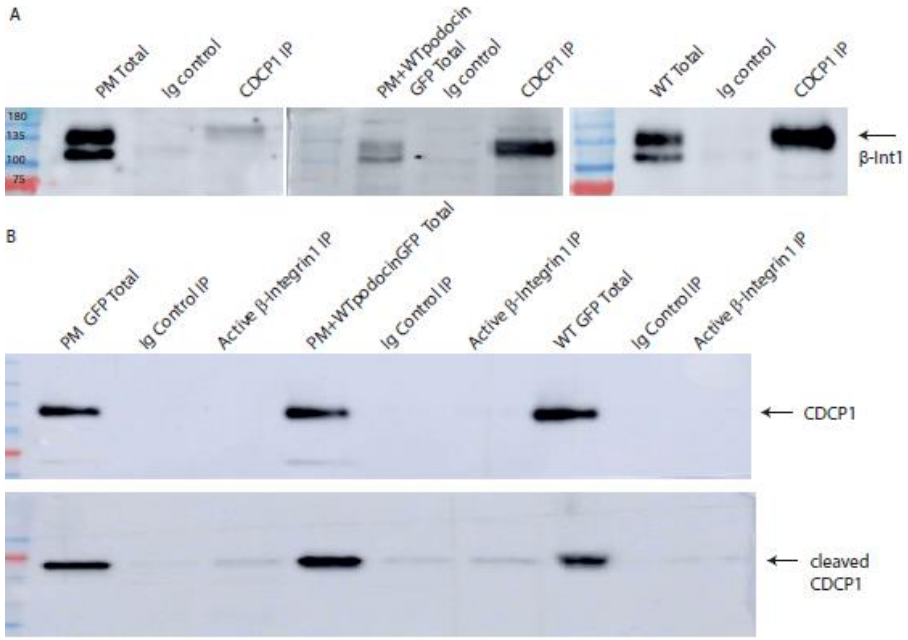

Figure 7.3 CDCP1 and beta integrin 1. (A) A representative western blot of co-immunoprecipitation between CDCP1 and total β-integrin 1 in differentiated PM, PM+WT podocin GFP and WT Human ciPods. (B) Co-immunoprecipitation of active β-integrin1 with full length and cleaved CDCP1.

7.3.4 Functional rescue

Since podocin is known to associate with lipid rafts, a flotation gradient centrifugation was performed to see whether CDCP1 is present in these lipid microdomain, and how its recruitment is affected by the R138Q mutation. Flotillin-1 was used as a lipid raft marker. In WT cells, CDCP1 is correctly recruited to the lipid rafts, while this association is

disrupted in PM cells, however, is rescued in the presence of WT podocin GFP (Figure

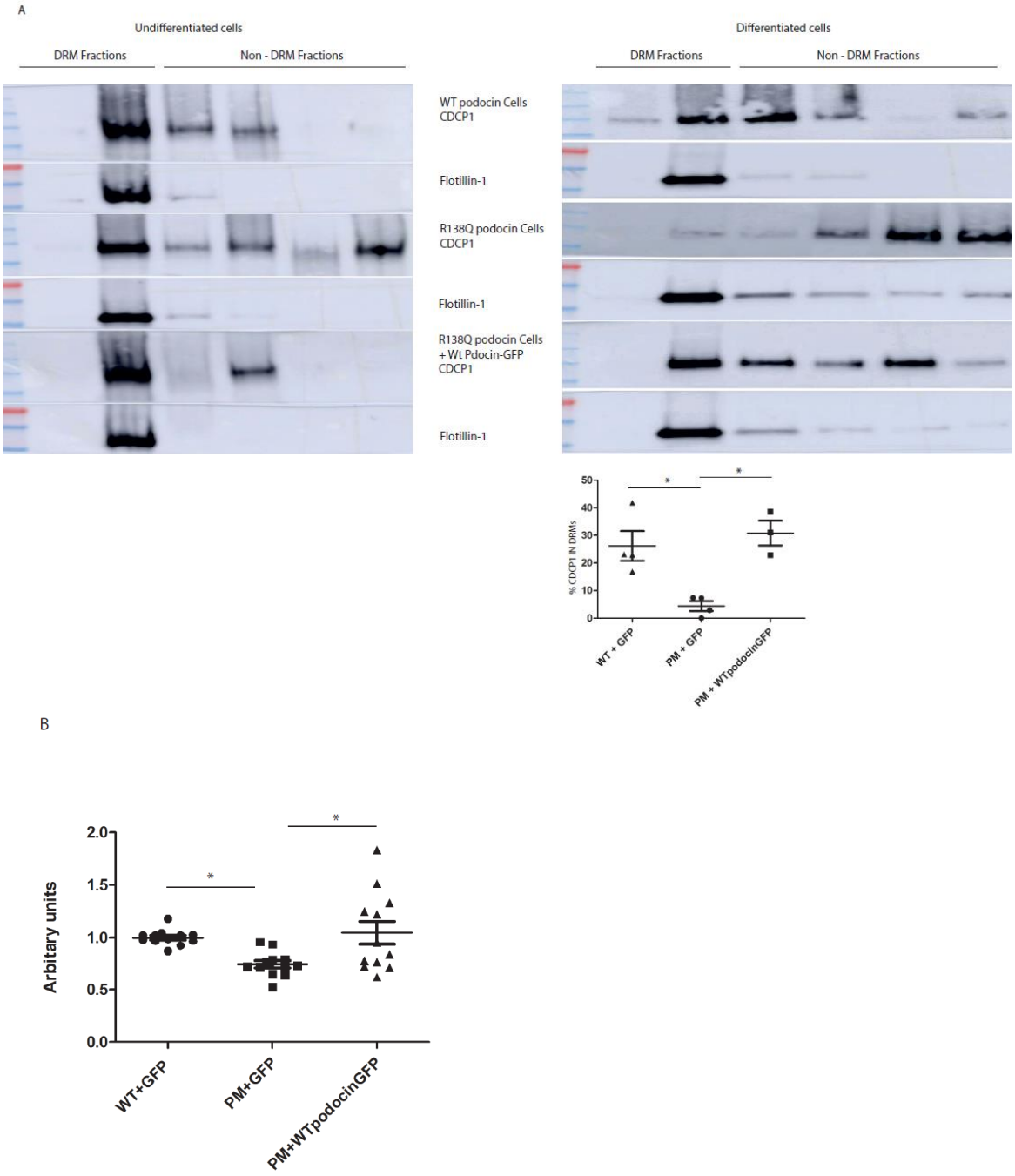

Figure 7.4 Rescue experiments. (A) Representative western blots of DRMs extraction from undifferentiated and differentiated WT, PM and PM+WT podocin GFP Human ciPods. Results were analysed by ANOVA and Bonferonni's multiple comparison test, significance *, n=4. (B) Adhesion assay of differentiated WT, PM and PM+WT podocin GFP Human cipods. Results were analysed by ANOVA and Bonferonni's multiple comparison test, significance * P≤0.05, ** P≤0.01, n=3.

7.4 Discussion

One of the novel proteins that came up on the proteomic screen was CUB domain-containing protein 1 (CDCP1), and was shown to interact with WT podocin (Figure 7.1A and B). Human tumor associated gene, *CDCP1*, was first identified and mapped to a chromosome 3p21-p23 from human colorectal cancer cells, due to its elevated expression in these cell lines in comparison with normal tissue [220]. CDCP1 is an integral membrane glycoprotein located on the cell membrane that has been previously reported to play a role in cancer metastasis [221]. Importantly, in animal models of cancer, such as prostrate, melanoma and lung adenocarcinoma, CDCP1 has been reported to play a role in metastasis progression [222], [223]. CDCP1 is mostly expressed in epithelial linings with no expression detected in fibroblasts and other mesenchymal-derived cells [224]. This protein was found to regulate cellular migration and adhesion, and it is known that both loss of and gain of functions of CDCP1 can ultimately result in the inhibition of migration [225]. CDCP1 is a 836 amino acid protein made of a 29 amino acid signal peptide at the N-terminus, followed by an extracellular domain, a transmembrane domain and a 150 amino acid cytoplasmic domain (Figure 7.5) [226]. Furthermore, the extracellular domain consists of three CUB (complement protein subcomponents C1r/C1s, urchin embryonic growth factor and bone morphogenetic protein 1) domains defined by immunoglobin-like folds and that are believed to be required for protein-protein interactions [226]. In addition, there are 14 N-glycosylation sites in the extracellular domain [226]. On the other hand, the cytoplasmic domain contains five evolutionary conserved tyrosine residues, which can be phosphorylated, and two proline-rich regions that are able to act as SH3 ligand-binding sites [226],[227].

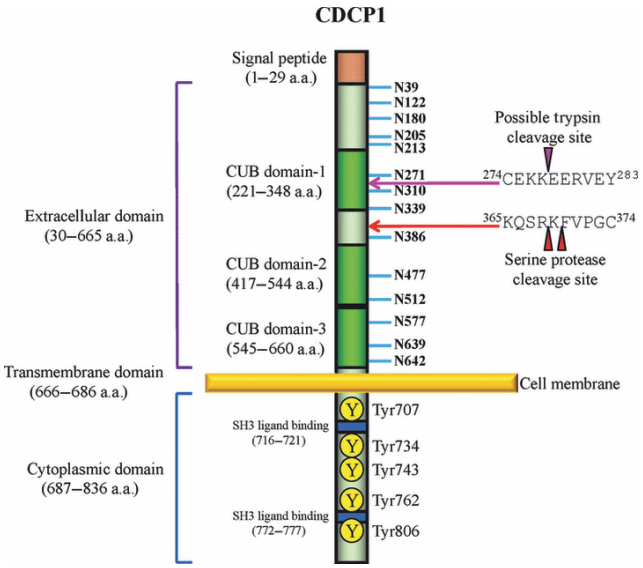

Figure 7.5 Schematic cartoon of human CDCP1. The full length CDCP1 consists of an extracellular domain made of three CUB domains containing 14 N-glycosylation sites, a transmembrane domain and a 150 amino acids cytoplasmic domain containing tyrosine residues. Reproduced from Uekita and Sakai [226].

The full-length, 135 kDa CDCP1 protein is also known to undergo a specific protease cleavage into a smaller 70 kDa cytoplasmic fragment and a 65 kDa protein portion on the extracellular part of the membrane [228], [226]. Proteases, such as plasmin and trypsin, have been shown to cleave CDCP1, and there is growing evidence to support the fact that this cleavage is required for the activity of the protein [223]. It has been demonstrated that the CDCP1 cleavage by plasmin-like serine proteases results in a signal transduction via a β1 integrin/FAK/PI3K/Akt signalling cascade that induces early stages of metastasis development leading to tumor cell invasion [223]. In addition to cleavage, activity of CDCP1 is dependent on its phosphorylation state; both full length and cleaved CDCP1 can be phosphorylated by Src family kinases (SFKs), such as Src, Fyn and Yes [222], [219]. Interestingly, the non-receptor tyrosine kinase focal adhesion kinase (FAK) was recently discovered to play a role in processes, such as cell adhesion and migration [229]. In particular, FAK is essential for integrin mediated signalling during cell adhesion, where integrin binding results in autophosphorylation of FAK at Y397, which, in turn, causes conformational changes and further Src phosphorylation of FAK at Y925, Y576/577, Y861 and Y407 [219].

Here, we demonstrate that total beta integrin 1 interacts with CDCP1, when podocin is correctly targeted to the plasma membrane (Figure 7.6). However, in the presence of the R138Q mutation, this interaction is reduced or diminished, which results in the elevated phosphorylation of FAK at Y397 and Y925, the sites associated with Src phosphorylation and autophosphorylation [230]. This, in turn, leads to FAs disassembly, which might explain the adhesive defect of the mutant cell line. Importantly, the introduction of WT podocin GFP resulted in the restoration of the mutant cells function and the recruitment of the CDCP1 back to the lipid raft microdomain.

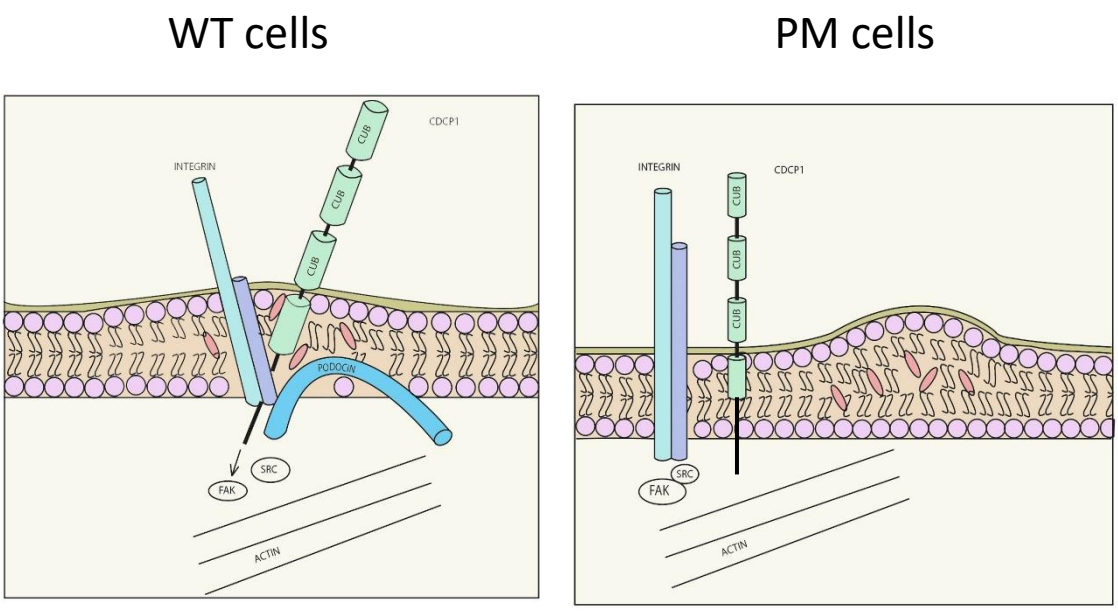

Figure 7.6 Proposed model of beta integrin 1/CDCP1/podocin complex formed at the plasma membrane of human podocytes. The R138Q mutation, results in the mutant protein being retained in the ER, resulting in the aberrant formation of the complex and adhesive defect of podocytes.

Altogether, it can be proposed that podocin interacts with and traffics CDCP1 to the plasma membrane in podocytes and aids its recruitment to the lipid raft microdomains. Moreover, the CDCP1-beta integrin 1 interaction only occur in the presence of podocin at the plasma membrane and is required for the normal adhesion and motility of podocytes. However, further work is required to identify the exact signalling events happening during the complex formation. It will be interesting to see if the introduction of WT podocin GFP to PM cells results in the decrease of FAK phosphorylation.

Chapter 8: Conclusions and Future Work

The work of this thesis describes a previously unknown molecular mechanism involved in the endoplasmic reticulum retention of the R138Q disease-causing mutation of podocin. Podocin is a podocyte specific integral membrane protein essential for intact glomerular filtration. To date, mutations in podocin represent the commonest form of the genetic NS. As described in Chapter 1, the most frequent podocin mutation is the R138Q missense mutation, which results in this protein being misfolded and retained in the ER. Therefore, a key aim of glomerular research is to discover small molecules that correct this trafficking defect. Using our unique conditionally immortalized human podocyte cell lines, derived from both wild-type and from patients bearing the R138Q podocin mutation, and various *in vitro* biochemical assays, such as PLA, IF and immunoprecipitation, the current work has demonstrated that the R138Q mutant but importantly not wild-type podocin associates with the intermediate filament keratin 8. Furthermore, treatment with the *in silico*-selected compound 407 resulted in the rescue of mutant podocin localization back to the plasma membrane, and more importantly restored the adhesive defect of mutant podocytes and structure of podocin-dependent lipid rafts (Figure 8.1). The same results were observed, when an shRNA-based approach was used to target the association between keratin 8 and R138Q podocin mutant in human podocytes. *In vivo*, a podocyte specific, doxycycline inducible triple transgenic mouse model of the R140Q mutation (a mouse analogue of the human R138Q mutation) was generated to test c407. Four weeks treatment with c407 by osmotic mini pumps led to prevention of the proteinuria in those mice with normal renal function and histology observed on PAS and EM.

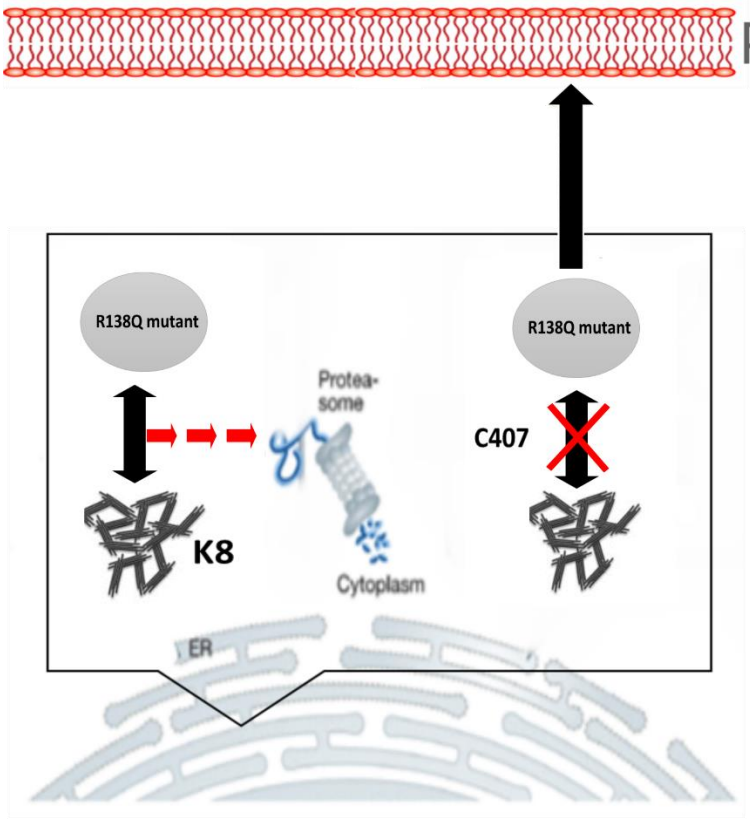

Figure 8.1 Proposed model for the mutant protein retention and rescue from the ER. The R138Q podocin associates with keratin 8 network, which, in turn, results in its ER accumulation and potential proteasomal degradation. However, if this interaction is inhibited by the corrector, such as c407, the R138Q podocin mutant can reach the plasma membrane and become functional.

Broadly, this work suggests a key role for the keratin 8 network in mutant podocin misprocessing and agrees with the previously published studies done by Colas *et al*., where the disruption of the mutant F508del-CFTR and keratin 8 interaction resulted in the functional form of the mutant protein at the plasma membrane [130]. Interestingly, keratin 8 has also been shown to be involved in alpha-1-antitrypsin (A1AT) secretion and/or degradation [231]. A1AT is a ubiquitously expressed inhibitor of inflammatory cells that appears to have its main physiological role in the lungs, where it protects them from degradation [232]. The Z mutation in alpha-1-antitrypsin (A1AT) represents one of the common forms of the genetic A1AT deficiency and also results in the misfolded form of protein, which is targeted for proteasomal degradation or for polymerization and autophagy [231]. A1AT deficiency is a rare genetic disease that presents as pulmonary emphysema, liver cirrhosis and, in rare cases, as the skin disease panniculitis, and is described by abnormally low plasma levels of A1AT [232]. Keratin 8 was shown to interact

with misfolded Z-A1AT, thus preventing it from correct targeting and secretion [231]. Based on the above, it will be interesting to investigate the role of keratin 8 in other protein misfolding disorders of the ER, such as Gaucher disease. Gaucher disease is an autosomal recessive disorder, in which patients present with the deficiency in the β-glucosidase, a membrane-associated lysosomal enzyme protein [233]. Similar to misfolded CFTR and podocin proteins, missense variant β-glucosidase protein is also accumulated in the ER and targeted for the proteasomal degradation in the cytosol [234]. While the precise effects of the R138Q podocin mutation on podocyte biology are incompletely understood, this work provides many potential leads and ideas. Experiments have been set up to see, whether the mutant podocin is targeted for proteasomal degradation *in vitro*. *In vivo*, mouse work has been started to see if a complete rescue of proteinuria can be achieved, when c407 is administrated after proteinuria has commenced. Further work should help to add new discoveries to what is already known, and hopefully start to lead to potential therapies for the disease course.

8.1 Complication of this work

Podocytes act as key players in the maintenance of the glomerular filtration barrier and a disruption in their function, as in the case of the R138Q mutation, ultimately results in glomerular disease, an understanding of the precise molecular mechanisms involved in the ER retention of the mutant protein is essential in the understanding of the underlying pathogenesis of SRNS. Work carried out in this thesis has developed a novel concept in understanding the effects of the R138Q podocin mutation on podocyte biology. It has established that the keratin 8 network is involved in the retention of the mutant protein. However, the main limitation of this work was that it had not conclusively proved that the two proteins interact directly, and this will require purified forms of both proteins for interaction studies.

During this project, PCR based molecular cloning methods were employed to generate pET-32(a) wt/R138Q podocin plasmids, which were used for protein purification. An overview of the process is shown graphically in Figure 8.2.

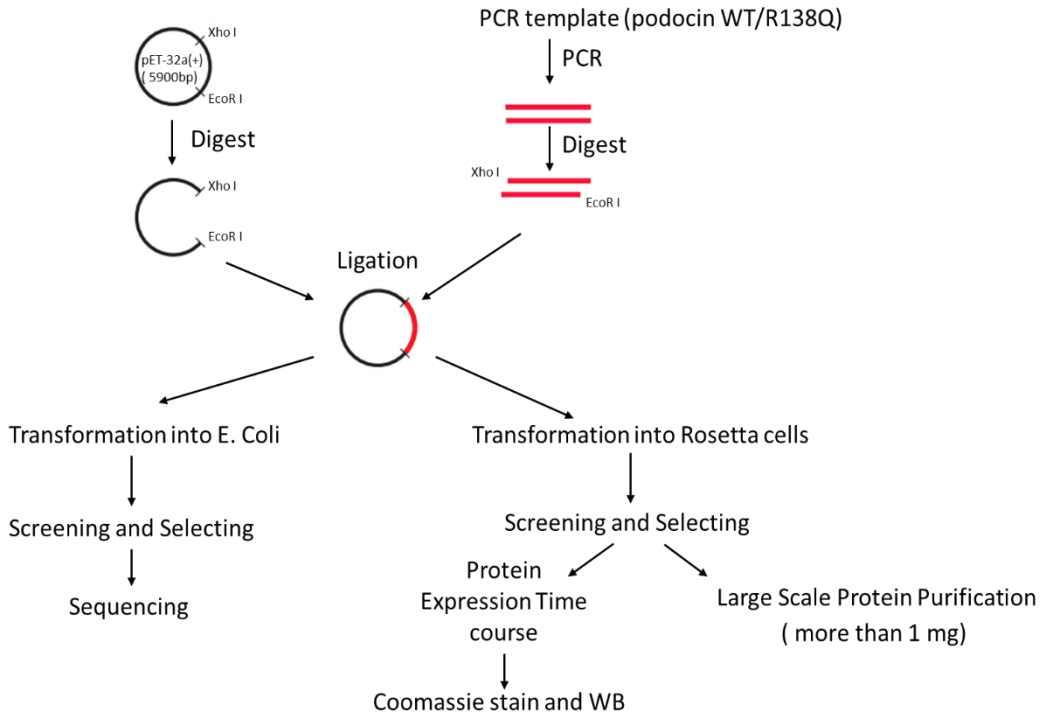

Figure 8.2 Schematic diagram showing the steps for PCR based molecular cloning, in which Xho I and EcoR I sites are incorporated into the WT and R138Q podocin prior to ligation into a pET-32(a) vector.

Unfortunately, multiple attempts to purify both the wild-type and mutant forms of podocin were unsuccessful. Integral membrane proteins, such as podocin, are known to be difficult to purify. Therefore, a collaboration was established with a drug discovery contract research organisation, DomaineX, in order to purify both keratin 8 and podocin to investigate their protein-protein interaction. To date, DomaineX have managed to obtain affinity purified full length keratin 8 and the portion of the podocin protein containing the R138Q missense mutation. Direct interaction between the two partner proteins has been demonstrated using a microscale thermophoresis (MST) assay. However, due to incorrect folding of purified podocin and hence aggregation, the assay has still to be optimised to allow calculation of binding affinity. This work is ongoing, as setting up a protein/protein interaction assay will allow for the development of a screening assay to test the ability of c407 and related drug compounds to block this binding.

8.2 On-going work

8.2.1 Development of c407 analogues

The lead compound in this project, c407 is a small-molecule selected from the National Cancer Institute's Diversity compound database, whose properties were shown to be within drug-like properties. The low molecular weight, lipophilicity and polar surface area of this compound allow for considerable scope for optimisation. One of the further aims of this project is to develop c407 into a series of novel molecules that can inhibit the R138Q podocin – keratin 8 association, for the eventual treatment of SRNS. Through the collaboration with Domainex, over 40 c407 analogues have so far been acquired or synthesized to be tested in a cell adhesion assay. The optimization of analogues systemically involves changes to the phosphinate, aromatic, and linker groups, and symmetry of the molecule in order to elevate their pharmacokinetical potency and properties (summarized in Figure 8.3).

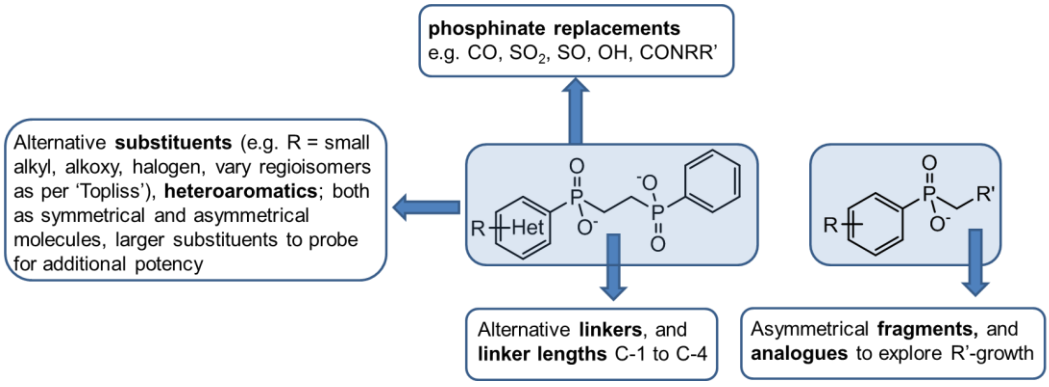

Figure 8.3 An example of the optimization protocol obtained from Domainex. The diagram shows various phosphinate replacements, alternative linkers and linker lengths, along with alternative substituents, such as small alkyl and halogen, and heteroaromatics.

Alongside, a small number of c407 analogues has been obtained from our French collaborators (Paris, INSERM) and tested in a robust cell adhesion assay. Mutant podocytes derived from a patient with a homozygous R138Q mutation have significantly less adhesion than healthy wild-type podocytes, which can be rescued using the small molecule c407. The assay has been used for a rapid quantification of adhesion plus or

minus c407 analogues, and the results obtained so far show that some selected analogues are able to (partially) restore the WT-phenotype, while others do not (Figure 8.4).

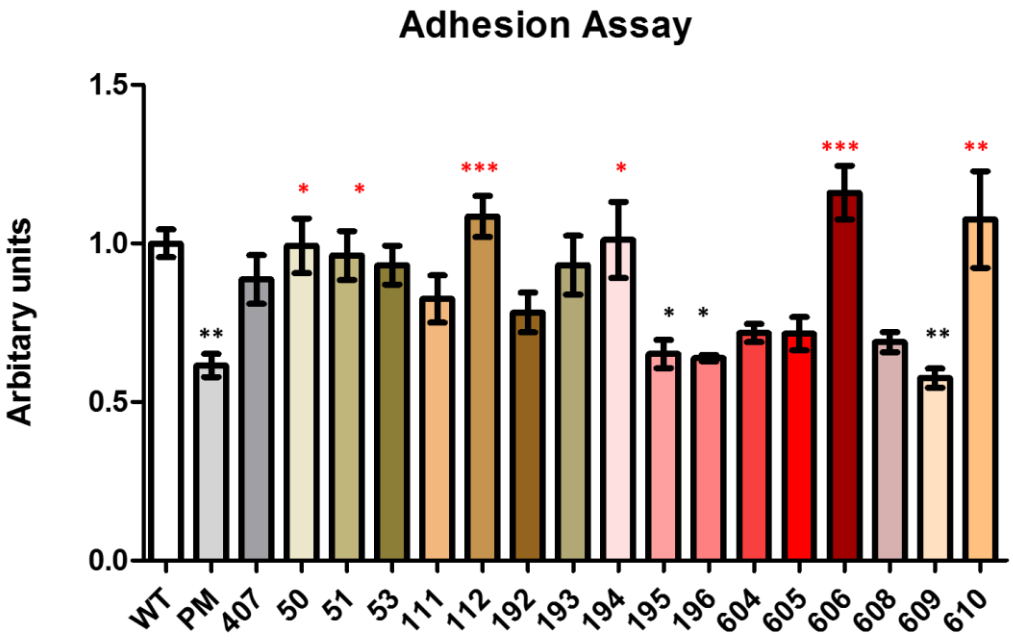

Figure 8.4 Cell adhesion assay of the c407 analogues. Some selected analogues, such as 112,194,606 and 610, are able to significantly restore the WT-phenotype, while other analogues, such as 195, 196 and 609, do not. Results are representative of 3 independent experiments; One-way ANOVA analysis P<0.0001.

These results have given significant clues as to how to optimize the c407 compound and this work is continuing. Further work will include testing of 20 different c407 related compounds generated by Domainex for dose and efficacy. The most suitable analogues derived from this test will be chosen and tested *in vivo*. Experiments will be performed in mouse knock-in model of podocin R140Q, using implantable minipumps and oral gavage (described in more details below) for effect and dose response. Readouts will be as before and include weekly proteinuria measurements, plasma renal profiles and renal histology/ultrastructure/immunofluorescence. The eventual aim of this project is to identify at least one candidate compound from the lead series, which demonstrates the most ideal pharmacokinetic (PK) profile in a mouse model of human R138Q mutation following minipump/oral administration.

8.2.2 Oral gavage of c407

To further test the efficacy of c407, it is important to determine whether it gets orally absorbed; whether it achieves relevant plasma concentration; and how long for does it stay in the blood. One of the best ways to answer these questions is to perform the administration of the drug directly into the stomach of mice or rats via a technique known as oral gavage [235]. This procedure involves the delivery of the compound into the stomach using stainless steel bulb tipped gavage needle or a flexible cannula attached to a syringe [235]. During this work, 2 mg of c407 was given orally twice a day for 17 days, alongside the doxycycline that was administered in the drinking water for the duration of the whole experiment. Urine was collected every 4 days, and blood samples were taken via facial vein at 4, 6, 8 hours after the c407 delivery for pharmacokinetic studies (PK) (Figure 8.5a). Blood samples were analysed by Domainex, and the mean plasma concentrations of c407 was shown to remain above 340ng/mL ($\geq$1µM) at 6 hours (Figure 8.5b). C407 was shown to be orally bioavailable following oral gavage administration, and the compound appeared to be well-tolerated during *in vivo* studies (clinical and behavioural observations Figure 8.5c). Moreover, c407 delivered orally prevented the development of proteinuria in mouse knock-in model of podocin R140Q starting from day 4 (Figure 8.5d). Orally given c407 also prevented the elevation of blood cholesterol, urea and creatinine (Figure 8.5e). Although phosphinate present in c407 is a relatively uncommon functional group in the pharmacopeia, the properties of c407 present no obvious liabilities, proving its oral bioavailability. This is supported by the fact that some drugs containing phosphinate groups, such as Fosinopril, are currently being used in clinic. Fosinopril is an approved phosphinate-containing drug that is used in patients with heart failure, and was seen to be beneficial in patients with renal or hepatic disfunction [236].

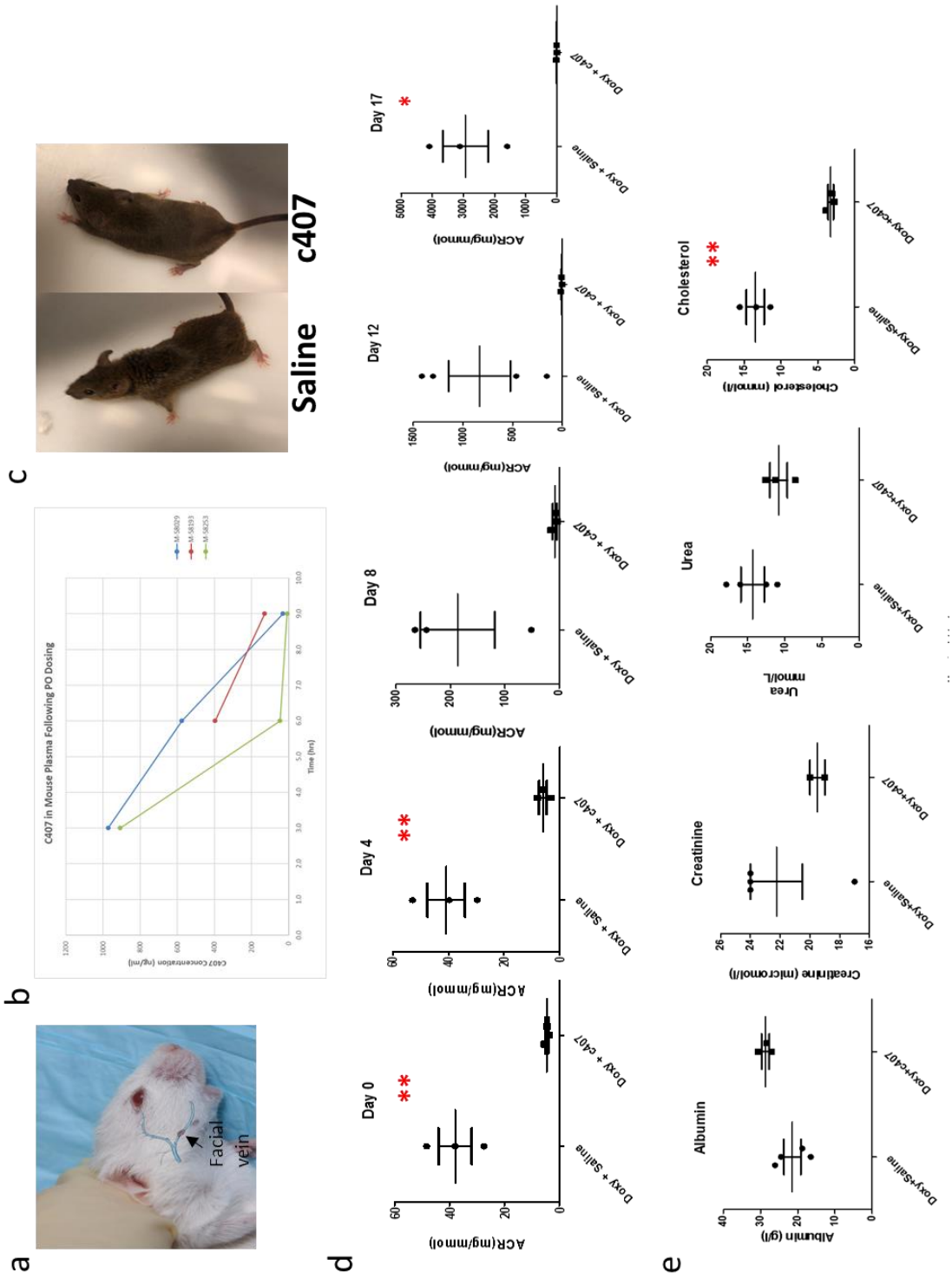

Figure 8.5 c407 administration by oral gavage. Blood samples were collected via facial vein (a) and (b) analysed for the mean plasma concentration of c407. (c) Clinical and behaviour signs were observed to be normal in c407 treated animals, while mice that were given saline had a scruffy appearance. (d) C407 oral administration prevented the development of proteinuria starting from the day 4 up to day 17. Two-tailed T-test

p=0.0054; p=0.0072; p=0.0158. (e) Normal plasma renal profiles were observed with c407 treatment. Two-tailed T-test, p=0.0012.

8.3 Summary of main conclusions

Multiple conclusions have been drawn from data obtained over the course of this work. The implications of many of these are extremely important, and they represent future leads and directions for the project to develop a novel treatment for Nephrotic Syndrome. The following table summarizes the findings addressed in each chapter (Table 8.1).

Chapter	Main Findings
Chapter 4 Creation of a conditional knock-in mouse model of the R140Q mutation	• a podocyte specific, doxycycline inducible triple transgenic mouse model of the R140Q mutation (a mouse analogue of the human R138Q mutation) was generated • Doxycycline induction of a hemizygous state in the *NPHS2*$^{flox/R140Q}$ mice led to severe proteinuria detectable within few days, which peaked to a maximum at 2-4 weeks and was maintained at week 12 • Animals presented with hypoalbuminemia, hypercholesterolemia, uremia and abnormally high plasma creatinine levels at the point of sacrifice • Loss of podocin and nephrin expression associated with the loss of podocytes was observed • Proteinuric animals develop global glomerulosclerosis, podocyte foot process effacement and global fusion with GBM thickening

Chapter 5 Disruption of cytokeratin-8 interaction with R138Q podocin corrects its functional defect both *in vitro* and *in vivo*	• R138Q podocin mutant is retained in the ER and not able to associate with lipid raft microdomains • Keratin 8 preferably associates with the R138Q mutant over its wild-type counterpart • Silencing of keratin 8 resulted in the rescue of mutant protein localization and function • C407 treatment rescued both the mutant protein localization back to the plasma membrane and adhesive defect of the mutant cells • *In vivo* treatment with c407 prevented the development of proteinuria with normal renal plasma levels and histology as seen on PAS and EM
Chapter 6 *TBC1D8B* loss-of-function mutations lead to X-linked Nephrotic Syndrome via defective trafficking pathways	• New gene mutated in SRNS was identified • TBC1D8B is present both in glomerular podocytes and in mature kidney • p.Phe291Ser mutation resulted in an increased adhesion and a decreased migration of human mutant podocytes • Foot process effacement and disappearance of slit diaphragms were seen in *tbc1d8b*$^{-/-}$ KO fish • Mutant cells displayed a delay in recycling processes
Chapter 7 CDCP1 is a novel interacting partner of podocin	• CDCP1 interacts with WT podocin • CDCP1 interacts with beta integrin 1 in WT cells • Introduction of the WT podocin GFP into the PM cells rescues the adhesive defect • CDCP1 is recruited to the lipid raft microdomains • FA disassembly occurs in the PM cells

Table 8.1 Summary of the major findings discovered in each chapter.

Achievements

PhD Scholarship

This PhD was funded by a Kidney Research UK PhD scholarship and Nephrotic Syndrome Trust: September 2016-August 2019

Publications

- Dorval, G., **Kuzmuk, V.**, Gribouval, O., Welsh, G., Bierzynska, A., Schmitt, A., Miserey-Lenkei, S., Koziell, A., Haq, S., Benmerah, A., Mollet, G., Boyer, O., Saleem, M. & Antignac, C., 7 Feb 2019, In : American Journal of Human Genetics. 104, 2, p.348-355. *TBC1D8B* Loss-of-Function Mutations Lead to X-Linked Nephrotic Syndrome via Defective Trafficking Pathways
- Keir, L. S., Firth, R., Aponik, L., Feitelberg, D., Sakimoto, S., Aguilar, E., Welsh, G. I., Richards, A., Usui, Y., Satchell, S. C., **Kuzmuk, V.,** Coward, R. J., Goult, J., Bull, K. R., Sharma, R., Bharti, K., Westenskow, P. D., Michael, I. P., Saleem, M. A. & Friedlander, M., 3 Jan 2017, In : Journal of Clinical Investigation. 127, 1, p.199-214. VEGF regulates local inhibitory complement proteins in the eye and kidney

Oral Presentations

- A novel small molecule therapy rescues trafficking of misfolded podocin and corrects Nephrotic Syndrome caused by a common podocin mutation. Submitted to ASN 2019, Washington, DC, USA
- A novel small molecule therapy rescues trafficking of misfolded podocin and corrects Nephrotic Syndrome caused by a common podocin mutation. Best Clinical and Scientific abstracts, UKKW 2019, Brighton, UK
- 12th International Podocyte Conference, May 2018, Montreal, Canada

Prizes

Best Clinical and Scientific abstract 2019, UK Kidney Week

Appendix 1

Cell culture and cell extraction reagents

Sigma Aldrich, Poole, UK:

RPMI Media 1640 (#R8758)

ITS liquid media supplement (#I3146)

Penicillin-Streptomycin (#P4333)

Foetal Bovine Serum (FBS) (#F7524)

DMEM x1 + Glutamax

DMSO (#D8418)

Trypsin-EDTA (#T3924)

Protease inhibitor cocktail (#P8340)

Gel electrophoresis and western blotting reagents

Severn Biotech Ltd, Worcester, UK

Acrylamide/Bis-acrylamide solution (#20-2100-05)

Millipore, MA, USA

PVDF Immobilon-P Transfer Membrane (#IPVH00010)

Sigma Aldrich, Poole, UK

Bovine Serum Albumin (BSA) (A9647)

Thermo Scientific, IL, USA

SuperSignal west femto maximum sensitivity substrate (#34096)

Solutions:

Solutions used in cell culture and protein extraction

1 x Phosphate Buffered Saline (PBS) (pH 7.4):

Reagent	**Concentration**
NaCl	137 mM
Na_2HPO_4	10 mM
KCl	2.7 mM
KH_2PO_4	2 mM

Podocyte culture medium (500ml RPMI 1640) containing:

Reagent	**Amount**
FBS	50ml (10%)
ITS	5ml
Pen Strep	5ml

HEK culture medium (500ml DMEM x1 + Glutamax) containing:

Reagent	**Amount**
FBS	50ml (10%)

Cell culture medium for cryoprecipitation (10 ml):

Reagent	**Amount**
Cell culture medium	5 ml
FBS	4 ml
DMSO (Sigma #D8418)	1 ml

TNE Buffer pH 7.4 (wash buffer):

Reagent	**Concentration**
Tris base (Sigma #T6791)	50 mM
NaCl	150 mM
EDTA	0.5 mM

NP40 Lysis Buffer (10ml):

Reagent	Concentration
1xTNE	10ml
NP40 (Sigma #I8896)	2%
Glycerol	10%
Protease inhibitor cocktail	100µl

Solutions used in gel electrophoresis and western blotting

Tris 0.5M pH 6.8 reagents list:

Reagent	Amount
Tris base (Sigma #T6791)	24.23g
dH_2O	250ml
Total	250ml

Tris 3M pH 8.8 reagents list:

Reagent	Amount
Tris base	90.85g
dH_2O	250ml
Total	250ml

Gel Compositions:

	STACK	RESOLVING		
	Standard (4%)	**10%**	**12.5%**	**15%**
30% Bis-Acrylamide (Severn Western, UK #20-2100-05)	1.25ml	6.7ml	8.4ml	10ml
Tris (0.5M) pH 6.8	2.5ml	-	-	-
3M Tris buffer	-	2.5ml	2.5ml	2.5ml
10% SDS	100µl	200µl	200µl	200µl
APS (Sigma #A3678) 30mg/ml	0.5ml	1ml	1ml	1ml
TEMED (Sigma #T9281)	5µl	10µl	10µl	10µl
dH_2O	5.65ml	9.6ml	7.9ml	6.3ml

Running buffer (10x) reagents list:

Reagent	Concentration
Tris base	0.25 M
Glycine (Sigma #G8898)	1.92 M
SDS (Sigma #L3771)	1% (w/v)

Transfer buffer (10x) reagents list:

Reagent	Concentration
Tris base	0.25 M
Glycine	1.92 M

TBS-T (10x) pH 7.6 reagents list:

Reagent	Concentration
Tris base	200 mM
NaCl	1.4 M
Tween-20	1 % (v/v)

BSA (5%) reagents list:

Reagent	Amount
BSA	12.5g
TBS-T (1x)	250ml
Total	250ml

BSA (3%) reagents list:

Reagent	Amount
BSA	7.5g
TBS-T (1x)	250ml
Total	250ml

SDS-Sample buffer (4x) reagents list:

Reagent	Concentration
SDS	8 %
Tris-HCl pH 6.8	240 mM
bromophenol blue	0.04 %
Glycerol	40% (v/v)

beta-mercaptoethanol	5 % (v/v)

Appendix 2

Images taken during osmotic mini-pump implantation.

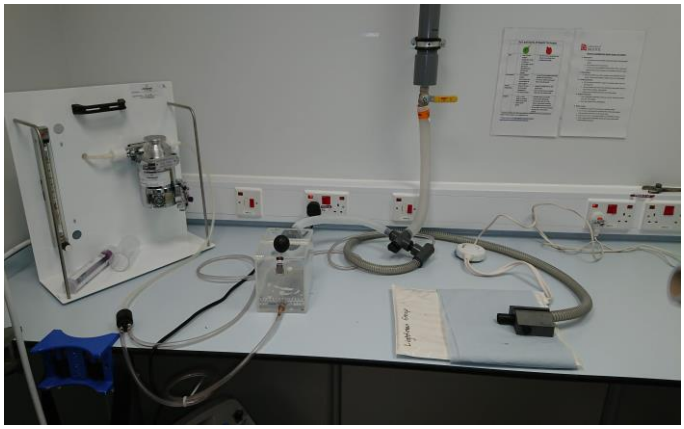

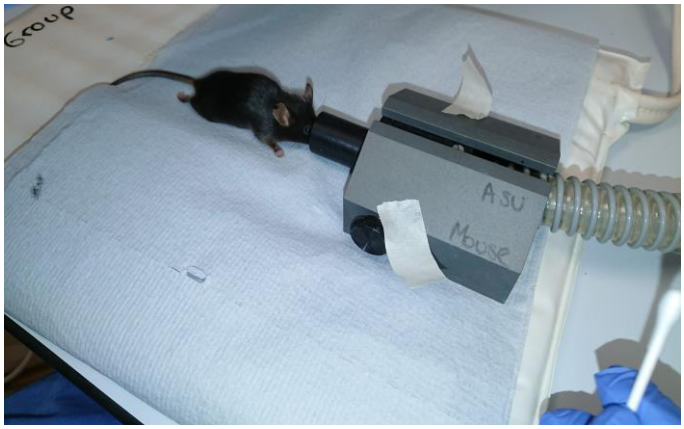




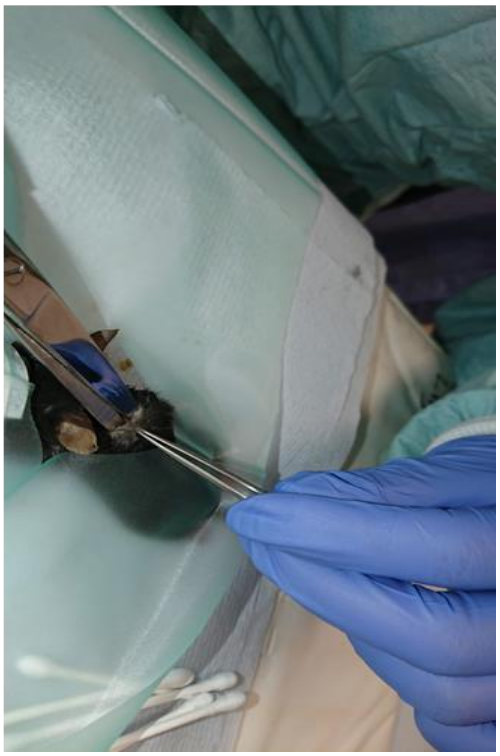

References

[1] "Kidneys | You and Your Hormones from the Society for Endocrinology." [Online]. Available: http://www.yourhormones.info/glands/kidneys/. [Accessed: 10-Apr-2019].

[2] R. E. Pratt, J. A. Flynn, P. M. Hobart, M. Paul, and V. J. Dzau, "Different secretory pathways of renin from mouse cells transfected with the human renin gene.," *J. Biol. Chem.*, vol. 263, no. 7, pp. 3137–41, Mar. 1988.

[3] "Kidney Pain: Symptoms, Pain Relief, Causes & Home Remedies." [Online]. Available: https://www.medicinenet.com/kidney_pain/article.htm#what_are_symptoms_and_signs_are_associated_with_kidney_pain. [Accessed: 10-Apr-2019].

[4] A. J. Vander, J. H. Sherman, and D. S. Luciano, *Human Physiology: The Mechanisms of Body Function*. McGraw-Hill, 2001.

[5] D. R. Abrahamson and R. Wang, *The Kidney*. Elsevier, 2003.

[6] "The Renal Tubule: Definition, Function & Terms - Video & Lesson Transcript | Study.com." [Online]. Available: https://study.com/academy/lesson/the-renal-tubule-definition-function-terms.html. [Accessed: 10-Apr-2019].

[7] "Microscopic Anatomy of the Kidney | Anatomy and Physiology II." [Online]. Available: https://courses.lumenlearning.com/cuny-kbcc-ap2/chapter/microscopic-anatomy-of-the-kidney/. [Accessed: 10-Apr-2019].

[8] C. C. Tisher, "Functional anatomy of the kidney.," *Hosp. Pract.*, vol. 13, no. 5, p. UNKNOWN, May 1978.

[9] S. E. Quaggin and J. A. Kreidberg, "Development of the renal glomerulus: good neighbors and good fences.," *Development*, vol. 135, no. 4, pp. 609–20, Feb. 2008.

[10] K. Tryggvason and J. Wartiovaara, "Molecular basis of glomerular permselectivity.," *Curr. Opin. Nephrol. Hypertens.*, vol. 10, no. 4, pp. 543–9, Jul. 2001.

[11] F. Costantini and R. Kopan, "Patterning a complex organ: branching morphogenesis and nephron segmentation in kidney development.," *Dev. Cell*, vol. 18, no. 5, pp. 698–712, May 2010.

[12] G. R. Dressler, "The Cellular Basis of Kidney Development," *Annu. Rev. Cell Dev. Biol.*, vol. 22, no. 1, pp. 509–529, Nov. 2006.

[13] S. Vainio and Y. Lin, "Coordinating early kidney development: lessons from gene targeting," *Nat. Rev. Genet.*, vol. 3, no. 7, pp. 533–543, Jul. 2002.

[14] G. R. Dressler, C. R. Altmann, R. A. Lang, A. Hemmati-Brivanlou, C. Kintner, and G. R. Dressler, "Advances in early kidney specification, development and patterning.," *Development*, vol. 136, no. 23, pp. 3863–74, Dec. 2009.

[15] C. Schell, N. Wanner, and T. B. Huber, "Glomerular development--shaping the

multi-cellular filtration unit.," *Semin. Cell Dev. Biol.*, vol. 36, pp. 39–49, Dec. 2014.

[16] B. Robert, X. Zhao, and D. R. Abrahamson, "Coexpression of neuropilin-1, Flk1, and VEGF164 in developing and mature mouse kidney glomeruli," *Am J Physiol Ren. Physiol*, vol. 279, no. 2, pp. F275-282, Aug. 2000.

[17] E. L. POTTER, "DEVELOPMENT OF THE HUMAN GLOMERULUS.," *Arch. Pathol.*, vol. 80, pp. 241–55, Sep. 1965.

[18] J. H. Miner, "Organogenesis of the kidney glomerulus: focus on the glomerular basement membrane.," *Organogenesis*, vol. 7, no. 2, pp. 75–82, Jan. 2011.

[19] M. C. Menon, P. Y. Chuang, and C. J. He, "The glomerular filtration barrier: components and crosstalk.," *Int. J. Nephrol.*, vol. 2012, p. 749010, Jan. 2012.

[20] H. Pavenstädt, W. Kriz, and M. Kretzler, "Cell biology of the glomerular podocyte.," *Physiol. Rev.*, vol. 83, no. 1, pp. 253–307, Jan. 2003.

[21] R. P. Scott and S. E. Quaggin, "The cell biology of renal filtration.," *J. Cell Biol.*, vol. 209, no. 2, pp. 199–210, Apr. 2015.

[22] J. Patrakka and K. Tryggvason, "Molecular make-up of the glomerular filtration barrier.," *Biochem. Biophys. Res. Commun.*, vol. 396, no. 1, pp. 164–9, May 2010.

[23] K. Ichimura, R. V. Stan, H. Kurihara, and T. Sakai, "Glomerular Endothelial Cells Form Diaphragms during Development and Pathologic Conditions," *J. Am. Soc. Nephrol.*, vol. 19, no. 8, pp. 1463–1471, Aug. 2008.

[24] S. C. Satchell and F. Braet, "Glomerular endothelial cell fenestrations: an integral component of the glomerular filtration barrier," *Am. J. Physiol. Physiol.*, vol. 296, no. 5, pp. F947–F956, May 2009.

[25] T. Kamba, B. Y. Y. Tam, H. Hashizume, A. Haskell, B. Sennino, M. R. Mancuso, S. M. Norberg, S. M. O'Brien, R. B. Davis, L. C. Gowen, K. D. Anderson, G. Thurston, S. Joho, M. L. Springer, C. J. Kuo, and D. M. McDonald, "VEGF-dependent plasticity of fenestrated capillaries in the normal adult microvasculature.," *Am. J. Physiol. Heart Circ. Physiol.*, vol. 290, no. 2, pp. H560-76, Feb. 2006.

[26] J. Rostgaard and K. Qvortrup, "Electron microscopic demonstrations of filamentous molecular sieve plugs in capillary fenestrae.," *Microvasc. Res.*, vol. 53, no. 1, pp. 1–13, Jan. 1997.

[27] A. R. Pries, T. W. Secomb, and P. Gaehtgens, "The endothelial surface layer.," *Pflugers Arch.*, vol. 440, no. 5, pp. 653–66, Sep. 2000.

[28] C. Hjalmarsson, B. R. Johansson, and B. Haraldsson, "Electron microscopic evaluation of the endothelial surface layer of glomerular capillaries," *Microvasc. Res.*, vol. 67, no. 1, pp. 9–17, Jan. 2004.

[29] M. J. C. Dane, B. M. van den Berg, M. C. Avramut, F. G. A. Faas, J. van der Vlag, A. L. W. M. M. Rops, R. B. G. Ravelli, B. J. Koster, A. J. van Zonneveld, H. Vink, and T. J. Rabelink, "Glomerular Endothelial Surface Layer Acts as a Barrier against Albumin Filtration," *Am. J. Pathol.*, vol. 182, no. 5, pp. 1532–1540, May 2013.

[30] M. Jeansson, K. Björck, O. Tenstad, and B. Haraldsson, "Adriamycin alters

glomerular endothelium to induce proteinuria.," *J. Am. Soc. Nephrol.*, vol. 20, no. 1, pp. 114–22, Jan. 2009.

[31] A. Singh, S. C. Satchell, C. R. Neal, E. A. McKenzie, J. E. Tooke, and P. W. Mathieson, "Glomerular endothelial glycocalyx constitutes a barrier to protein permeability.," *J. Am. Soc. Nephrol.*, vol. 18, no. 11, pp. 2885–93, Nov. 2007.

[32] P. Kundra and S. Goswami, "Endothelial glycocalyx: Role in body fluid homeostasis and fluid management," *Indian J. Anaesth.*, vol. 63, no. 1, p. 6, Jan. 2019.

[33] A. Björnson, J. Moses, A. Ingemansson, B. Haraldsson, and J. Sörensson, "Primary human glomerular endothelial cells produce proteoglycans, and puromycin affects their posttranslational modification.," *Am. J. Physiol. Renal Physiol.*, vol. 288, no. 4, pp. F748-56, Apr. 2005.

[34] I. E. Stillman and S. A. Karumanchi, "The glomerular injury of preeclampsia.," *J. Am. Soc. Nephrol.*, vol. 18, no. 8, pp. 2281–4, Aug. 2007.

[35] M. F. Galvis-Ramírez, J. C. Quintana-Castillo, and J. C. Bueno-Sanchez, "Novel Insights Into the Role of Glycans in the Pathophysiology of Glomerular Endotheliosis in Preeclampsia.," *Front. Physiol.*, vol. 9, p. 1470, 2018.

[36] D. R. Abrahamson, "Origin of the glomerular basement membrane visualized after in vivo labeling of laminin in newborn rat kidneys.," *J. Cell Biol.*, vol. 100, no. 6, pp. 1988–2000, Jun. 1985.

[37] J. H. Miner, "The glomerular basement membrane.," *Exp. Cell Res.*, vol. 318, no. 9, pp. 973–8, May 2012.

[38] J. H. Suh and J. H. Miner, "The glomerular basement membrane as a barrier to albumin," *Nat. Rev. Nephrol.*, vol. 9, no. 8, pp. 470–477, Aug. 2013.

[39] J. H. Miner, "Glomerular basement membrane composition and the filtration barrier.," *Pediatr. Nephrol.*, vol. 26, no. 9, pp. 1413–7, Sep. 2011.

[40] J. H. Miner, B. L. Patton, S. I. Lentz, D. J. Gilbert, W. D. Snider, N. A. Jenkins, N. G. Copeland, and J. R. Sanes, "The laminin alpha chains: expression, developmental transitions, and chromosomal locations of alpha1-5, identification of heterotrimeric laminins 8-11, and cloning of a novel alpha3 isoform.," *J. Cell Biol.*, vol. 137, no. 3, pp. 685–701, May 1997.

[41] P. L. St John and D. R. Abrahamson, "Glomerular endothelial cells and podocytes jointly synthesize laminin-1 and -11 chains.," *Kidney Int.*, vol. 60, no. 3, pp. 1037–46, Sep. 2001.

[42] P. G. Noakes, J. H. Miner, M. Gautam, J. M. Cunningham, J. R. Sanes, and J. P. Merlie, "The renal glomerulus of mice lacking s-laminin/laminin beta 2: nephrosis despite molecular compensation by laminin beta 1.," *Nat. Genet.*, vol. 10, no. 4, pp. 400–6, Aug. 1995.

[43] B. G. Hudson, "The Molecular Basis of Goodpasture and Alport Syndromes: Beacons for the Discovery of the Collagen IV Family," *J. Am. Soc. Nephrol.*, vol. 15, no. 10, pp. 2514–2527, Oct. 2004.

[44] J. H. Miner and J. R. Sanes, "Collagen IV alpha 3, alpha 4, and alpha 5 chains in

rodent basal laminae: sequence, distribution, association with laminins, and developmental switches.," *J. Cell Biol.*, vol. 127, no. 3, pp. 879–91, Nov. 1994.

[45] D. R. Abrahamson, B. G. Hudson, L. Stroganova, D.-B. Borza, and P. L. St John, "Cellular origins of type IV collagen networks in developing glomeruli.," *J. Am. Soc. Nephrol.*, vol. 20, no. 7, pp. 1471–9, Jul. 2009.

[46] S. J. Harvey, G. Jarad, J. Cunningham, A. L. Rops, J. van der Vlag, J. H. Berden, M. J. Moeller, L. B. Holzman, R. W. Burgess, and J. H. Miner, "Disruption of Glomerular Basement Membrane Charge through Podocyte-Specific Mutation of Agrin Does Not Alter Glomerular Permselectivity," *Am. J. Pathol.*, vol. 171, no. 1, pp. 139–152, Jul. 2007.

[47] J. H. Miner, "Renal basement membrane components.," *Kidney Int.*, vol. 56, no. 6, pp. 2016–24, Dec. 1999.

[48] D. Kerjaschki, D. J. Sharkey, and M. G. Farquhar, "Identification and characterization of podocalyxin--the major sialoprotein of the renal glomerular epithelial cell.," *J. Cell Biol.*, vol. 98, no. 4, pp. 1591–6, Apr. 1984.

[49] *Molecular and Genetic Basis of Renal Disease*. Elsevier, 2008.

[50] D. Kerjaschki, A. T. Vernillo, and M. G. Farquhar, "Reduced sialylation of podocalyxin--the major sialoprotein of the rat kidney glomerulus--in aminonucleoside nephrosis.," *Am. J. Pathol.*, vol. 118, no. 3, pp. 343–9, Mar. 1985.

[51] K. Ichimura, S. Kakuta, Y. Kawasaki, T. Miyaki, T. Nonami, N. Miyazaki, T. Nakao, S. Enomoto, S. Arai, M. Koike, K. Murata, and T. Sakai, "Morphological process of podocyte development revealed by block-face scanning electron microscopy," 2017.

[52] K. Ichimura, N. Miyazaki, S. Sadayama, K. Murata, M. Koike, K.-I. Nakamura, K. Ohta, and T. Sakai, "Three-dimensional architecture of podocytes revealed by block-face scanning electron microscopy.," *Sci. Rep.*, vol. 5, p. 8993, Jan. 2015.

[53] K. Ichimura, H. Kurihara, and T. Sakai, "Actin Filament Organization of Foot Processes in Rat Podocytes," *J. Histochem. Cytochem.*, vol. 51, no. 12, pp. 1589–1600, Dec. 2003.

[54] P. Garg, "A Review of Podocyte Biology," *Am. J. Nephrol.*, vol. 47, no. 1, pp. 3–13, 2018.

[55] S. K. Mitra, D. A. Hanson, and D. D. Schlaepfer, "Focal adhesion kinase: in command and control of cell motility," *Nat. Rev. Mol. Cell Biol.*, vol. 6, no. 1, pp. 56–68, Jan. 2005.

[56] E. Arif, M. C. Wagner, D. B. Johnstone, H. N. Wong, B. George, P. A. Pruthi, M. J. Lazzara, and D. Nihalani, "Motor Protein Myo1c Is a Podocyte Protein That Facilitates the Transport of Slit Diaphragm Protein Neph1 to the Podocyte Membrane," *Mol. Cell. Biol.*, vol. 31, no. 10, pp. 2134–2150, May 2011.

[57] E. Schnabel, "The tight junction protein ZO-1 is concentrated along slit diaphragms of the glomerular epithelium," *J. Cell Biol.*, vol. 111, no. 3, pp. 1255–1263, Sep. 1990.

[58] M. T. Tassin, A. Beziau, M. C. Gubler, and B. Boyer, “Spatiotemporal expression of molecules associated with junctional complexes during the in vivo maturation of renal podocytes.,” *Int. J. Dev. Biol.*, vol. 38, no. 1, pp. 45–54, Mar. 1994.

[59] V. Ruotsalainen, P. Ljungberg, J. Wartiovaara, U. Lenkkeri, M. Kestilä, H. Jalanko, C. Holmberg, and K. Tryggvason, “Nephrin is specifically located at the slit diaphragm of glomerular podocytes.,” *Proc. Natl. Acad. Sci. U. S. A.*, vol. 96, no. 14, pp. 7962–7, Jul. 1999.

[60] J. Wartiovaara, L.-G. Öfverstedt, J. Khoshnoodi, J. Zhang, E. Mäkelä, S. Sandin, V. Ruotsalainen, R. H. Cheng, H. Jalanko, U. Skoglund, and K. Tryggvason, “Nephrin strands contribute to a porous slit diaphragm scaffold as revealed by electron tomography,” *J. Clin. Invest.*, vol. 114, no. 12, pp. 1820–1820, Dec. 2004.

[61] J. M. Kaplan, S. H. Kim, K. N. North, H. Rennke, L. A. Correia, H. Q. Tong, B. J. Mathis, J. C. Rodríguez-Pérez, P. G. Allen, A. H. Beggs, and M. R. Pollak, “Mutations in ACTN4, encoding alpha-actinin-4, cause familial focal segmental glomerulosclerosis.,” *Nat. Genet.*, vol. 24, no. 3, pp. 251–6, Mar. 2000.

[62] E. J. Brown, J. S. Schlöndorff, D. J. Becker, H. Tsukaguchi, S. J. Tonna, A. L. Uscinski, H. N. Higgs, J. M. Henderson, and M. R. Pollak, “Mutations in the formin gene INF2 cause focal segmental glomerulosclerosis.,” *Nat. Genet.*, vol. 42, no. 1, pp. 72–6, Jan. 2010.

[63] T. B. Huber and T. Benzing, “The slit diaphragm: a signaling platform to regulate podocyte function.,” *Curr. Opin. Nephrol. Hypertens.*, vol. 14, no. 3, pp. 211–6, May 2005.

[64] F. Grahammer, C. Schell, and T. B. Huber, “The podocyte slit diaphragm—from a thin grey line to a complex signalling hub,” *Nat. Rev. Nephrol.*, vol. 9, no. 10, pp. 587–598, Oct. 2013.

[65] P. Garg, R. Verma, L. Cook, A. Soofi, M. Venkatareddy, B. George, K. Mizuno, C. Gurniak, W. Witke, and L. B. Holzman, “Actin-depolymerizing factor cofilin-1 is necessary in maintaining mature podocyte architecture.,” *J. Biol. Chem.*, vol. 285, no. 29, pp. 22676–88, Jul. 2010.

[66] B. George, R. Verma, A. A. Soofi, P. Garg, J. Zhang, T.-J. Park, L. Giardino, L. Ryzhova, D. B. Johnstone, H. Wong, D. Nihalani, D. J. Salant, S. K. Hanks, T. Curran, M. P. Rastaldi, and L. B. Holzman, “Crk1/2-dependent signaling is necessary for podocyte foot process spreading in mouse models of glomerular disease,” *J. Clin. Invest.*, vol. 122, no. 2, pp. 674–692, Feb. 2012.

[67] W. Kriz, I. Shirato, M. Nagata, M. LeHir, and K. V. Lemley, “The podocyte’s response to stress: the enigma of foot process effacement,” *Am. J. Physiol. Physiol.*, vol. 304, no. 4, pp. F333–F347, Feb. 2013.

[68] P. Garg and T. Rabelink, “Glomerular proteinuria: a complex interplay between unique players,” *Adv. Chronic Kidney Dis.*, 2011.

[69] N. Boute, O. Gribouval, S. Roselli, F. Benessy, H. Lee, A. Fuchshuber, K. Dahan, M. C. Gubler, P. Niaudet, and C. Antignac, “NPHS2, encoding the glomerular protein podocin, is mutated in autosomal recessive steroid-resistant nephrotic syndrome.,” *Nat. Genet.*, vol. 24, no. 4, pp. 349–54, Apr. 2000.

[70] T.-S. Ha, “Genetics of hereditary nephrotic syndrome: a clinical review,” *Korean J. Pediatr.*, vol. 60, no. 3, p. 55, 2017.

[71] A. Sinha and A. Bagga, “Nephrotic Syndrome,” *Indian J. Pediatr.*, vol. 79, no. 8, pp. 1045–1055, Aug. 2012.

[72] W. Wong, “Idiopathic nephrotic syndrome in New Zealand children, demographic, clinical features, initial management and outcome after twelve-month follow-up: results of a three-year national surveillance study.,” *J. Paediatr. Child Health*, vol. 43, no. 5, pp. 337–41, May 2007.

[73] M. A. Saleem, “New developments in steroid-resistant nephrotic syndrome.,” *Pediatr. Nephrol.*, vol. 28, no. 5, pp. 699–709, May 2013.

[74] N. Daskalakis and M. P. Winn, “Focal and segmental glomerulosclerosis.,” *Cell. Mol. Life Sci.*, vol. 63, no. 21, pp. 2506–11, Nov. 2006.

[75] O. Gribouval, O. Boyer, A. Hummel, J. Dantal, F. Martinez, R. Sberro-Soussan, I. Etienne, D. Chauveau, M. Delahousse, A. Lionet, J. Allard, C. P. Noble, M.-J. Tête, L. Heidet, C. Antignac, and A. Servais, “Identification of genetic causes for sporadic steroid-resistant nephrotic syndrome in adults,” *Kidney Int.*, vol. 94, no. 5, pp. 1013–1022, Nov. 2018.

[76] M.-C. Gubler, “Podocyte Differentiation and Hereditary Proteinuria/Nephrotic Syndromes,” *J. Am. Soc. Nephrol.*, vol. 14, no. 90001, p. 22S–26, Jun. 2003.

[77] A. Bierzynska, K. Soderquest, and A. Koziell, “Genes and podocytes - new insights into mechanisms of podocytopathy.,” *Front. Endocrinol. (Lausanne).*, vol. 5, p. 226, Jan. 2014.

[78] M. Kestilä, U. Lenkkeri, M. Männikkö, J. Lamerdin, P. McCready, H. Putaala, V. Ruotsalainen, T. Morita, M. Nissinen, R. Herva, C. E. Kashtan, L. Peltonen, C. Holmberg, A. Olsen, and K. Tryggvason, “Positionally Cloned Gene for a Novel Glomerular Protein—Nephrin—Is Mutated in Congenital Nephrotic Syndrome,” *Mol. Cell*, vol. 1, no. 4, pp. 575–582, Mar. 1998.

[79] N. P. Huttunen, “Congenital nephrotic syndrome of Finnish type. Study of 75 patients.,” *Arch. Dis. Child.*, vol. 51, no. 5, pp. 344–8, May 1976.

[80] C. Holmberg, M. Antikainen, K. R�nnholm, M. Ala-Houhala, and H. Jalanko, “Management of congenital nephrotic syndrome of the Finnish type,” *Pediatr. Nephrol.*, vol. 9, no. 1, pp. 87–93, Feb. 1995.

[81] J. Patrakka and K. Tryggvason, “Nephrin--a unique structural and signaling protein of the kidney filter.,” *Trends Mol. Med.*, vol. 13, no. 9, pp. 396–403, Sep. 2007.

[82] H. Putaala, “The murine nephrin gene is specifically expressed in kidney, brain and pancreas: inactivation of the gene leads to massive proteinuria and neonatal death,” *Hum. Mol. Genet.*, vol. 10, no. 1, pp. 1–8, Jan. 2001.

[83] J. Khoshnoodi, S. Hill, K. Tryggvason, B. Hudson, and D. B. Friedman, “Identification of N-linked glycosylation sites in human nephrin using mass spectrometry,” *J. MASS Spectrom. J. Mass Spectrom*, vol. 42, pp. 370–379, 2007.

[84] H. A. Dworak, M. A. Charles, L. B. Pellerano, and H. Sink, “Characterization of

Drosophila hibris, a gene related to human nephrin.," *Development*, vol. 128, no. 21, pp. 4265–76, Nov. 2001.

[85] G.-M. Barletta, I. A. Kovari, R. K. Verma, D. Kerjaschki, and L. B. Holzman, "Nephrin and Neph1 Co-localize at the Podocyte Foot Process Intercellular Junction and Form cis Hetero-oligomers," *J. Biol. Chem.*, vol. 278, no. 21, pp. 19266–19271, Mar. 2003.

[86] G. Liu, B. Kaw, J. Kurfis, S. Rahmanuddin, Y. S. Kanwar, and S. S. Chugh, "Neph1 and nephrin interaction in the slit diaphragm is an important determinant of glomerular permeability," *J. Clin. Invest.*, vol. 112, no. 2, pp. 209–221, Jul. 2003.

[87] R. Verma, B. Wharram, I. Kovari, R. Kunkel, D. Nihalani, K. K. Wary, R. C. Wiggins, P. Killen, and L. B. Holzman, "Fyn binds to and phosphorylates the kidney slit diaphragm component Nephrin.," *J. Biol. Chem.*, vol. 278, no. 23, pp. 20716–23, Jun. 2003.

[88] R. Verma, "Nephrin ectodomain engagement results in Src kinase activation, nephrin phosphorylation, Nck recruitment, and actin polymerization," *J. Clin. Invest.*, vol. 116, no. 5, pp. 1346–1359, May 2006.

[89] B. D. Adair, M. M. Altintas, C. C. Möller, M. A. Arnaout, and J. Reiser, "Structure of the kidney slit diaphragm adapter protein CD2-associated protein as determined with electron microscopy.," *J. Am. Soc. Nephrol.*, vol. 25, no. 7, pp. 1465–73, Jul. 2014.

[90] N. Y. Shih, J. Li, R. Cotran, P. Mundel, J. H. Miner, and A. S. Shaw, "CD2AP localizes to the slit diaphragm and binds to nephrin via a novel C-terminal domain.," *Am. J. Pathol.*, vol. 159, no. 6, pp. 2303–8, Dec. 2001.

[91] N. Shih, "Congenital Nephrotic Syndrome in Mice Lacking CD2-Associated Protein," *Science (80-.).*, vol. 286, no. 5438, pp. 312–315, Oct. 1999.

[92] J. M. Kim, H. Wu, G. Green, C. A. Winkler, J. B. Kopp, J. H. Miner, E. R. Unanue, and A. S. Shaw, "CD2-associated protein haploinsufficiency is linked to glomerular disease susceptibility.," *Science*, vol. 300, no. 5623, pp. 1298–300, May 2003.

[93] J. A. Grunkemeyer, C. Kwoh, T. B. Huber, and A. S. Shaw, "CD2-associated Protein (CD2AP) Expression in Podocytes Rescues Lethality of CD2AP Deficiency," *J. Biol. Chem.*, vol. 280, no. 33, pp. 29677–29681, Aug. 2005.

[94] "CD2AP (CD2 associated protein)." [Online]. Available: http://atlasgeneticsoncology.org/Genes/GC_CD2AP.html. [Accessed: 13-Jul-2019].

[95] T. B. Huber, B. Hartleben, J. Kim, M. Schmidts, B. Schermer, A. Keil, L. Egger, R. L. Lecha, C. Borner, H. Pavenstadt, A. S. Shaw, G. Walz, and T. Benzing, "Nephrin and CD2AP Associate with Phosphoinositide 3-OH Kinase and Stimulate AKT-Dependent Signaling," *Mol. Cell. Biol.*, vol. 23, no. 14, pp. 4917–4928, Jul. 2003.

[96] J. S. Schlöndorff and M. R. Pollak, "TRPC6 in glomerular health and disease: what we know and what we believe.," *Semin. Cell Dev. Biol.*, vol. 17, no. 6, pp. 667–74, Dec. 2006.

[97] C. C. Möller, J. Flesche, and J. Reiser, "Sensitizing the Slit Diaphragm with TRPC6

Ion Channels," *J. Am. Soc. Nephrol.*, vol. 20, no. 5, pp. 950–953, May 2009.

[98] D. E. Clapham, "TRP channels as cellular sensors.," *Nature*, vol. 426, no. 6966, pp. 517–24, Dec. 2003.

[99] S. E. Dryer and J. Reiser, "TRPC6 channels and their binding partners in podocytes: role in glomerular filtration and pathophysiology," *Am. J. Physiol. Physiol.*, vol. 299, no. 4, pp. F689–F701, Oct. 2010.

[100] A. Dietrich, H. Kalwa, B. R. Rost, and T. Gudermann, "The diacylgylcerol-sensitive TRPC3/6/7 subfamily of cation channels: functional characterization and physiological relevance.," *Pflugers Arch.*, vol. 451, no. 1, pp. 72–80, Oct. 2005.

[101] M. P. Winn, P. J. Conlon, K. L. Lynn, M. K. Farrington, T. Creazzo, A. F. Hawkins, N. Daskalakis, S. Y. Kwan, S. Ebersviller, J. L. Burchette, M. A. Pericak-Vance, D. N. Howell, J. M. Vance, and P. B. Rosenberg, "A mutation in the TRPC6 cation channel causes familial focal segmental glomerulosclerosis.," *Science*, vol. 308, no. 5729, pp. 1801–4, Jun. 2005.

[102] J. Reiser, K. R. Polu, C. C. Möller, P. Kenlan, M. M. Altintas, C. Wei, C. Faul, S. Herbert, I. Villegas, C. Avila-Casado, M. McGee, H. Sugimoto, D. Brown, R. Kalluri, P. Mundel, P. L. Smith, D. E. Clapham, and M. R. Pollak, "TRPC6 is a glomerular slit diaphragm-associated channel required for normal renal function.," *Nat. Genet.*, vol. 37, no. 7, pp. 739–44, Jul. 2005.

[103] T. B. Huber, B. Schermer, and T. Benzing, "Podocin organizes ion channel-lipid supercomplexes: implications for mechanosensation at the slit diaphragm.," *Nephron. Exp. Nephrol.*, vol. 106, no. 2, pp. e27-31, Jan. 2007.

[104] T. B. Huber, M. Kottgen, B. Schilling, G. Walz, and T. Benzing, "Interaction with podocin facilitates nephrin signaling.," *J. Biol. Chem.*, vol. 276, no. 45, pp. 41543–6, Nov. 2001.

[105] T. B. Huber, B. Schermer, R. U. Müller, M. Höhne, M. Bartram, A. Calixto, H. Hagmann, C. Reinhardt, F. Koos, K. Kunzelmann, E. Shirokova, D. Krautwurst, C. Harteneck, M. Simons, H. Pavenstädt, D. Kerjaschki, C. Thiele, G. Walz, M. Chalfie, and T. Benzing, "Podocin and MEC-2 bind cholesterol to regulate the activity of associated ion channels.," *Proc. Natl. Acad. Sci. U. S. A.*, vol. 103, no. 46, pp. 17079–86, Nov. 2006.

[106] C. Hisatsune, Y. Kuroda, K. Nakamura, T. Inoue, T. Nakamura, T. Michikawa, A. Mizutani, and K. Mikoshiba, "Regulation of TRPC6 Channel Activity by Tyrosine Phosphorylation," *J. Biol. Chem.*, vol. 279, no. 18, pp. 18887–18894, Apr. 2004.

[107] C. C. Möller, C. Wei, M. M. Altintas, J. Li, A. Greka, T. Ohse, J. W. Pippin, M. P. Rastaldi, S. Wawersik, S. Schiavi, A. Henger, M. Kretzler, S. J. Shankland, and J. Reiser, "Induction of TRPC6 channel in acquired forms of proteinuric kidney disease.," *J. Am. Soc. Nephrol.*, vol. 18, no. 1, pp. 29–36, Jan. 2007.

[108] E. S. Chhabra, V. Ramabhadran, S. A. Gerber, and H. N. Higgs, "INF2 is an endoplasmic reticulum-associated formin protein.," *J. Cell Sci.*, vol. 122, no. Pt 9, pp. 1430–40, May 2009.

[109] R. Rollason, M. Wherlock, J. A. Heath, K. J. Heesom, M. A. Saleem, and G. I. Welsh, "Disease causing mutations in inverted formin 2 regulate its binding to G-actin, F-

actin capping protein (CapZ α-1) and profilin 2.," *Biosci. Rep.*, vol. 36, no. 1, p. e00302, Jan. 2016.

[110] S. Roselli, O. Gribouval, N. Boute, M. Sich, F. Benessy, T. Attié, M.-C. Gubler, and C. Antignac, "Podocin localizes in the kidney to the slit diaphragm area.," *Am. J. Pathol.*, vol. 160, no. 1, pp. 131–9, Jan. 2002.

[111] S. Roselli, L. Heidet, M. Sich, A. Henger, M. Kretzler, M.-C. Gubler, and C. Antignac, "Early Glomerular Filtration Defect and Severe Renal Disease in Podocin-Deficient Mice," *Mol. Cell. Biol.*, vol. 24, no. 2, pp. 550–560, Dec. 2003.

[112] E.-M. Schurek, L. A. Völker, J. Tax, T. Lamkemeyer, M. M. Rinschen, D. Ungrue, J. E. Kratz, L. Sirianant, K. Kunzelmann, M. Chalfie, B. Schermer, T. Benzing, and M. Höhne, "A disease-causing mutation illuminates the protein membrane topology of the kidney-expressed prohibitin homology (PHB) domain protein podocin.," *J. Biol. Chem.*, vol. 289, no. 16, pp. 11262–71, Apr. 2014.

[113] M. Anderson, E. Y. Kim, H. Hagmann, T. Benzing, and S. E. Dryer, "Opposing effects of podocin on the gating of podocyte TRPC6 channels evoked by membrane stretch or diacylglycerol.," *Am. J. Physiol. Cell Physiol.*, vol. 305, no. 3, pp. C276-89, Aug. 2013.

[114] A. Tabassum, T. Rajeshwari, N. Soni, D. Raju, M. Yadav, A. Nayarisseri, and P. Jahan, "Structural Characterization and Mutational Assessment of Podocin-A Novel Drug Target to Nephrotic Syndrome-An in silico Approach," *Interdiscip Sci Comput Life Sci*, vol. 6, pp. 32–39, 2014.

[115] M. Relle, H. Cash, C. Brochhausen, D. Strand, J. Menke, P. R. Galle, and A. Schwarting, "New perspectives on the renal slit diaphragm protein podocin," *Mod. Pathol.*, vol. 24, no. 8, pp. 1101–1110, Aug. 2011.

[116] M. Simons, K. Schwarz, W. Kriz, A. Miettinen, J. Reiser, P. Mundel, and H. Holthöfer, "Involvement of lipid rafts in nephrin phosphorylation and organization of the glomerular slit diaphragm.," *Am. J. Pathol.*, vol. 159, no. 3, pp. 1069–77, Sep. 2001.

[117] M. B. Fessler and J. S. Parks, "Intracellular lipid flux and membrane microdomains as organizing principles in inflammatory cell signaling.," *J. Immunol.*, vol. 187, no. 4, pp. 1529–35, Aug. 2011.

[118] A. Fornoni, S. Merscher, and J. B. Kopp, "Lipid biology of the podocyte--new perspectives offer new opportunities.," *Nat. Rev. Nephrol.*, vol. 10, no. 7, pp. 379–88, Jul. 2014.

[119] T. B. Huber, M. Simons, B. Hartleben, L. Sernetz, M. Schmidts, E. Gundlach, M. A. Saleem, G. Walz, and T. Benzing, "Molecular basis of the functional podocin-nephrin complex: mutations in the NPHS2 gene disrupt nephrin targeting to lipid raft microdomains.," *Hum. Mol. Genet.*, vol. 12, no. 24, pp. 3397–405, Dec. 2003.

[120] K. Bouchireb, O. Boyer, O. Gribouval, F. Nevo, E. Huynh-Cong, V. Morinière, R. Campait, E. Ars, D. Brackman, J. Dantal, P. Eckart, M. Gigante, B. S. Lipska, A. Liutkus, A. Megarbane, N. Mohsin, F. Ozaltin, M. A. Saleem, F. Schaefer, K. Soulami, R. Torra, N. Garcelon, G. Mollet, K. Dahan, and C. Antignac, "NPHS2 mutations in steroid-resistant nephrotic syndrome: a mutation update and the associated phenotypic spectrum.," *Hum. Mutat.*, vol. 35, no. 2, pp. 178–86, Feb. 2014.

[121] I. Horinouchi, H. Nakazato, T. Kawano, K.-I. Iyama, A. Furuse, K. Arizono, J. Machida, T. Sakamoto, F. Endo, and S. Hattori, “In situ evaluation of podocin in normal and glomerular diseases,” *Kidney Int.*, vol. 64, no. 6, pp. 2092–2099, Dec. 2003.

[122] K. Schwarz, M. Simons, J. Reiser, M. A. Saleem, C. Faul, W. Kriz, A. S. Shaw, L. B. Holzman, and P. Mundel, “Podocin, a raft-associated component of the glomerular slit diaphragm, interacts with CD2AP and nephrin.,” *J. Clin. Invest.*, vol. 108, no. 11, pp. 1621–9, Dec. 2001.

[123] E. Machuca, A. Hummel, F. Nevo, J. Dantal, F. Martinez, E. Al-Sabban, V. Baudouin, L. Abel, J.-P. Grünfeld, and C. Antignac, “Clinical and epidemiological assessment of steroid-resistant nephrotic syndrome associated with the NPHS2 R229Q variant,” *Kidney Int.*, vol. 75, no. 7, pp. 727–735, Apr. 2009.

[124] S. Weber, O. Gribouval, E. L. Esquivel, V. Morinière, M.-J. Tête, C. Legendre, P. Niaudet, and C. Antignac, “NPHS2 mutation analysis shows genetic heterogeneity of steroid-resistant nephrotic syndrome and low post-transplant recurrence.,” *Kidney Int.*, vol. 66, no. 2, pp. 571–9, Aug. 2004.

[125] B. Hinkes, C. Vlangos, S. Heeringa, B. Mucha, R. Gbadegesin, J. Liu, K. Hasselbacher, F. Ozaltin, and F. Hildebrandt, “Specific podocin mutations correlate with age of onset in steroid-resistant nephrotic syndrome.,” *J. Am. Soc. Nephrol.*, vol. 19, no. 2, pp. 365–71, Feb. 2008.

[126] S. Roselli, I. Moutkine, O. Gribouval, A. Benmerah, and C. Antignac, “Plasma membrane targeting of podocin through the classical exocytic pathway: effect of NPHS2 mutations.,” *Traffic*, vol. 5, no. 1, pp. 37–44, Jan. 2004.

[127] M. A. Saleem, M. J. O’Hare, J. Reiser, R. J. Coward, C. D. Inward, T. Farren, C. Y. Xing, L. Ni, P. W. Mathieson, and P. Mundel, “A conditionally immortalized human podocyte cell line demonstrating nephrin and podocin expression.,” *J. Am. Soc. Nephrol.*, vol. 13, no. 3, pp. 630–8, Mar. 2002.

[128] N. Odolczyk, J. Fritsch, C. Norez, N. Servel, M. F. da Cunha, S. Bitam, A. Kupniewska, L. Wiszniewski, J. Colas, K. Tarnowski, D. Tondelier, A. Roldan, E. L. Saussereau, P. Melin-Heschel, G. Wieczorek, G. L. Lukacs, M. Dadlez, G. Faure, H. Herrmann, M. Ollero, F. Becq, P. Zielenkiewicz, and A. Edelman, “Discovery of novel potent ΔF508-CFTR correctors that target the nucleotide binding domain.,” *EMBO Mol. Med.*, vol. 5, no. 10, pp. 1484–501, Oct. 2013.

[129] A. L. Mattheyses, S. M. Simon, and J. Z. Rappoport, “Imaging with total internal reflection fluorescence microscopy for the cell biologist.,” *J. Cell Sci.*, vol. 123, no. Pt 21, pp. 3621–8, Nov. 2010.

[130] J. Colas, G. Faure, E. Saussereau, S. Trudel, W. M. Rabeh, S. Bitam, I. C. Guerrera, J. Fritsch, I. Sermet-Gaudelus, N. Davezac, F. Brouillard, G. L. Lukacs, H. Herrmann, M. Ollero, and A. Edelman, “Disruption of cytokeratin-8 interaction with F508del-CFTR corrects its functional defect.,” *Hum. Mol. Genet.*, vol. 21, no. 3, pp. 623–34, Feb. 2012.

[131] K. Di Gregoli, N. N. Mohamad Anuar, R. Bianco, S. J. White, A. C. Newby, S. J. George, and J. L. Johnson, “MicroRNA-181b Controls Atherosclerosis and Aneurysms Through Regulation of TIMP-3 and Elastin.,” *Circ. Res.*, vol. 120, no. 1,

pp. 49–65, Jan. 2017.

[132] N. Boute, O. Gribouval, S. Roselli, F. Benessy, H. Lee, A. Fuchshuber, K. Dahan, M. C. Gubler, P. Niaudet, and C. Antignac, “NPHS2, encoding the glomerular protein podocin, is mutated in autosomal recessive steroid-resistant nephrotic syndrome.,” *Nat. Genet.*, vol. 24, no. 4, pp. 349–54, Apr. 2000.

[133] M. Tabatabaeifar, T. Wlodkowski, I. Simic, H. Denc, G. Mollet, S. Weber, J. J. Moyers, B. Brühl, M. J. Randles, R. Lennon, C. Antignac, and F. Schaefer, “An inducible mouse model of podocin-mutation-related nephrotic syndrome.,” *PLoS One*, vol. 12, no. 10, p. e0186574, 2017.

[134] T. Shigehara, C. Zaragoza, C. Kitiyakara, H. Takahashi, H. Lu, M. Moeller, L. B. Holzman, and J. B. Kopp, “Inducible podocyte-specific gene expression in transgenic mice.,” *J. Am. Soc. Nephrol.*, vol. 14, no. 8, pp. 1998–2003, Aug. 2003.

[135] A. Philippe, S. Weber, E. L. Esquivel, C. Houbron, G. Hamard, J. Ratelade, W. Kriz, F. Schaefer, M.-C. Gubler, and C. Antignac, “A missense mutation in podocin leads to early and severe renal disease in mice.,” *Kidney Int.*, vol. 73, no. 9, pp. 1038–47, May 2008.

[136] R. L. Miller, “Transgenic mice: beyond the knockout.,” *Am. J. Physiol. Renal Physiol.*, vol. 300, no. 2, pp. F291-300, Feb. 2011.

[137] M. J. Moeller, S. K. Sanden, A. Soofi, R. C. Wiggins, and L. B. Holzman, “Two gene fragments that direct podocyte-specific expression in transgenic mice.,” *J. Am. Soc. Nephrol.*, vol. 13, no. 6, pp. 1561–7, Jun. 2002.

[138] J. Juhila, R. Roozendaal, M. Lassila, S. J. Verbeek, and H. Holthofer, “Podocyte cell-specific expression of doxycycline inducible Cre recombinase in mice.,” *J. Am. Soc. Nephrol.*, vol. 17, no. 3, pp. 648–54, Mar. 2006.

[139] G. Mollet, J. Ratelade, O. Boyer, A. O. Muda, L. Morisset, T. A. Lavin, D. Kitzis, M. J. Dallman, L. Bugeon, N. Hubner, M.-C. Gubler, C. Antignac, and E. L. Esquivel, “Podocin inactivation in mature kidneys causes focal segmental glomerulosclerosis and nephrotic syndrome.,” *J. Am. Soc. Nephrol.*, vol. 20, no. 10, pp. 2181–9, Oct. 2009.

[140] I. M. Redelsperger, T. Taldone, E. R. Riedel, M. L. Lepherd, N. S. Lipman, and F. R. Wolf, “Stability of Doxycycline in Feed and Water and Minimal Effective Doses in Tetracycline-Inducible Systems.,” *J. Am. Assoc. Lab. Anim. Sci.*, vol. 55, no. 4, pp. 467–74, 2016.

[141] J. H. Miner, G. Go, J. Cunningham, B. L. Patton, and G. Jarad, “Transgenic isolation of skeletal muscle and kidney defects in laminin beta2 mutant mice: implications for Pierson syndrome.,” *Development*, vol. 133, no. 5, pp. 967–75, Mar. 2006.

[142] B. L. Wharram, M. Goyal, J. E. Wiggins, S. K. Sanden, S. Hussain, W. E. Filipiak, T. L. Saunders, R. C. Dysko, K. Kohno, L. B. Holzman, and R. C. Wiggins, “Podocyte Depletion Causes Glomerulosclerosis: Diphtheria Toxin–Induced Podocyte Depletion in Rats Expressing Human Diphtheria Toxin Receptor Transgene,” *J. Am. Soc. Nephrol.*, vol. 16, no. 10, pp. 2941–2952, Oct. 2005.

[143] C. Zoja, M. Abbate, and G. Remuzzi, “Progression of renal injury toward interstitial inflammation and glomerular sclerosis is dependent on abnormal protein

filtration," *Nephrol. Dial. Transplant.*, vol. 30, no. 5, pp. 706–712, May 2015.

[144] "How Many Ways Can a Podocyte Die?," *Semin. Nephrol.*, vol. 32, no. 4, pp. 394–404, Jul. 2012.

[145] T. Ohashi, K. Uchida, S. Uchida, S. Sasaki, and H. Nihei, "Intracellular mislocalization of mutant podocin and correction by chemical chaperones.," *Histochem. Cell Biol.*, vol. 119, no. 3, pp. 257–64, Mar. 2003.

[146] M. Ollero, F. Brouillard, and A. Edelman, "Cystic fibrosis enters the proteomics scene: New answers to old questions," *Proteomics*, vol. 6, no. 14, pp. 4084–4099, Jul. 2006.

[147] D. Gadsby, A. N.-P. reviews, and undefined 1999, "Control of CFTR channel gating by phosphorylation and nucleotide hydrolysis," *physiology.org*.

[148] J. R. Riordan, J. M. Rommens, B. Kerem, N. Alon, R. Rozmahel, Z. Grzelczak, J. Zielenski, S. Lok, N. Plavsic, J. L. Chou, and et al., "Identification of the cystic fibrosis gene: cloning and characterization of complementary DNA.," *Science*, vol. 245, no. 4922, pp. 1066–73, Sep. 1989.

[149] G. M. Denning, M. P. Anderson, J. F. Amara, J. Marshall, A. E. Smith, and M. J. Welsh, "Processing of mutant cystic fibrosis transmembrane conductance regulator is temperature-sensitive.," *Nature*, vol. 358, no. 6389, pp. 761–4, Aug. 1992.

[150] W. Dalemans, P. Barbry, G. Champigny, S. Jallat, S. Jallat, K. Dott, D. Dreyer, R. G. Crystal, A. Pavirani, J.-P. Lecocq, and M. Lazdunski, "Altered chloride ion channel kinetics associated with the ΔF508 cystic fibrosis mutation," *Nature*, vol. 354, no. 6354, pp. 526–528, Dec. 1991.

[151] G. W. Carlile, R. Robert, D. Zhang, K. A. Teske, Y. Luo, J. W. Hanrahan, and D. Y. Thomas, "Correctors of Protein Trafficking Defects Identified by a Novel High-Throughput Screening Assay," *ChemBioChem*, vol. 8, no. 9, pp. 1012–1020, Jun. 2007.

[152] J. Paccou, P. Fardellone, and B. Cortet, "Cystic fibrosis-related bone disease," *Curr. Opin. Pulm. Med.*, vol. 19, no. 6, pp. 681–686, Nov. 2013.

[153] O. Kalid, M. Mense, S. Fischman, A. Shitrit, H. Bihler, E. Ben-Zeev, N. Schutz, N. Pedemonte, P. J. Thomas, R. J. Bridges, D. R. Wetmore, Y. Marantz, and H. Senderowitz, "Small molecule correctors of F508del-CFTR discovered by structure-based virtual screening," *J. Comput. Aided. Mol. Des.*, vol. 24, no. 12, pp. 971–991, Dec. 2010.

[154] J. R. Riordan, "CFTR Function and Prospects for Therapy," *Annu. Rev. Biochem.*, vol. 77, no. 1, pp. 701–726, Jun. 2008.

[155] H. Yu, B. Burton, C.-J. Huang, J. Worley, D. Cao, J. P. Johnson, A. Urrutia, J. Joubran, S. Seepersaud, K. Sussky, B. J. Hoffman, and F. Van Goor, "Ivacaftor potentiation of multiple CFTR channels with gating mutations," *J. Cyst. Fibros.*, vol. 11, no. 3, pp. 237–245, May 2012.

[156] G. Wieczorek and P. Zielenkiewicz, "ΔF508 mutation increases conformational flexibility of CFTR protein," *J. Cyst. Fibros.*, vol. 7, no. 4, pp. 295–300, Jul. 2008.

[157] N. Odolczyk, J. Fritsch, C. Norez, N. Servel, M. F. da Cunha, S. Bitam, A. Kupniewska, L. Wiszniewski, J. Colas, K. Tarnowski, D. Tondelier, A. Roldan, E. L. Saussereau, P. Melin-Heschel, G. Wieczorek, G. L. Lukacs, M. Dadlez, G. Faure, H. Herrmann, M. Ollero, F. Becq, P. Zielenkiewicz, and A. Edelman, "Discovery of novel potent ΔF508-CFTR correctors that target the nucleotide binding domain," *EMBO Mol. Med.*, vol. 5, no. 10, pp. 1484–1501, Oct. 2013.

[158] P. A. Coulombe, L. Ma, S. Yamada, and M. Wawersik, "Intermediate filaments at a glance," *J. Cell Sci.*, vol. 114, no. 24, pp. 4345–4347, Dec. 2001.

[159] M. Hesse, T. M. Magin, and K. Weber, "Genes for intermediate filament proteins and the draft sequence of the human genome: novel keratin genes and a surprisingly high number of pseudogenes related to keratin genes 8 and 18," *J. Cell Sci.*, vol. 114, no. 14, pp. 2569–2575, Jul. 2001.

[160] F. Brouillard, J. Fritsch, A. Edelman, and M. Ollero, "Contribution of proteomics to the study of the role of cytokeratins in disease and physiopathology.," *Proteomics. Clin. Appl.*, vol. 2, no. 2, pp. 264–85, Mar. 2008.

[161] R. Windoffer, S. Wöll, P. Strnad, and R. E. Leube, "Identification of novel principles of keratin filament network turnover in living cells.," *Mol. Biol. Cell*, vol. 15, no. 5, pp. 2436–48, May 2004.

[162] E. Fuchs and K. Weber, "Intermediate filaments: structure, dynamics, function, and disease.," *Annu. Rev. Biochem.*, vol. 63, pp. 345–82, Jan. 1994.

[163] P. A. Coulombe and P. Wong, "Cytoplasmic intermediate filaments revealed as dynamic and multipurpose scaffolds.," *Nat. Cell Biol.*, vol. 6, no. 8, pp. 699–706, Aug. 2004.

[164] C. R. Robbins, *Chemical and physical behavior of human hair*. Springer, 2012.

[165] J. Schweizer, P. E. Bowden, P. A. Coulombe, L. Langbein, E. B. Lane, T. M. Magin, L. Maltais, M. B. Omary, D. A. D. Parry, M. A. Rogers, and M. W. Wright, "New consensus nomenclature for mammalian keratins.," *J. Cell Biol.*, vol. 174, no. 2, pp. 169–74, Jul. 2006.

[166] T. M. Magin, P. Vijayaraj, and R. E. Leube, "Structural and regulatory functions of keratins.," *Exp. Cell Res.*, vol. 313, no. 10, pp. 2021–32, Jun. 2007.

[167] N.-O. Ku and M. B. Omary, "A disease- and phosphorylation-related nonmechanical function for keratin 8.," *J. Cell Biol.*, vol. 174, no. 1, pp. 115–25, Jul. 2006.

[168] D. Toivola, M. I. Nieminen, M. Hesse, T. He, H. Baribault, T. M. Magin, M. B. Omary, and J. E. Eriksson, "Disturbances in hepatic cell-cycle regulation in mice with assembly-deficient keratins 8/18," *Hepatology*, vol. 34, no. 6, pp. 1174–1183, Dec. 2001.

[169] S. Gilbert, A. Loranger, and N. Marceau, "Keratins modulate c-Flip/extracellular signal-regulated kinase 1 and 2 antiapoptotic signaling in simple epithelial cells.," *Mol. Cell. Biol.*, vol. 24, no. 16, pp. 7072–81, Aug. 2004.

[170] D. M. Toivola, G.-Z. Tao, A. Habtezion, J. Liao, and M. B. Omary, "Cellular integrity plus: organelle-related and protein-targeting functions of intermediate

filaments.," *Trends Cell Biol.*, vol. 15, no. 11, pp. 608–17, Nov. 2005.

[171] S. M. Karle, B. Uetz, V. Ronner, L. Glaeser, F. Hildebrandt, and A. Fuchshuber, "Novel mutations in NPHS2 detected in both familial and sporadic steroid-resistant nephrotic syndrome.," *J. Am. Soc. Nephrol.*, vol. 13, no. 2, pp. 388–93, Feb. 2002.

[172] B. Zhong, Q. Zhou, D. M. Toivola, G.-Z. Tao, E. Z. Resurreccion, and M. B. Omary, "Organ-specific stress induces mouse pancreatic keratin overexpression in association with NF-kappaB activation.," *J. Cell Sci.*, vol. 117, no. Pt 9, pp. 1709–19, Apr. 2004.

[173] S. Djudjaj, M. Papasotiriou, R. D. Bü Low, A. Wagnerova, M. T. Lindenmeyer, C. D. Cohen, P. Strnad, D. S. Goumenos, J. Rgen Floege, and P. Boor, "Keratins are novel markers of renal epithelial cell injury," *Kidney Int.*, vol. 89, pp. 792–808, 2016.

[174] H. Tamura, H. Nakazato, S. Kuraoka, K. Yoneda, W. Takahashi, and F. Endo, "Reduced INF2 expression in nephrotic syndrome is possibly related to clinical severity of steroid resistance in children," *Nephrology*, vol. 21, no. 6, pp. 467–475, Jun. 2016.

[175] S.-Y. Zhang, M. Kamal, K. Dahan, A. Pawlak, V. Ory, D. Desvaux, V. Audard, M. Candelier, F. BenMohamed, F. Ben Mohamed, M. Matignon, C. Christov, X. Decrouy, V. Bernard, G. Mangiapan, P. Lang, G. Guellaën, P. Ronco, and D. Sahali, "c-mip impairs podocyte proximal signaling and induces heavy proteinuria.," *Sci. Signal.*, vol. 3, no. 122, p. ra39, May 2010.

[176] Y. Morishita, H. Yoshizawa, M. Watanabe, K. Ishibashi, S. Muto, E. Kusano, and D. Nagata, "siRNAs targeted to Smad4 prevent renal fibrosis in vivo.," *Sci. Rep.*, vol. 4, p. 6424, Sep. 2014.

[177] F. Liu, Z. Chen, J. Wang, X. Shao, Z. Cui, C. Yang, Z. Zhu, and D. Xiong, "Overexpression of Cell Surface Cytokeratin 8 in Multidrug-Resistant MCF-7/MX Cells Enhances Cell Adhesion to the Extracellular Matrix," *Neoplasia*, vol. 10, no. 11, pp. 1275–1284, Nov. 2008.

[178] H. Long, V. Boczonadi, … L. M.-J. of cell, and undefined 2006, "Periplakin-dependent re-organisation of keratin cytoskeleton and loss of collective migration in keratin-8-downregulated epithelial sheets," *jcs.biologists.org*.

[179] N. Davezac, D. Tondelier, J. Lipecka, P. Fanen, F. Demaugre, J. Debski, M. Dadlez, A. Schrattenholz, M. A. Cahill, and A. Edelman, "Global proteomic approach unmasks involvement of keratins 8 and 18 in the delivery of cystic fibrosis transmembrane conductance regulator (CFTR)/?F508-CFTR to the plasma membrane," *Proteomics*, vol. 4, no. 12, pp. 3833–3844, Dec. 2004.

[180] C. Le Henaff, M. Faria, D. Cunha, A. Hatton, D. Tondelier, C. Marty, C. Collet, M. Zarka, V. Geoffroy, K. Zatloukal, E. Laplantine, A. Edelman, I. Sermet-Gaudelus, and P. J. Marie, "Genetic deletion of keratin 8 corrects the altered bone formation and osteopenia in a mouse model of cystic fibrosis," 2016.

[181] A. Jaitovich, S. Mehta, N. Na, A. Ciechanover, R. D. Goldman, and K. M. Ridge, "Ubiquitin-Proteasome-mediated Degradation of Keratin Intermediate Filaments in Mechanically Stimulated A549 Cells," *J. Biol. Chem.*, vol. 283, no. 37, pp. 25348–25355, Sep. 2008.

[182] O. Cil and F. Perwad, “Monogenic Causes of Proteinuria in Children,” *Front. Med.*, vol. 5, p. 55, Mar. 2018.

[183] M. Aridor and L. A. Hannan, “Traffic jams II: an update of diseases of intracellular transport.,” *Traffic*, vol. 3, no. 11, pp. 781–90, Nov. 2002.

[184] Y. Nishibori, L. Liu, M. Hosoyamada, H. Endou, A. Kudo, H. Takenaka, E. Higashihara, F. Bessho, S. Takahashi, D. Kershaw, V. Ruotsalainen, K. Tryggvason, J. Khoshnoodi, and K. Yan, “Disease-causing missense mutations in NPHS2 gene alter normal nephrin trafficking to the plasma membrane.,” *Kidney Int.*, vol. 66, no. 5, pp. 1755–65, Nov. 2004.

[185] V. D’Agati, “Pathologic classification of focal segmental glomerulosclerosis,” *Semin. Nephrol.*, vol. 23, no. 2, pp. 117–134, Mar. 2003.

[186] J. B. Pereira-Leal and M. C. Seabra, “Evolution of the rab family of small GTP-binding proteins,” *J. Mol. Biol.*, vol. 313, no. 4, pp. 889–901, Nov. 2001.

[187] M. Fukuda, “Membrane traffic in the secretory pathway,” *Cell. Mol. Life Sci.*, vol. 65, no. 18, pp. 2801–2813, Sep. 2008.

[188] M. Fukuda, “TBC proteins: GAPs for mammalian small GTPase Rab?,” *Biosci. Rep.*, vol. 31, no. 3, pp. 159–168, Jun. 2011.

[189] M. Fukuda, “How can mammalian Rab small GTPases be comprehensively analyzed?: Development of new tools to comprehensively analyze mammalian Rabs in membrane traffic.,” *Histol. Histopathol.*, vol. 25, no. 11, pp. 1473–80, 2010.

[190] M. Fukuda, E. Kanno, K. Ishibashi, and T. Itoh, “Large Scale Screening for Novel Rab Effectors Reveals Unexpected Broad Rab Binding Specificity,” *Mol. Cell. Proteomics*, vol. 7, no. 6, pp. 1031–1042, Jun. 2008.

[191] F. Barr and D. G. Lambright, “Rab GEFs and GAPs,” *Curr. Opin. Cell Biol.*, vol. 22, no. 4, pp. 461–470, Aug. 2010.

[192] L. I. Gallo, Y. Liao, W. G. Ruiz, D. R. Clayton, M. Li, Y.-J. Liu, Y. Jiang, M. Fukuda, G. Apodaca, and X.-M. Yin, “TBC1D9B functions as a GTPase-activating protein for Rab11a in polarized MDCK cells,” *Mol. Biol. Cell*, vol. 25, no. 23, pp. 3779–3797, Nov. 2014.

[193] B. Vollenbröker, B. George, M. Wolfgart, M. A. Saleem, H. Pavenstädt, and T. Weide, “mTOR regulates expression of slit diaphragm proteins and cytoskeleton structure in podocytes,” *Am. J. Physiol. Physiol.*, vol. 296, no. 2, pp. F418–F426, Feb. 2009.

[194] D. Rapaport, Y. Lugassy, E. Sprecher, and M. Horowitz, “Loss of SNAP29 Impairs Endocytic Recycling and Cell Motility,” *PLoS One*, vol. 5, no. 3, p. e9759, Mar. 2010.

[195] J. M. Smith, D. M. Stablein, R. Munoz, D. Hebert, and R. A. McDonald, “Contributions of the Transplant Registry: The 2006 Annual Report of the North American Pediatric Renal Trials and Collaborative Studies (NAPRTCS),” *Pediatr. Transplant.*, vol. 11, no. 4, pp. 366–373, Jun. 2007.

[196] S. Lovric, S. Ashraf, W. Tan, and F. Hildebrandt, “Genetic testing in steroid-resistant nephrotic syndrome: when and how?,” *Nephrol. Dial. Transplant.*, vol. 31, no. 11,

pp. 1802–1813, Nov. 2016.

[197] A. Bierzynska, H. McCarthy, K. Soderquest, E. S.-K. international, and undefined 2017, “Genomic and clinical profiling of a national nephrotic syndrome cohort advocates a precision medicine approach to disease management,” *Elsevier*.

[198] C. Faul, K. Asanuma, E. Yanagida-Asanuma, … K. K.-T. in cell, and undefined 2007, “Actin up: regulation of podocyte structure and function by components of the actin cytoskeleton,” *Elsevier*.

[199] I. Tossidou, B. Teng, J. Menne, N. Shushakova, J.-K. Park, J. U. Becker, F. Modde, M. Leitges, H. Haller, and M. Schiffer, “Podocytic PKC-Alpha Is Regulated in Murine and Human Diabetes and Mediates Nephrin Endocytosis,” *PLoS One*, vol. 5, no. 4, p. e10185, Apr. 2010.

[200] T. Hermle, R. Schneider, … D. S.-J. of the, and undefined 2018, “GAPVD1 and ANKFY1 mutations implicate RAB5 regulation in nephrotic syndrome,” *Am Soc Nephrol*.

[201] A. Kramer-Zucker, S. Wiessner, … A. J.-D., and undefined 2005, “Organization of the pronephric filtration apparatus in zebrafish requires Nephrin, Podocin and the FERM domain protein Mosaic eyes,” *Elsevier*.

[202] X. Pan, S. Eathiraj, M. Munson, D. L.- Nature, and undefined 2006, “TBC-domain GAPs for Rab GTPases accelerate GTP hydrolysis by a dual-finger mechanism,” *nature.com*.

[203] S. R. Pfeffer, “Rab GTPases: master regulators that establish the secretory and endocytic pathways,” *Mol. Biol. Cell*, vol. 28, no. 6, pp. 712–715, Mar. 2017.

[204] K. M. Mayle, A. M. Le, and D. T. Kamei, “The intracellular trafficking pathway of transferrin.,” *Biochim. Biophys. Acta*, vol. 1820, no. 3, pp. 264–81, Mar. 2012.

[205] B. Grant, J. D.-N. reviews M. cell biology, and undefined 2009, “Pathways and mechanisms of endocytic recycling,” *nature.com*.

[206] S. Mukherjee, R. N. Ghosh, and F. R. Maxfield, “Endocytosis,” *Physiol. Rev.*, vol. 77, no. 3, pp. 759–803, Jul. 1997.

[207] M. Kann, S. Ettou, Y. L. Jung, M. O. Lenz, M. E. Taglienti, P. J. Park, B. Schermer, T. Benzing, and J. A. Kreidberg, “Genome-Wide Analysis of Wilms’ Tumor 1-Controlled Gene Expression in Podocytes Reveals Key Regulatory Mechanisms.,” *J. Am. Soc. Nephrol.*, vol. 26, no. 9, pp. 2097–104, Sep. 2015.

[208] L. Lapierre, M. Dorn, … C. Z.-E. cell, and undefined 2003, “Rab11b resides in a vesicular compartment distinct from Rab11a in parietal cells and other epithelial cells,” *Elsevier*.

[209] X. Li, M. D.-P. in neurobiology, and undefined 2012, “The recycling endosome and its role in neurological disorders,” *Elsevier*.

[210] N. Grimsey, L. Coronel, … I. C.-J. of B., and undefined 2016, “Recycling and endosomal sorting of protease-activated Receptor-1 is distinctly regulated by Rab11A and Rab11B proteins,” *ASBMB*.

[211] K. Inoue and S. Ishibe, “Podocyte endocytosis in the regulation of the glomerular filtration barrier,” *Am. J. Physiol. Physiol.*, vol. 309, no. 5, pp. F398–F405, Sep. 2015.

[212] T. B. Huber, B. Schermer, and T. Benzing, “Podocin organizes ion channel-lipid supercomplexes: implications for mechanosensation at the slit diaphragm.,” *Nephron. Exp. Nephrol.*, vol. 106, no. 2, pp. e27-31, Jan. 2007.

[213] B. Schermer and T. Benzing, “Lipid–Protein Interactions along the Slit Diaphragm of Podocytes,” *J. Am. Soc. Nephrol.*, vol. 20, no. 3, pp. 473–478, Mar. 2009.

[214] M. M. Rinschen, P. Bharill, X. Wu, P. Kohli, M. J. Reinert, O. Kretz, I. S. Martinez, B. Schermer, M. Höhne, M. P. Bartram, S. Aravamudhan, B. R. Brooks, D. Vilchez, T. B. Huber, R.-U. Müller, M. Krüger, and T. Benzing, “The ubiquitin ligase Ubr4 controls stability of podocin/MEC-2 supercomplexes.,” *Hum. Mol. Genet.*, Jan. 2016.

[215] A. Doerr, “Targeted proteomics,” *Nat. Methods*, vol. 8, no. 1, pp. 43–43, Jan. 2011.

[216] C. E.-C. opinion in cell biology and undefined 1990, “Cell migration in the embryo and adult organism,” *Elsevier*.

[217] A. Ridley, M. Schwartz, K. Burridge, … R. F.-, and undefined 2003, “Cell migration: integrating signals from front to back,” *science.sciencemag.org*.

[218] X. Zhao and J.-L. Guan, “Focal adhesion kinase and its signaling pathways in cell migration and angiogenesis,” *Adv. Drug Deliv. Rev.*, vol. 63, no. 8, pp. 610–615, Jul. 2011.

[219] A. Wortmann, Y. He, M. E. Christensen, M. Linn, J. W. Lumley, P. M. Pollock, N. J. Waterhouse, and J. D. Hooper, “Cellular settings mediating Src substrate switching between focal adhesion kinase (FAK) tyrosine 861 and CUB-domain containing protein 1 (CDCP1) tyrosine 734,” 2011.

[220] M. Scherl-Mostageer, W. Sommergruber, R. Abseher, R. Hauptmann, P. Ambros, and N. Schweifer, “Identification of a novel gene, CDCP1, overexpressed in human colorectal cancer,” *Oncogene*, vol. 20, no. 32, pp. 4402–4408, Jul. 2001.

[221] J. D. Hooper, A. Zijlstra, R. T. Aimes, H. Liang, G. F. Claassen, D. Tarin, J. E. Testa, and J. P. Quigley, “Subtractive immunization using highly metastatic human tumor cells identifies SIMA135/CDCP1, a 135 kDa cell surface phosphorylated glycoprotein antigen.,” *Oncogene*, vol. 22, no. 12, pp. 1783–94, Mar. 2003.

[222] T. Uekita, L. Jia, M. Narisawa-Saito, J. Yokota, T. Kiyono, and R. Sakai, “CUB Domain-Containing Protein 1 Is a Novel Regulator of Anoikis Resistance in Lung Adenocarcinoma,” *Mol. Cell. Biol.*, vol. 27, no. 21, pp. 7649–7660, Nov. 2007.

[223] B. Casar, I. Rimann, H. Kato, S. J. Shattil, J. P. Quigley, and E. I. Deryugina, “In vivo cleaved CDCP1 promotes early tumor dissemination via complexing with activated β1 integrin and induction of FAK/PI3K/Akt motility signaling,” *Oncogene*, vol. 33, no. 2, pp. 255–268, Jan. 2014.

[224] D. S. Spassov, F. L. Baehner, C. H. Wong, S. McDonough, and M. M. Moasser, “The transmembrane src substrate Trask is an epithelial protein that signals during anchorage deprivation.,” *Am. J. Pathol.*, vol. 174, no. 5, pp. 1756–65, May 2009.

[225] D. S. Spassov, C. H. Wong, N. Sergina, D. Ahuja, M. Fried, D. Sheppard, and M. M. Moasser, “Phosphorylation of Trask by Src kinases inhibits integrin clustering and functions in exclusion with focal adhesion signaling.,” *Mol. Cell. Biol.*, vol. 31, no. 4, pp. 766–82, Feb. 2011.

[226] T. Uekita and R. Sakai, “Roles of CUB domain-containing protein 1 signaling in cancer invasion and metastasis,” *Cancer Sci.*, vol. 102, no. 11, pp. 1943–1948, Nov. 2011.

[227] T. A. Brown, T. M. Yang, T. Zaitsevskaia, Y. Xia, C. A. Dunn, R. O. Sigle, B. Knudsen, and W. G. Carter, “Adhesion or plasmin regulates tyrosine phosphorylation of a novel membrane glycoprotein p80/gp140/CUB domain-containing protein 1 in epithelia.,” *J. Biol. Chem.*, vol. 279, no. 15, pp. 14772–83, Apr. 2004.

[228] B. Casar, Y. He, M. Iconomou, J. D. Hooper, J. P. Quigley, and E. I. Deryugina, “Blocking of CDCP1 cleavage in vivo prevents Akt-dependent survival and inhibits metastatic colonization through PARP1-mediated apoptosis of cancer cells.,” *Oncogene*, vol. 31, no. 35, pp. 3924–38, Aug. 2012.

[229] S. M. Frisch, K. Vuori, E. Ruoslahti, and P. Y. Chan-Hui, “Control of adhesion-dependent cell survival by focal adhesion kinase.,” *J. Cell Biol.*, vol. 134, no. 3, pp. 793–9, Aug. 1996.

[230] D. Lietha, X. Cai, D. F. J. Ceccarelli, Y. Li, M. D. Schaller, and M. J. Eck, “Structural basis for the autoinhibition of focal adhesion kinase.,” *Cell*, vol. 129, no. 6, pp. 1177–87, Jun. 2007.

[231] I. Pranke, K. Tomaszewski, S. Bitam, G. Faure, E. Chevet, I. Sermet-Gaudelus, and A. Edelman, “The role of cytokeratin 8 in alpha-1-antitrypsin secretion and/or degradation,” *Rev. Mal. Respir.*, vol. 32, no. 3, pp. 319–320, Mar. 2015.

[232] L. Fregonese and J. Stolk, “Hereditary alpha-1-antitrypsin deficiency and its clinical consequences.,” *Orphanet J. Rare Dis.*, vol. 3, p. 16, Jun. 2008.

[233] K. S. Hruska, M. E. LaMarca, C. R. Scott, and E. Sidransky, “Gaucher disease: mutation and polymorphism spectrum in the glucocerebrosidase gene (GBA),” *Hum. Mutat.*, vol. 29, no. 5, pp. 567–583, May 2008.

[234] N. Gregersen, “Protein misfolding disorders: Pathogenesis and intervention; Protein misfolding disorders: Pathogenesis and intervention,” *J Inherit Metab Dis*, vol. 29, pp. 456–470, 2006.

[235] “Administration by Oral Gavage — Research at Penn State.” [Online]. Available: https://www.research.psu.edu/arp/experimental-guidelines/administration-by-oral-gavage.html. [Accessed: 29-Jul-2019].

[236] R. Davis, A. Coukell, and donna McTavish, “Fosinopril,” *Drugs*, vol. 54, no. 1, pp. 103–116, Jul. 1997.